MS Analysis Report

Ribolytix Project Number: Internal

Ribolytix Report Number: Internal-MS-2v2

Client / laboratory: Internal

Report date: 2026-11-15

Report status: Final

Prepared By:

Ribolytix, Inc.

701 West Main Street, Suite 200

Durham, NC, 27701

QUALITY CONTROL STATEMENT

It is the objective of Ribolytix, Inc., that all studies conducted by our facility shall be of the highest quality to ensure the integrity of the data generated.

The MS analysis report for project Internal was reviewed before finalization.

JohnCarlo Kristofich, PhD

Founder & CEO

Ribolytix, Inc.

1. Purpose and Scope

This study profiles cellular responses to RBP-targeting compounds in HCT116 cells. It identifies compound-responsive proteins and potential markers of cellular activity, examines relationships among their responses, and interprets the observed patterns in the context of the compounds' reported mechanisms.

This report summarizes the results from LC–MS/MS analysis of the sample fractions identified in Section 4, including protein coverage, sample variability, differential analysis, and functional annotation of differentially abundant proteins. The supporting data package contains results and figures for all protein panels defined below. This report focuses on the filtered GO RNA-binding protein panel, which includes proteins with annotated RNA-binding functions while excluding those with historical evidence that free protein contributed more than 25% of their measured signal.

Protein panel	Definition
Total identified proteins	Proteins identified by LC–MS/MS in the analyzed sample fractions, excluding contaminants and technical standards.
GO RNA-binding proteins	Identified proteins with Gene Ontology annotations for RNA binding (GO:0003723).
Filtered GO RNA-binding proteins	GO RNA-binding proteins excluding those with previously reported free-protein contributions greater than 25% of their measured signal ($S/N < 3$). Proteins without previously reported S/N measurements remain included.

2. Abbreviations and Definitions

The following abbreviations and definitions are aligned with terminology previously defined by Kristofich and Nicchitta (*Nature Communications*, 2023; *RNA*, 2024; *Bio-protocol*, 2024).

RBP: RNA-binding protein.

Ribonucleoprotein (RNP) fractions: Sample fraction containing total RNA and RNA-bound protein.

Total protein (Input) fractions: Sample fraction containing total protein.

Fragmented RNP (frag RNP) fractions: Sample fraction containing both protein-bound and protein-free RNA fragments (fragment-size peak: approximately 200 nt).

Fragmented and free RNA depleted RNP (frag clRNP) fractions: Sample fraction containing protein-bound RNA fragments (fragment-size peak: approximately 200 nt).

PK: Proteinase K.

PK-treated, fragmented RNP (PK frag RNP) fractions: RNA fraction recovered following proteinase K treatment of a frag RNP fraction.

PK-treated, fragmented, and free RNA depleted RNP (PK frag clRNP) fractions: RNA fraction recovered following proteinase K treatment of a frag clRNP fraction.

Signal (*S*): RNA-bound protein.

Noise (*N*): Unbound counterpart of an RNA-bound protein.

Background (*B*): Protein without an RNA-bound counterpart.

Signal-to-noise ratio (*S*/*N*): The ratio of RNA-bound protein to its unbound counterpart.

Yield: Quantity of RNA or protein recovered by a given process expressed as micrograms per one percent of starting sample fraction (e.g., µg/% fraction).

RNP composition: The ratio of protein to RNA in RNP fractions, estimated by dividing protein yields by their corresponding RNA yields.

LC-MS/MS: Liquid chromatography-tandem mass spectrometry.

GO: Gene Ontology, a reference system describing molecular functions, biological processes, and cellular components.

Sum peptide intensities (SPI): The sum of MS peptide intensities assigned to a protein; used to estimate protein quantity.

Total Protein Approach (TPA): An approach for estimating protein abundances from protein SPI values relative to total MS signal of the sample (total SPI).

Protein abundance (%TP): Protein abundance estimated as 100 × protein SPI divided by total SPI across all eligible proteins in the sample. Protein panels retain this complete eligible-protein denominator.

Fold change (FC): In this report, the ratio of geometric mean protein abundances (%TP) in the numerator and denominator groups.

Differentially abundant protein: A protein showing a statistically significant difference in abundance between the compared sample groups after correction for multiple testing.

False discovery rate (FDR): The expected proportion of significant results that are actually false positives.

Coefficient of variation (CV): Standardized measure of dispersion of a probability distribution or frequency distribution, calculated as the ratio of the standard deviation to the mean.

Principal component analysis (PCA): A method that summarizes variation across many measurements using uncorrelated components, ordered by the amount of variation they explain, to display similarities and differences among samples.

MA plot: A plot of M (minus, or the difference between log-transformed values) versus A (average). In this report, M represents the $\log_2$ ratio of protein abundances (%TP), and A represents the average $\log_{10}$(%TP) across all samples.

Over-representation analysis (ORA): A statistical analysis testing whether a functional category is represented more frequently in a selected gene or protein list than expected relative to a defined reference background.

Gene set enrichment analysis (GSEA): An analysis testing whether members of a predefined gene set are concentrated toward the top or bottom of a gene list ranked by a specified measurement or statistic.

Normalized enrichment score (NES): A GSEA enrichment score scaled relative to permutation-derived scores to account for differences in gene-set size. Positive and negative values indicate enrichment toward the top and bottom of the ranked list, respectively. Statistical significance is assessed separately.

3. Study and Sample Metadata

3.1 Experimental Sample List

Sample group	Biological replicate	Cell line	UV irradiation	Treatment / condition
H3B-8800	R1	HCT116	0.4 J/cm²; 254 nm	10 µM H3B-8800; 90 min
H3B-8800	R2	HCT116	0.4 J/cm²; 254 nm	10 µM H3B-8800; 90 min
RK-33	R1	HCT116	0.4 J/cm²; 254 nm	10 µM RK-33; 90 min
RK-33	R2	HCT116	0.4 J/cm²; 254 nm	10 µM RK-33; 90 min
MS-444	R1	HCT116	0.4 J/cm²; 254 nm	100 µM MS-444; 90 min
MS-444	R2	HCT116	0.4 J/cm²; 254 nm	100 µM MS-444; 90 min
UZH1a	R1	HCT116	0.4 J/cm²; 254 nm	100 µM UZH1a; 90 min
UZH1a	R2	HCT116	0.4 J/cm²; 254 nm	100 µM UZH1a; 90 min
Untreated	R1	HCT116	0.4 J/cm²; 254 nm	Untreated; 90-min timepoint
Untreated	R2	HCT116	0.4 J/cm²; 254 nm	Untreated; 90-min timepoint

4. Sample Fractions Covered by This Report

The following table identifies the sample fractions included in this MS analysis and accompanying data package.

Client-provided sample ID	Internally assigned sample ID	Sample fraction type	Sample fraction ID
Not provided	Not provided	Not provided	Not provided
Not provided	Not provided	Not provided	Not provided
Not provided	Not provided	Not provided	Not provided
Not provided	Not provided	Not provided	Not provided
Not provided	Not provided	Not provided	Not provided
Not provided	Not provided	Not provided	Not provided
Not provided	Not provided	Not provided	Not provided
Not provided	Not provided	Not provided	Not provided
Not provided	Not provided	Not provided	Not provided
Not provided	Not provided	Not provided	Not provided

5. Execution and Source-Data Traceability

Execution records, source files, internal software versions, and reference dates used for this report are summarized below.

Component	Execution and source information
MS sample submission	Aliquots for the 10 analyzed sample fractions were prepared on July 27, 2026, following SOP-P-0029-0001. Supporting equipment, material, and reagent records are provided in 05_Traceability.
LC–MS/MS acquisition and database searching	Acquisition and search methods are summarized in Methods_and_Data_Analysis.docx. Additional details may be requested from the facility.
MS data analysis	Ribolytix MS analysis workflow 3.4.5; executed November 14, 2026.
Databases and annotations	Accessed November 14, 2026: UniProtKB 2026_04 for protein functions, KEGG 2026, Reactome 98, InterPro domains 111.0, GO biological process 2026-11-13, GO molecular function 2026-11-13, GO cellular component 2026-11-13, STRING 12.5 (functional associations). Reference check November 14, 2026: UniProtKB 2026_04, Pfam 39.0, InterPro 111.0 (protein features). Accessed November 14, 2026: GOA/QuickGO annotations; GO release 2026-11-13.
Report assembly	Ribolytix Deliverable builder 1.12.19; report assembled November 15, 2026.

Supporting data and traceability records are provided in the data package.

6. Protein Coverage

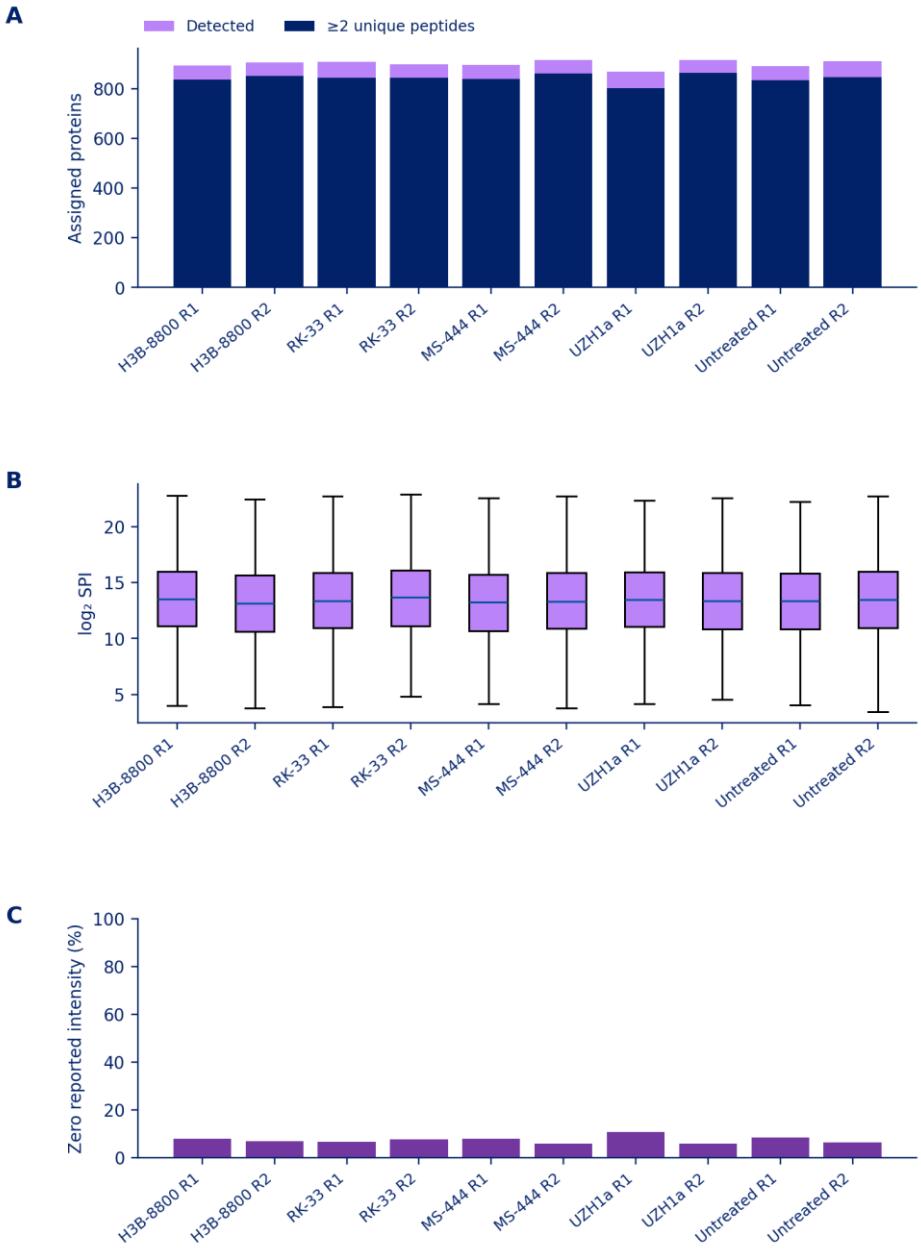


Figure 1. Protein coverage and signal distributions for filtered GO RNA-binding proteins. (A) Numbers of proteins detected per sample. Total bar height represents proteins detected with ≥1 unique peptide; dark blue indicates the subset supported by ≥2 unique peptides. **(B)** Distributions of positive protein intensities after $\log_2$ transformation, before sample normalization. Boxes span the interquartile range (IQR), horizontal lines indicate medians, and whiskers extend to the most extreme values within 1.5 × IQR of the box edges. Outliers are not displayed. **(C)** Percentage of proteins in the panel with zero reported intensity in each sample. Differential-abundance testing requires ≥2 unique peptides per protein in every included replicate of both comparison groups.

Across samples, 869–916 proteins were identified, including 802–863 identified with ≥2 unique peptides.

7. Within- and Between-Group Variability

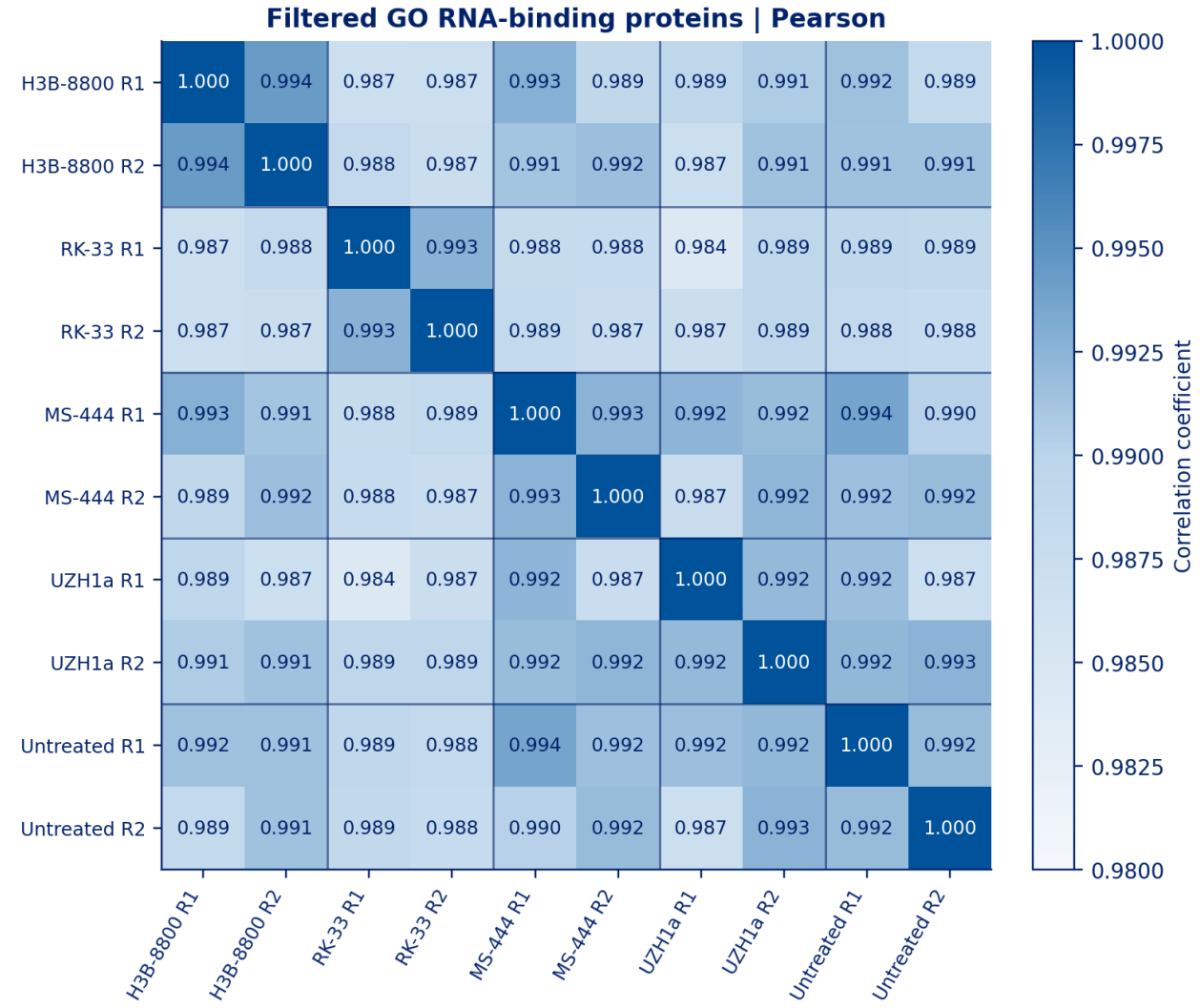


Figure 2. Pairwise Pearson correlations among samples. Correlations were calculated using $\log_2$(%TP) values in the analyzed RNP fractions for filtered GO RNA-binding proteins identified with at least two unique peptide matches in every included sample. Each cell shows Pearson's *r* for the corresponding sample pair; diagonal cells represent self-correlations.

Principal component analysis

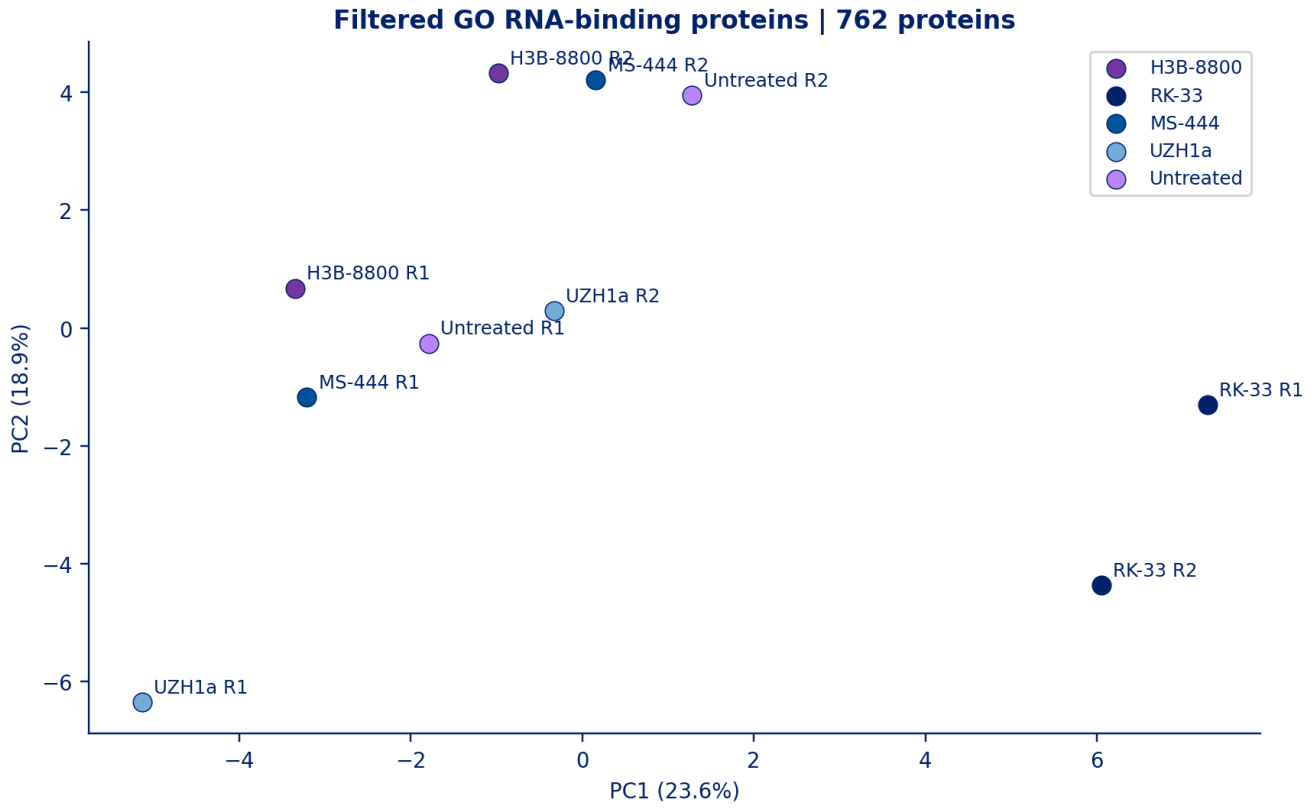


Figure 3. Principal component analysis of filtered GO RNA-binding proteins. PCA was performed using $\log_2$(%TP) values in the analyzed RNP fractions for proteins identified with at least two unique peptide matches in every included sample. Points represent individual biological replicates, colored by sample group. Axis labels indicate the percentage of total variance explained by each principal component.

The first two principal components accounted for 42.4% of the total variance (PC1, 23.6%; PC2, 18.9%).

8. Differential Analysis

Common contaminants and spike-ins were excluded, and sum peptide intensities (SPI) were calculated by summing the intensities of unique peptides assigned to each protein. Proteins identified with at least two unique peptide matches in every included sample were retained. Samples were mean-normalized to total SPI across these proteins. Protein abundances (%TP) were estimated using the Total Protein Approach and expressed as a percentage of total SPI across all eligible proteins. Protein panels retained this complete eligible-protein denominator.

Within the filtered GO RNA-binding proteins panel, $\log_2$(%TP) values in the analyzed RNP fractions were used to test for differences in protein abundance using two-tailed moderated *t* tests using limma. The Benjamini–Hochberg procedure was used to correct for multiple hypothesis testing across all proteins tested in this panel within each comparison, with a false discovery rate of 5%. The adjusted *p* values are reported as *q* values ($q < .05$). Fold changes represent ratios of geometric mean protein abundances (%TP) between groups. No minimum fold-change threshold was applied.

Short protein function and feature descriptions accompany the heatmaps. Descriptions summarize recorded UniProtKB functions, selected positive Gene Ontology annotations, and Pfam/InterPro features. They are independent of the observed abundance differences. Complete annotations, source evidence, database releases, and selection rules for every retained identified protein are provided in the supporting Protein_Annotations folder.

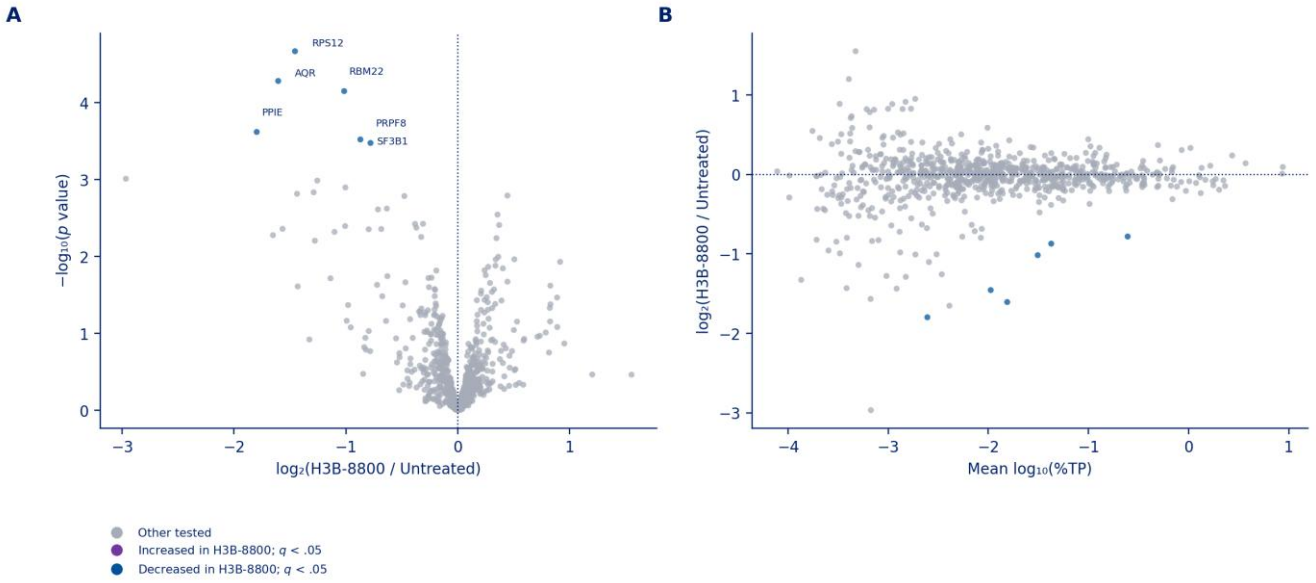


Figure 4. Differential analyses of filtered GO RNA-binding proteins between H3B-8800 and Untreated. 6 of 797 tested proteins met $q < .05$. **(A)** Volcano plot showing $-\log_{10}$-transformed *p* values before FDR correction as a function of $\log_2$(H3B-8800/Untreated). Point colors indicate differential abundance after Benjamini–Hochberg correction ($q < .05$) in both panels. **(B)** MA plot showing $\log_2$(H3B-8800/Untreated) as a function of mean $\log_{10}$(%TP) across all samples.

Of the 797 proteins tested, 6 (0.8%) differed significantly in abundance, including 0 with increased and 6 with decreased abundance in H3B-8800 relative to Untreated.

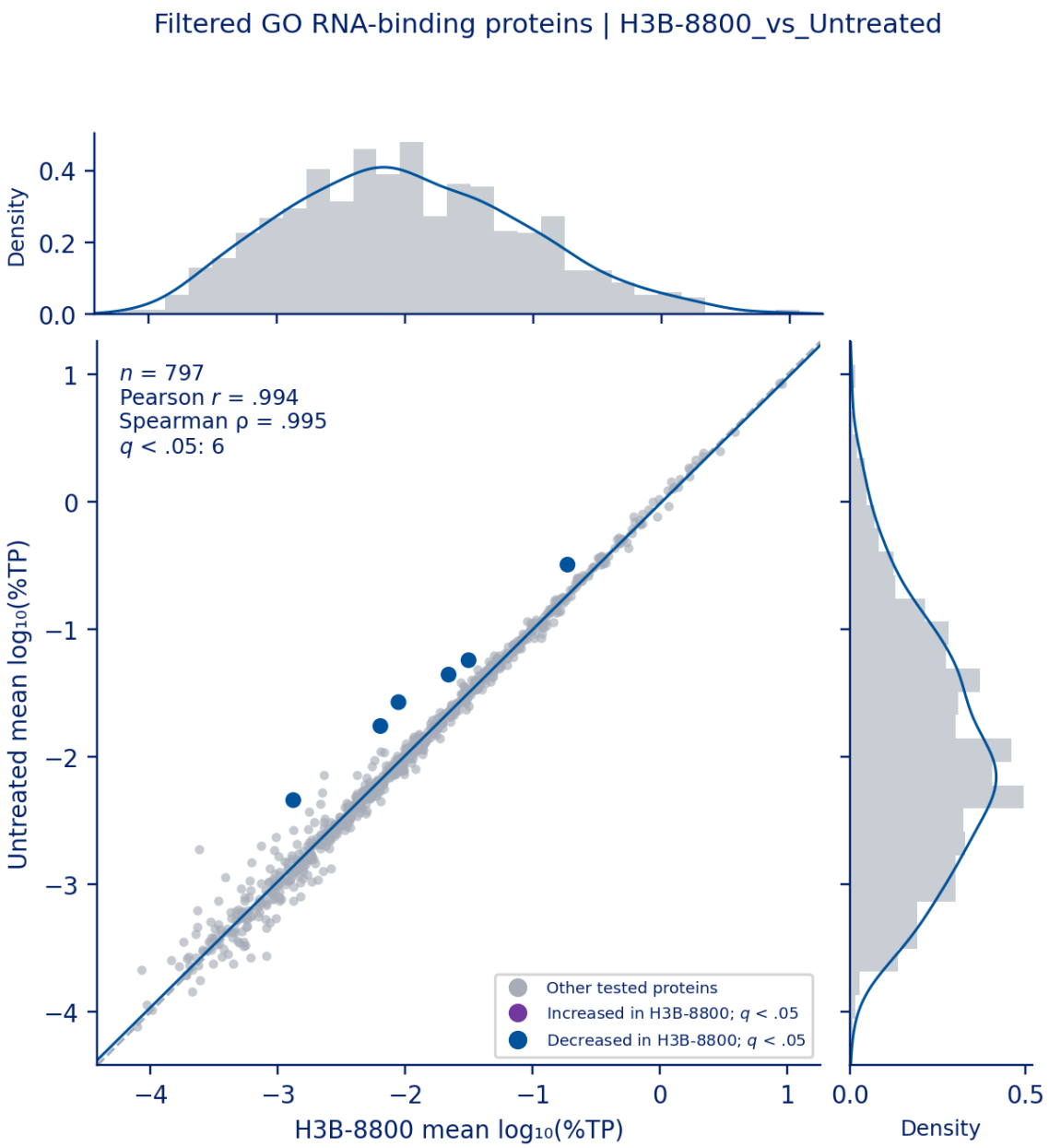


Figure 5. Comparison of observed protein abundances between H3B-8800 and Untreated. Scatterplot comparing group means of $\log_{10}$(%TP) for filtered GO RNA-binding proteins. Each point represents a protein tested for differential abundance. Corresponding histograms and probability density curves show the distributions for the horizontal-axis group (top) and vertical-axis group (right). Purple and blue identify proteins with significantly increased and decreased abundance, respectively, in H3B-8800 relative to Untreated after Benjamini–Hochberg correction ($q < .05$). Other tested proteins are shown in gray. The dashed line indicates equal abundance, and the solid blue line shows the linear regression fit.

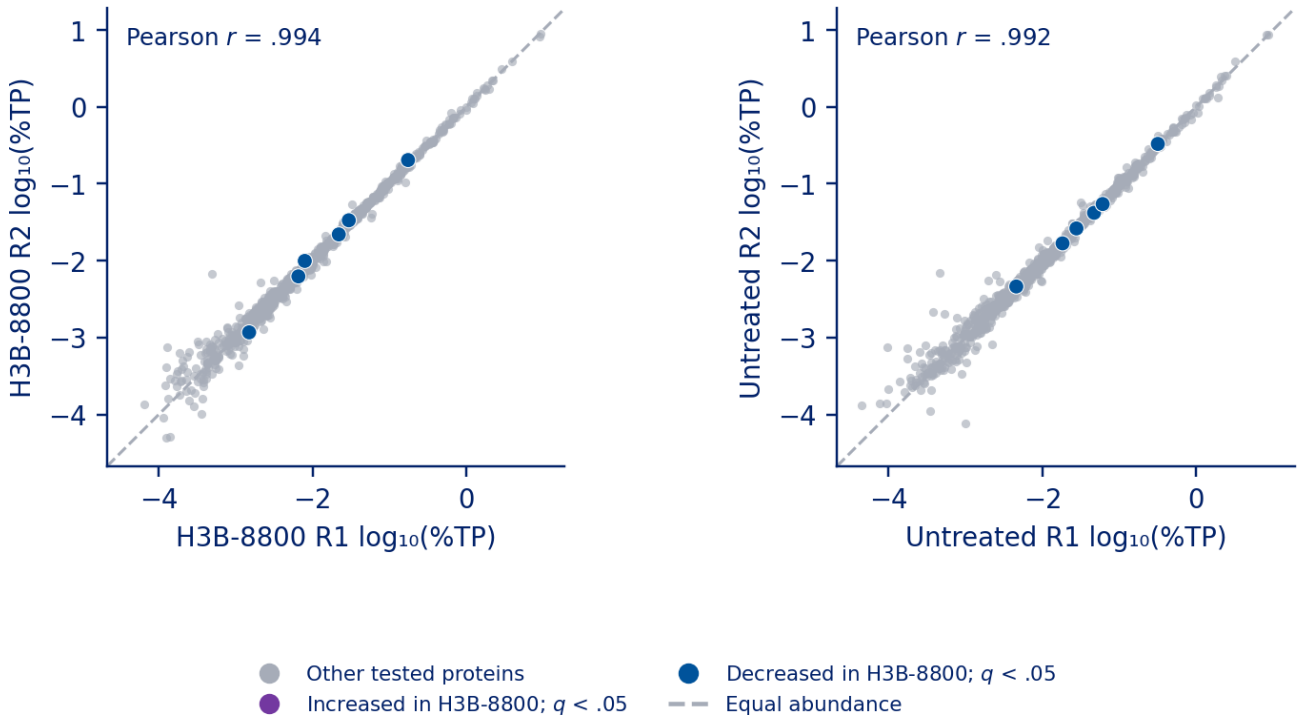


Figure 6. Within-group comparisons of biological replicates for H3B-8800 and Untreated. Each point represents a protein tested in the filtered GO RNA-binding proteins panel; axes show $\log_{10}$(%TP) in the analyzed RNP fractions for individual replicates. Pearson *r* summarizes all plotted proteins. The dashed line indicates equal abundance. Purple and blue identify proteins with significantly increased and decreased abundance, respectively, in H3B-8800 relative to Untreated (BH-adjusted $q < .05$). Other tested proteins are gray. The colors refer to the between-group comparison, not a within-group test.

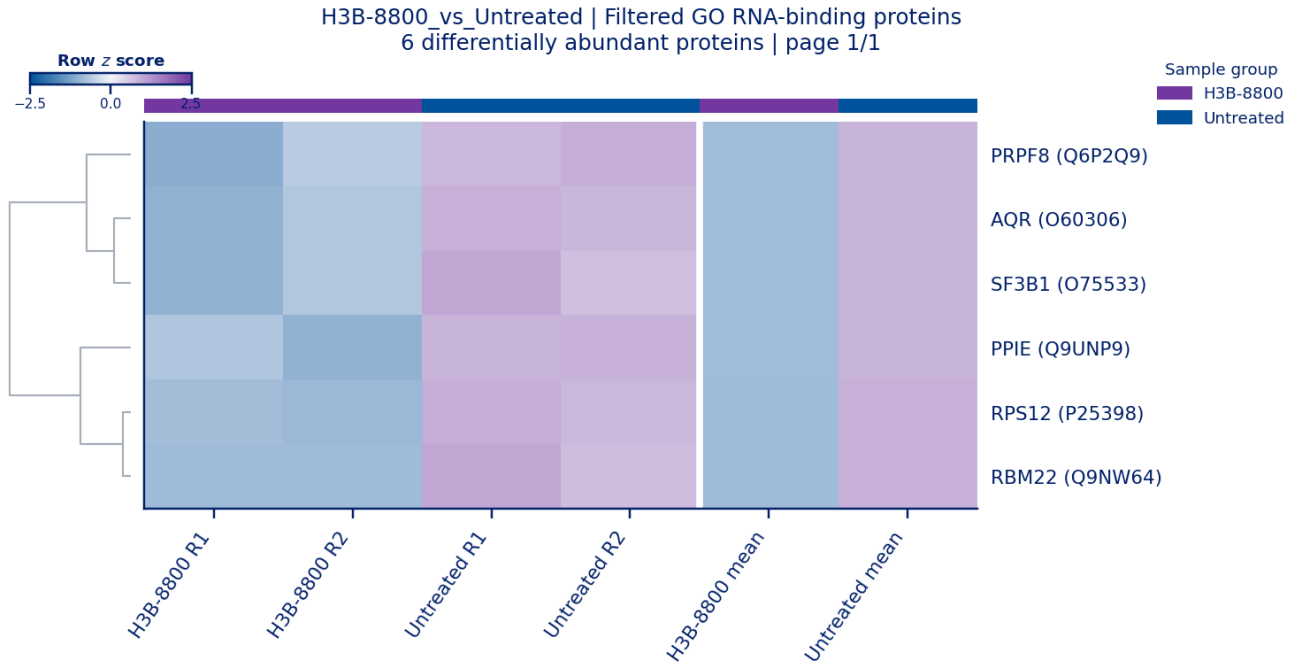


Figure 7. Protein abundance patterns of differentially abundant proteins. Heatmap showing $\log_2$(%TP) values in the analyzed RNP fractions, standardized within each protein across biological replicates (row *z* scores). Purple and blue indicate abundances above and below the mean for each protein, respectively; the color scale is limited to ±2.5. Rows were clustered using average linkage and correlation distance across replicate samples. The dendrogram branches show the hierarchical clustering of proteins by their abundance patterns; the merge positions reflect average correlation distances, not evidence of direct interactions. Sample columns retain their experimental order. The final columns show the group means of the row *z* scores and were excluded from clustering. All proteins meeting $q < .05$ are included.

Protein functions and features (Figure 7)

PRPF8 (Q6P2Q9). Plays a role in pre-mRNA splicing as core component of precatalytic, catalytic and postcatalytic spliceosomal complexes, both of the predominant U2-type spliceosome and the minor U12-type spliceosome. Annotated features: JAB1/Mov34/MPN/PAD-1 ubiquitin protease; PRO8NT (NUC069), PrP8 N-terminal domain.

AQR (O60306). Involved in pre-mRNA splicing as component of the spliceosome; GO annotations include 3'-5' RNA helicase activity; mRNA splicing, via spliceosome. Annotated features: AAA domain; Intron-binding protein aquarius insert domain.

SF3B1 (O75533). Component of the 17S U2 SnRNP complex of the spliceosome, a large ribonucleoprotein complex that removes introns from transcribed pre-mRNAs. Annotated features: Splicing factor 3B subunit 1; PPP2R1A-like HEAT repeat (repeat).

PPIE (Q9UNP9). Involved in pre-mRNA splicing as component of the spliceosome; GO annotations include poly(A) binding; mRNA splicing, via spliceosome. Annotated features: Cyclophilin type peptidyl-prolyl cis-trans isomerase/CLD; RNA recognition motif.

RPS12 (P25398). Part of the small subunit (SSU) processome, first precursor of the small eukaryotic ribosomal subunit. Annotated features: Ribosomal protein L7Ae/L30e/S12e/Gadd45 family.

RBM22 (Q9NW64). Required for pre-mRNA splicing as component of the activated spliceosome; GO annotations include U6 snRNA binding; positive regulation of protein import into nucleus. Annotated features: RBM22 CCCH zinc finger domain; RNA recognition motif.

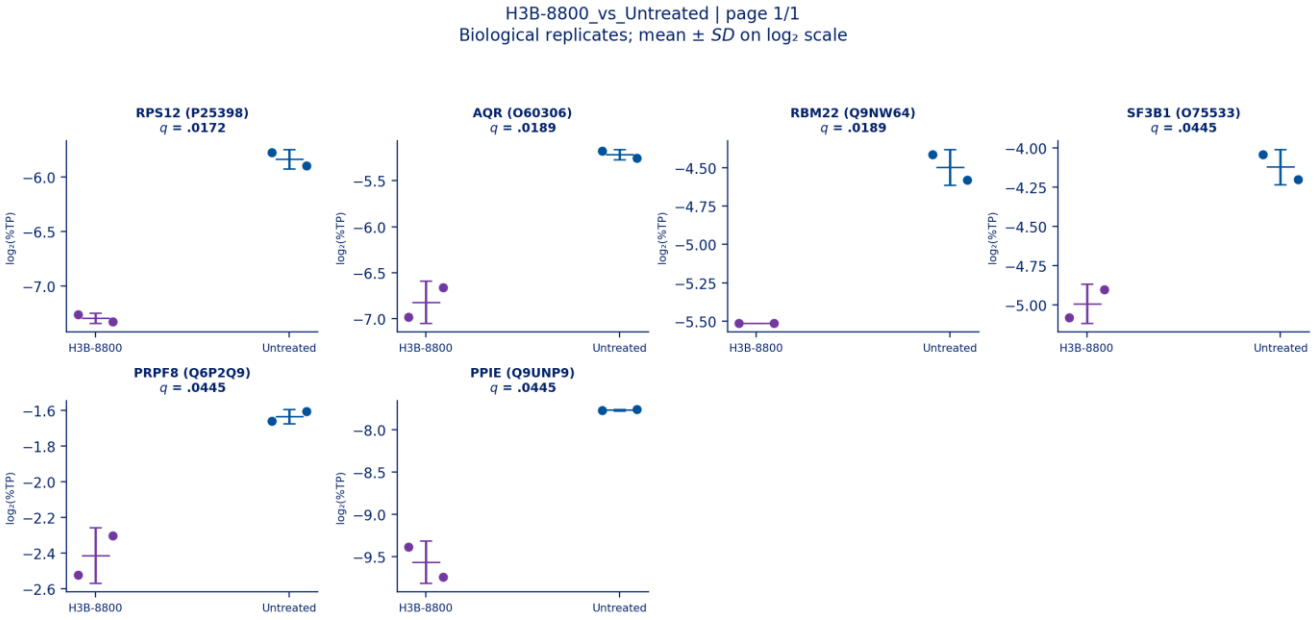


Figure 8. Replicate abundances of differentially abundant proteins between H3B-8800 and Untreated. Points show $\log_2$(%TP) for individual biological replicates (n = 2 per sample group); horizontal bars and whiskers show the group mean and standard deviation on this scale. Panels identify the protein by gene symbol and UniProt accession and report its q value. All significant proteins are shown across 1 pages (page 1 of 1).

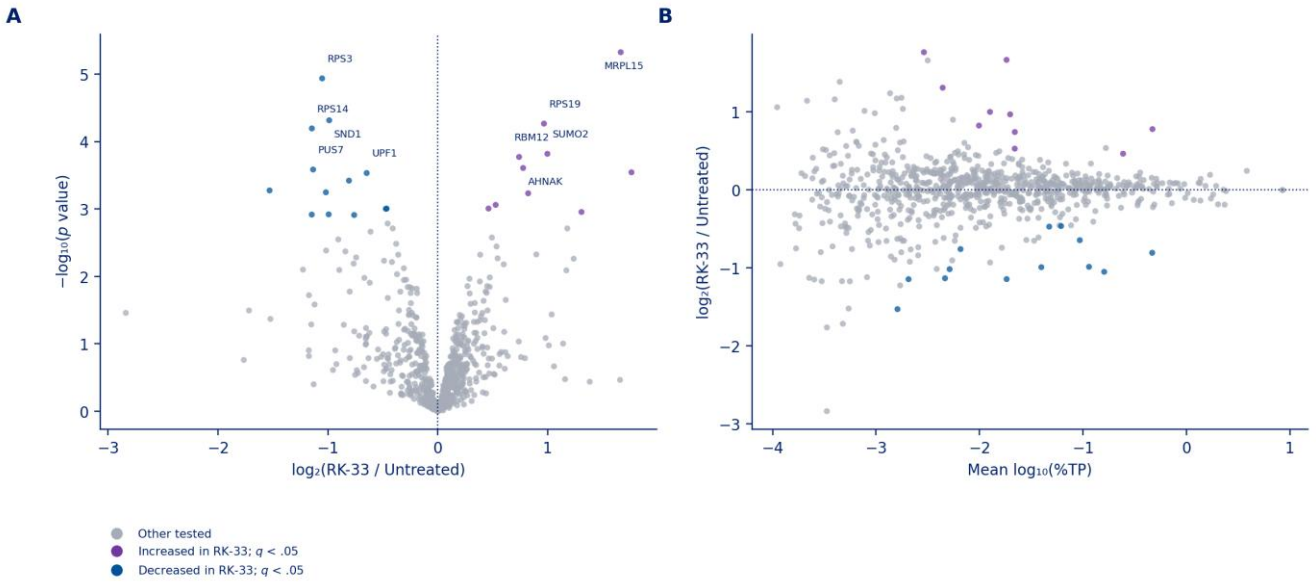


Figure 9. Differential analyses of filtered GO RNA-binding proteins between RK-33 and Untreated. 23 of 797 tested proteins met q < .05. **(A)** Volcano plot showing $-\log_{10}$-transformed p values before FDR correction as a function of $\log_2$(RK-33/Untreated). Point colors indicate differential abundance after Benjamini–Hochberg correction (q < .05) in both panels. **(B)** MA plot showing $\log_2$(RK-33/Untreated) as a function of mean $\log_{10}$(%TP) across all samples.

Of the 797 proteins tested, 23 (2.9%) differed significantly in abundance, including 10 with increased and 13 with decreased abundance in RK-33 relative to Untreated.

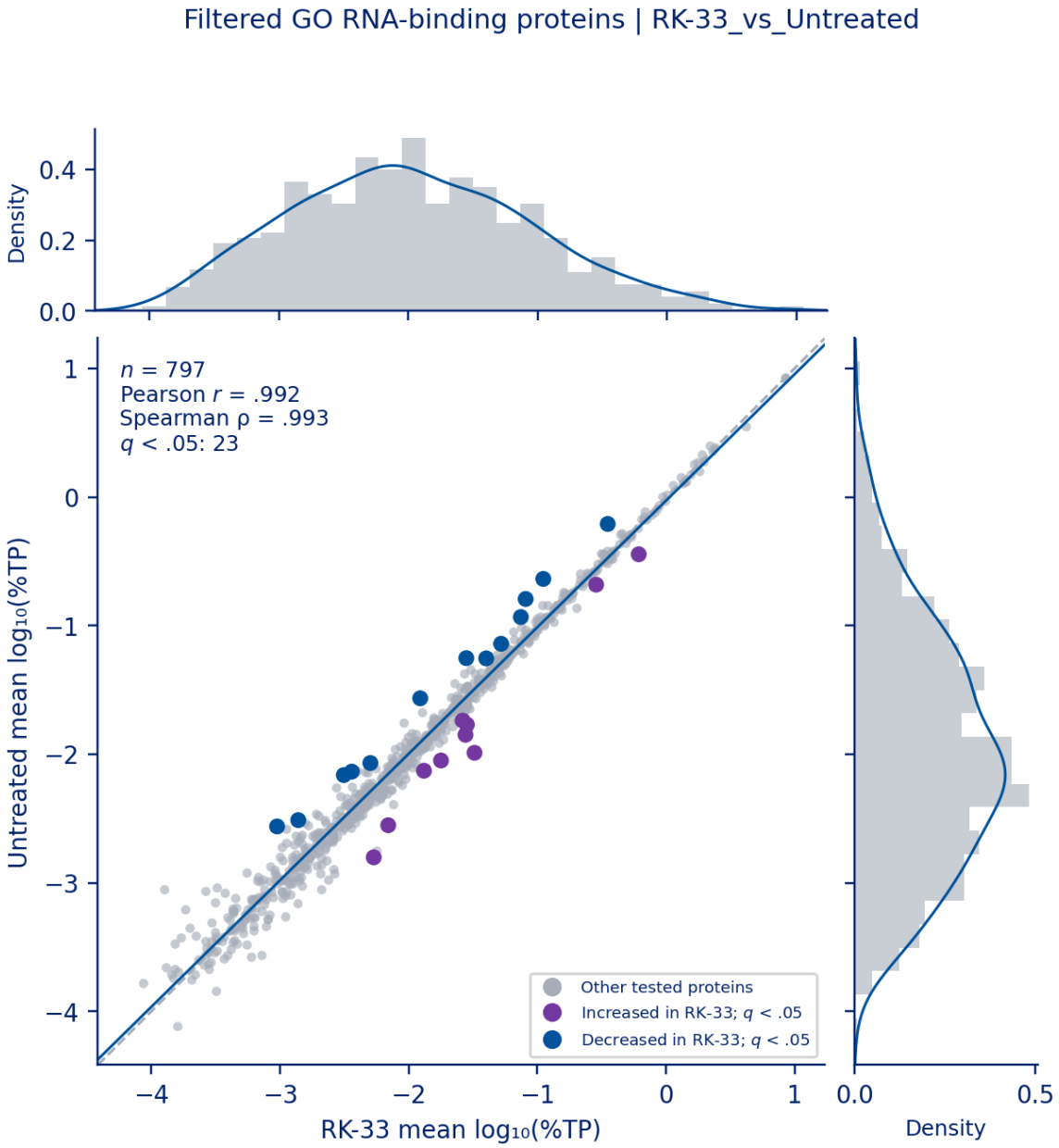


Figure 10. Comparison of observed protein abundances between RK-33 and Untreated. Scatterplot comparing group means of $\log_{10}$(%TP) for filtered GO RNA-binding proteins. Each point represents a protein tested for differential abundance. Corresponding histograms and probability density curves show the distributions for the horizontal-axis group (top) and vertical-axis group (right). Purple and blue identify proteins with significantly increased and decreased abundance, respectively, in RK-33 relative to Untreated after Benjamini–Hochberg correction ($q < .05$). Other tested proteins are shown in gray. The dashed line indicates equal abundance, and the solid blue line shows the linear regression fit.

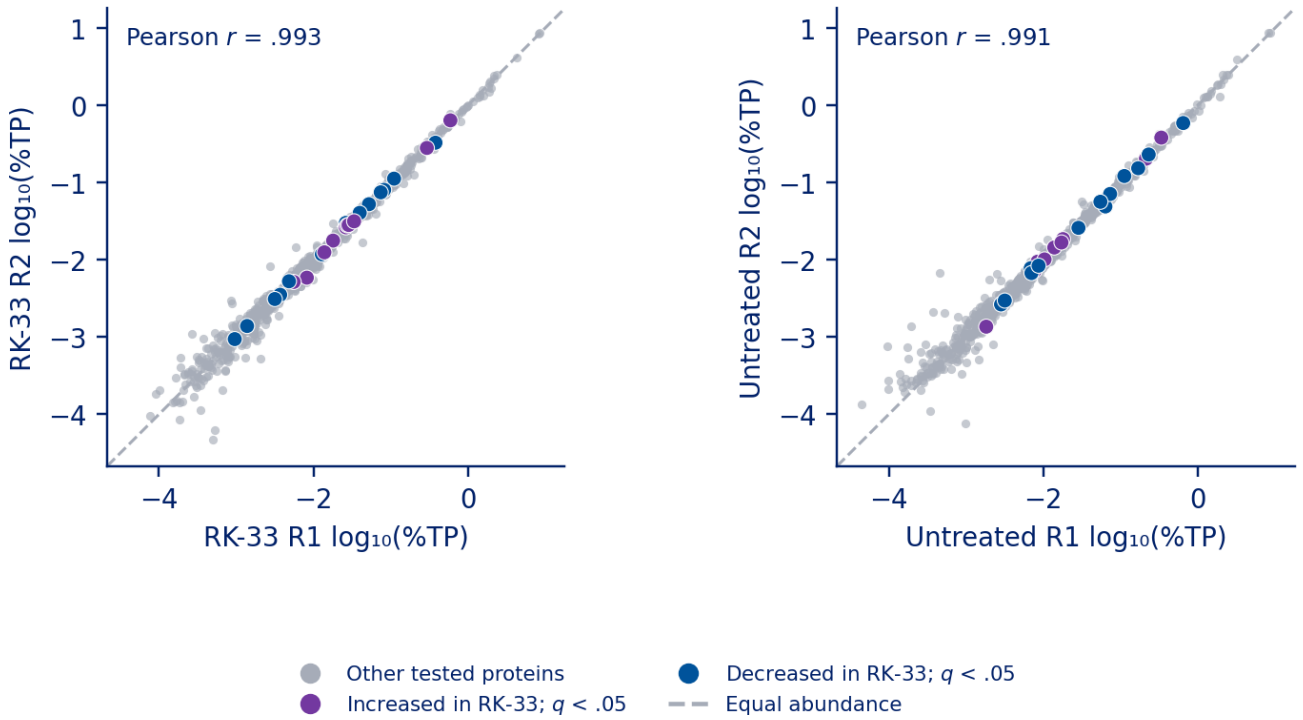


Figure 11. Within-group comparisons of biological replicates for RK-33 and Untreated. Each point represents a protein tested in the filtered GO RNA-binding proteins panel; axes show $\log_{10}$(%TP) in the analyzed RNP fractions for individual replicates. Pearson *r* summarizes all plotted proteins. The dashed line indicates equal abundance. Purple and blue identify proteins with significantly increased and decreased abundance, respectively, in RK-33 relative to Untreated (BH-adjusted $q < .05$). Other tested proteins are gray. The colors refer to the between-group comparison, not a within-group test.

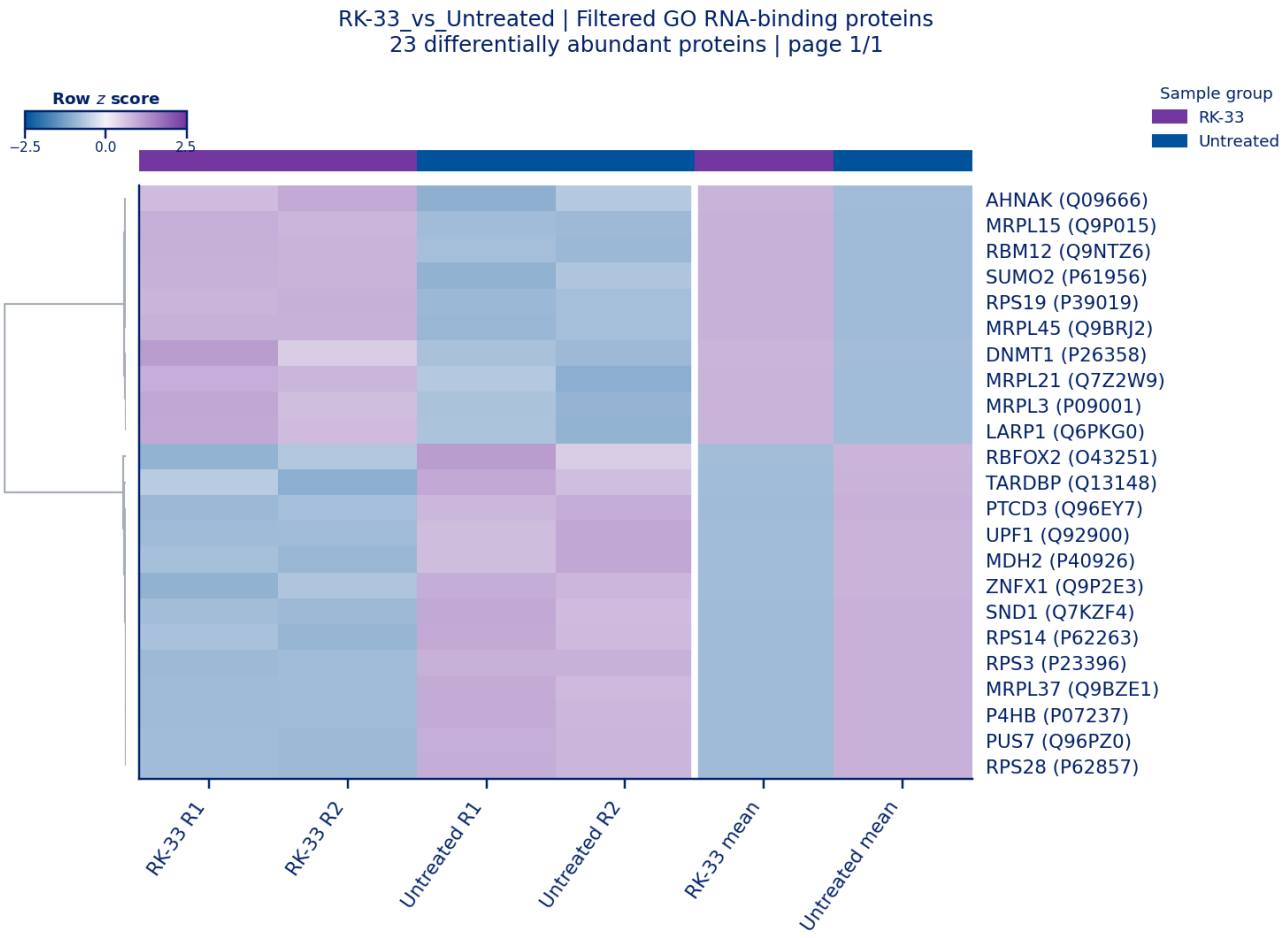


Figure 12. Protein abundance patterns of differentially abundant proteins. Heatmap showing $\log_2$(%TP) values in the analyzed RNP fractions, standardized within each protein across biological replicates (row *z* scores). Purple and blue indicate abundances above and below the mean for each protein, respectively; the color scale is limited to ±2.5. Rows were clustered using average linkage and correlation distance across replicate samples. The dendrogram branches show the hierarchical clustering of proteins by their abundance patterns; the merge positions reflect average correlation distances, not evidence of direct interactions. Sample columns retain their experimental order. The final columns show the group means of the row *z* scores and were excluded from clustering. All proteins meeting $q < .05$ are included.

Protein functions and features (Figure 12)

AHNAK (Q09666). May be required for neuronal cell differentiation; GO annotations include cadherin binding; positive regulation of plasma membrane repair. Annotated features: PDZ domain.

MRPL15 (Q9P015). GO annotations include structural constituent of ribosome; mitochondrial translation. Annotated features: Ribosomal proteins 50S-L15, 50S-L18e, 60S-L27A.

RBM12 (Q9NTZ6). RNA binding protein; GO annotations include nucleic acid binding; negative regulation of cAMP/PKA signal transduction. Annotated features: RNA recognition motif; RRM domain.

SUMO2 (P61956). Ubiquitin-like protein that can be covalently attached to proteins as a monomer or as a lysine-linked polymer. Annotated features: Rad60/SUMO-like domain; Ubiquitin-like domain.

RPS19 (P39019). Component of the small ribosomal subunit; GO annotations include fibroblast growth factor binding; antimicrobial humoral immune response mediated by antimicrobial peptide. Annotated features: Ribosomal protein S19e (family).

MRPL45 (Q9BRJ2). Component of the mitochondrial large ribosomal subunit (mt-LSU); GO annotations include mitochondrial translation. Annotated features: Tim44-like domain.

DNMT1 (P26358). DNA methyltransferase that methylates CpG residues; GO annotations include DNA (cytosine-5-)-methyltransferase activity; negative regulation of gene expression via chromosomal CpG island methylation. Annotated features: BAH domain; C-5 cytosine-specific DNA methylase.

MRPL21 (Q7Z2W9). GO annotations include structural constituent of ribosome; mitochondrial translation. Annotated features: Ribosomal prokaryotic L21 protein (family).

MRPL3 (P09001). GO annotations include structural constituent of ribosome; mitochondrial translation. Annotated features: Ribosomal protein L3 (family).

LARP1 (Q6PKG0). RNA-binding protein that regulates the translation of specific target mRNA species downstream of the mTORC1 complex, in function of growth signals and nutrient availability. Annotated features: La domain; LARP1 HEAT repeat region (repeat).

RBFOX2 (O43251). RNA-binding protein that regulates alternative splicing events by binding to 5'-UGCAUGU-3' elements. Annotated features: RNA recognition motif.

TARDBP (Q13148). RNA-binding protein that is involved in various steps of RNA biogenesis and processing. Annotated features: RNA recognition motif; TAR DNA-binding protein 43, N-terminal domain.

PTCD3 (Q96EY7). Mitochondrial RNA-binding protein that has a role in mitochondrial translation. ; GO annotations include ribosomal small subunit binding; mitochondrial translation. Annotated features: Pentatricopeptide repeat domain (repeat); Small ribosomal subunit protein mS39, PPR (repeat).

UPF1 (Q92900). RNA-dependent helicase required for nonsense-mediated decay (NMD) of aberrant mRNAs containing premature stop codons and which modulates the expression level of normal mRNAs. Annotated features: AAA domain; RNA helicase (UPF2 interacting domain).

MDH2 (P40926). Mitochondrial malate dehydrogenase that catalyzes the reversible conversion of malate to oxaloacetate using NAD(+) as a cofactor. Annotated features: lactate/malate dehydrogenase, NAD binding domain; lactate/malate dehydrogenase, alpha/beta C-terminal domain.

ZNFX1 (Q9P2E3). RNA-activated non-canonical E3 ubiquitin ligase required for cell survival during interferon (IFN) responses. Annotated features: AAA domain; RZ type zinc finger domain.

SND1 (Q7KZF4). Endonuclease that mediates miRNA decay of both protein-free and AGO2-loaded miRNAs; GO annotations include 3' overhang single-stranded DNA endonuclease activity; mRNA catabolic process. Annotated features: Staphylococcal nuclease homologue; Tudor domain.

RPS14 (P62263). Component of the small ribosomal subunit; GO annotations include mRNA 5'-UTR binding; negative regulation of transcription by RNA polymerase II. Annotated features: Ribosomal protein S11 (family).

RPS3 (P23396). Component of the small ribosomal subunit; GO annotations include class I DNA-(apurinic or apyrimidinic site) endonuclease activity; positive regulation of intrinsic apoptotic signaling pathway in response to DNA damage. Annotated features: KH domain; Ribosomal protein S3, C-terminal domain.

MRPL37 (Q9BZE1). GO annotations include structural constituent of ribosome; mitochondrial translation. Annotated features: Mitochondrial 28S ribosomal protein S30 (PDCD9) (family).

P4HB (P07237). This multifunctional protein catalyzes the formation, breakage and rearrangement of disulfide bonds. Annotated features: Thioredoxin; Thioredoxin-like domain.

PUS7 (Q96PZ0). Pseudouridylate synthase that catalyzes pseudouridylation of RNAs; GO annotations include tRNA pseudouridine(13) synthase activity; negative regulation of translation. Annotated features: Pseudouridine synthase, TruD, insertion domain.

RPS28 (P62857). Component of the small ribosomal subunit; GO annotations include structural constituent of ribosome; cytoplasmic translation. Annotated features: Ribosomal protein S28e.

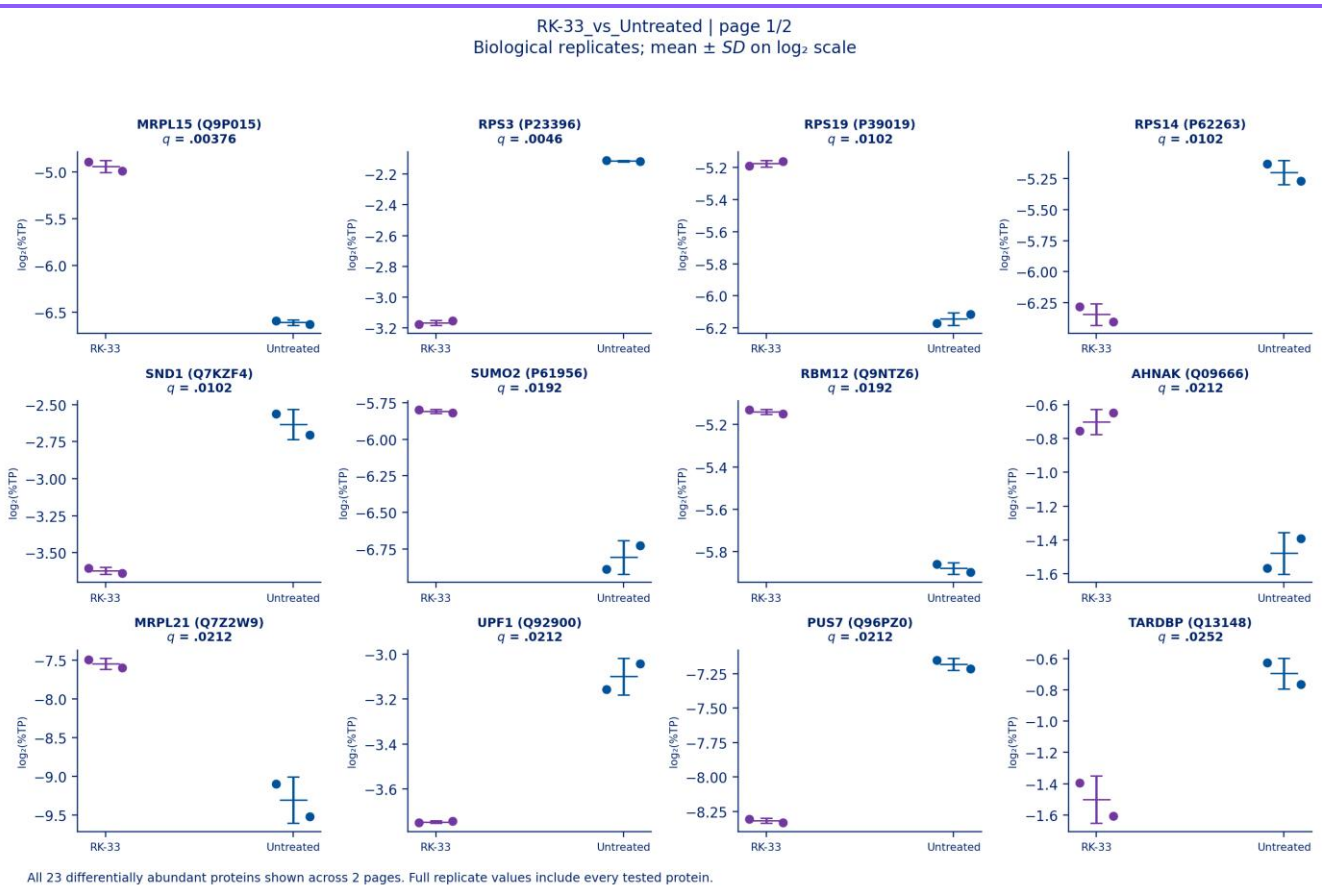


Figure 13. Replicate abundances of differentially abundant proteins between RK-33 and Untreated. Points show $\log_2$(%TP) for individual biological replicates (n = 2 per sample group); horizontal bars and whiskers show the group mean and standard deviation on this scale. Panels identify the protein by gene symbol and UniProt accession and report its q value. All significant proteins are shown across 2 pages (page 1 of 2).

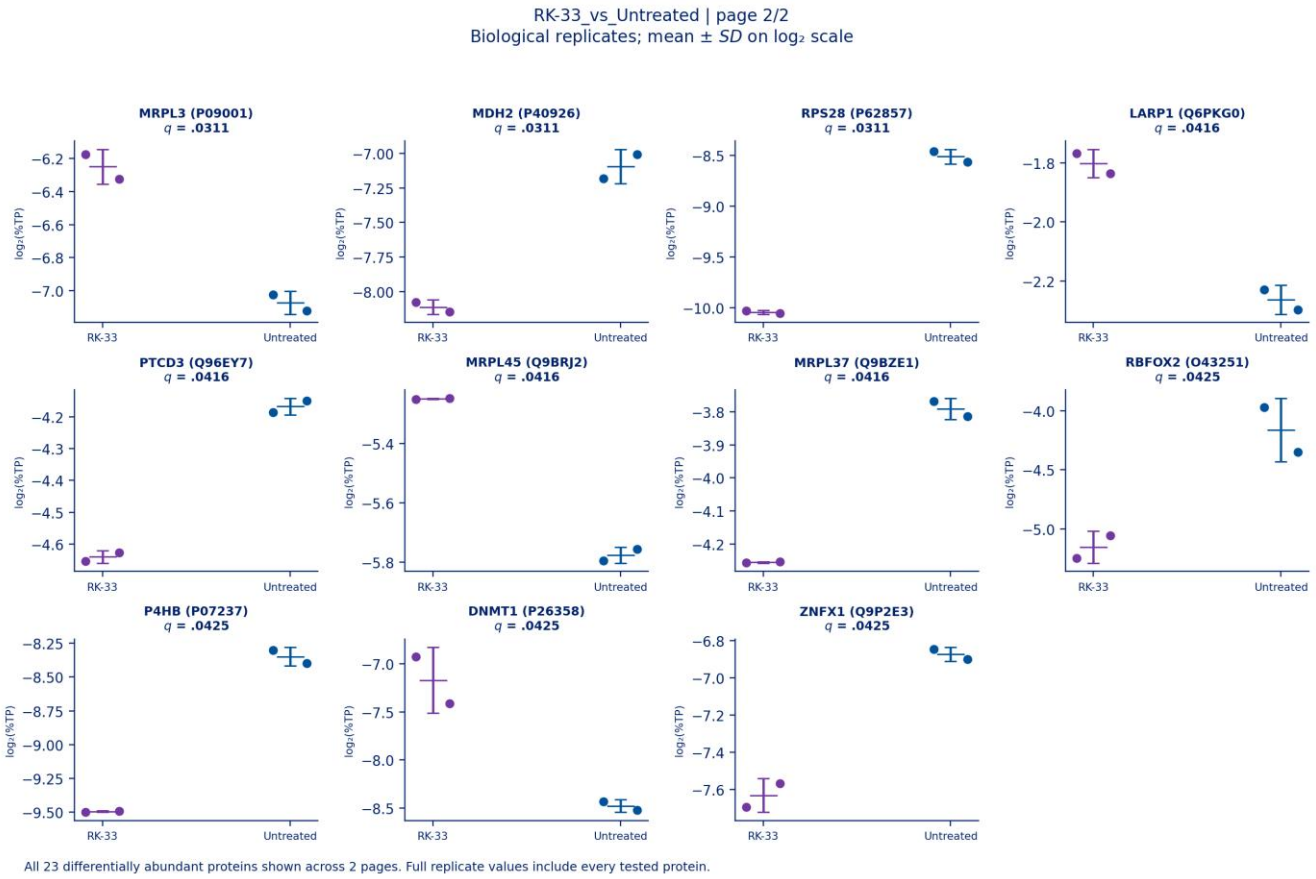


Figure 14. Replicate abundances of differentially abundant proteins between RK-33 and Untreated. Points show $\log_2$(%TP) for individual biological replicates (n = 2 per sample group); horizontal bars and whiskers show the group mean and standard deviation on this scale. Panels identify the protein by gene symbol and UniProt accession and report its q value. All significant proteins are shown across 2 pages (page 2 of 2).

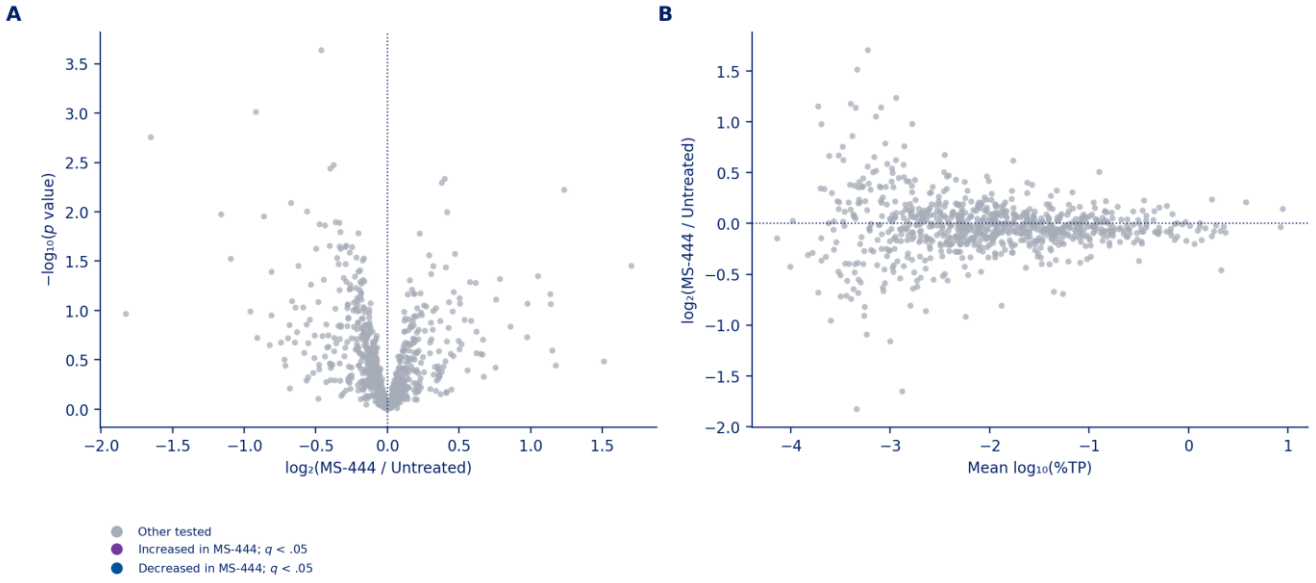


Figure 15. Differential analyses of filtered GO RNA-binding proteins between MS-444 and Untreated. 0 of 804 tested proteins met q < .05. **(A)** Volcano plot showing $-\log_{10}$-transformed p values before FDR correction as a function of $\log_2$(MS-444/Untreated). Point colors indicate differential abundance after Benjamini–Hochberg correction (q < .05) in both panels. **(B)** MA plot showing $\log_2$(MS-444/Untreated) as a function of mean $\log_{10}$(%TP) across all samples.

Of the 804 proteins tested, 0 (0.0%) differed significantly in abundance, including 0 with increased and 0 with decreased abundance in MS-444 relative to Untreated.

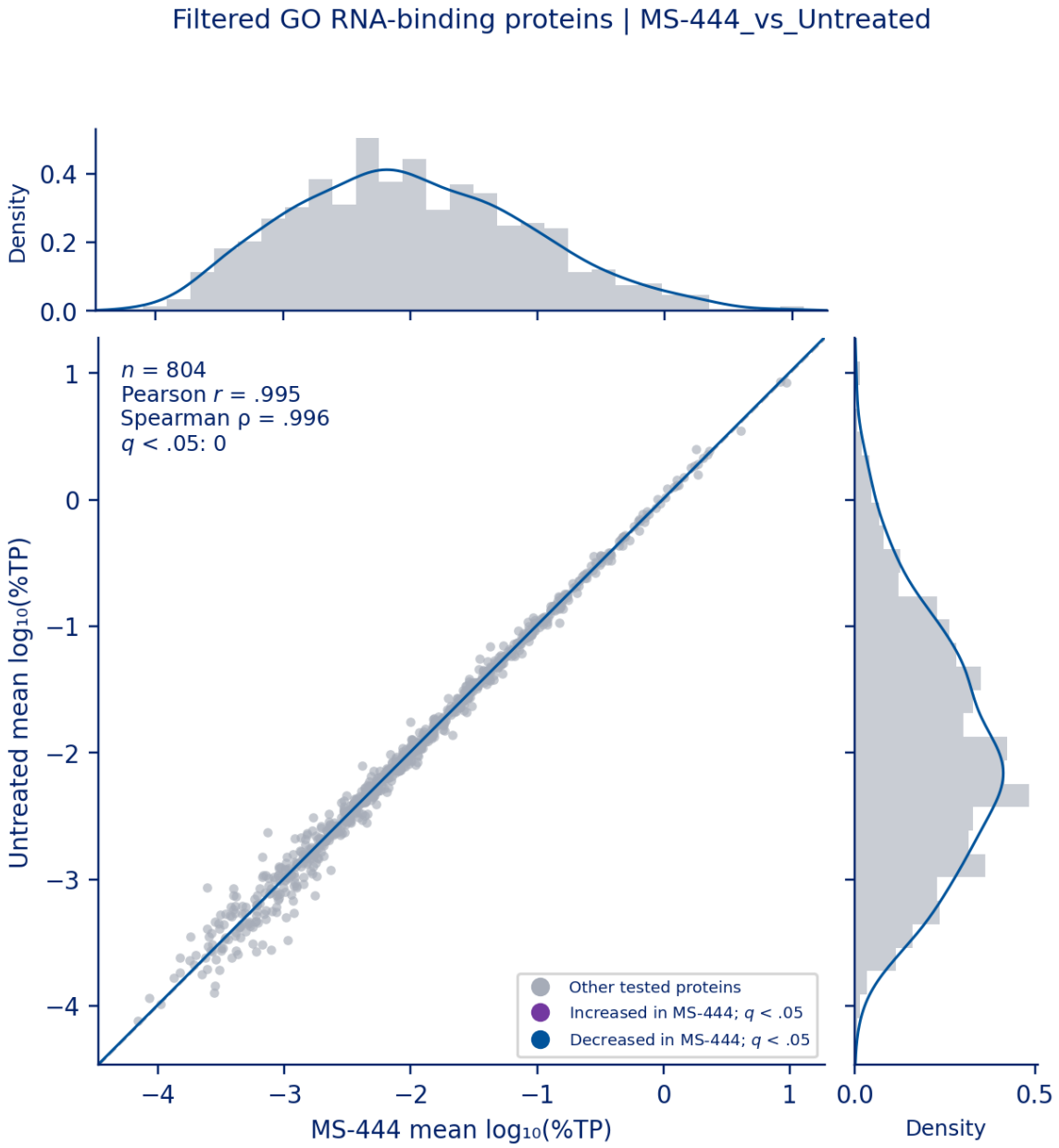


Figure 16. Comparison of observed protein abundances between MS-444 and Untreated. Scatterplot comparing group means of $\log_{10}$(%TP) for filtered GO RNA-binding proteins. Each point represents a protein tested for differential abundance. Corresponding histograms and probability density curves show the distributions for the horizontal-axis group (top) and vertical-axis group (right). Purple and blue identify proteins with significantly increased and decreased abundance, respectively, in MS-444 relative to Untreated after Benjamini–Hochberg correction ($q < .05$). Other tested proteins are shown in gray. The dashed line indicates equal abundance, and the solid blue line shows the linear regression fit.

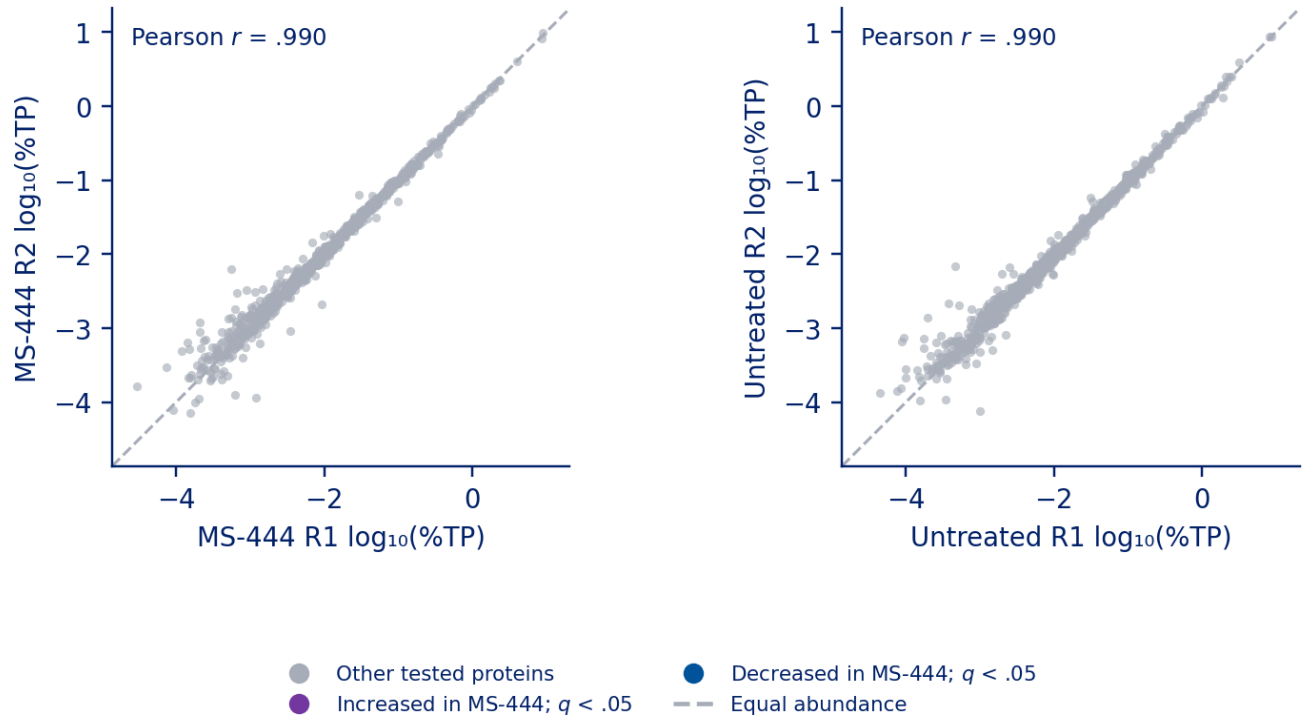


Figure 17. Within-group comparisons of biological replicates for MS-444 and Untreated. Each point represents a protein tested in the filtered GO RNA-binding proteins panel; axes show $\log_{10}$(%TP) in the analyzed RNP fractions for individual replicates. Pearson *r* summarizes all plotted proteins. The dashed line indicates equal abundance. Purple and blue identify proteins with significantly increased and decreased abundance, respectively, in MS-444 relative to Untreated (BH-adjusted $q < .05$). Other tested proteins are gray. The colors refer to the between-group comparison, not a within-group test.

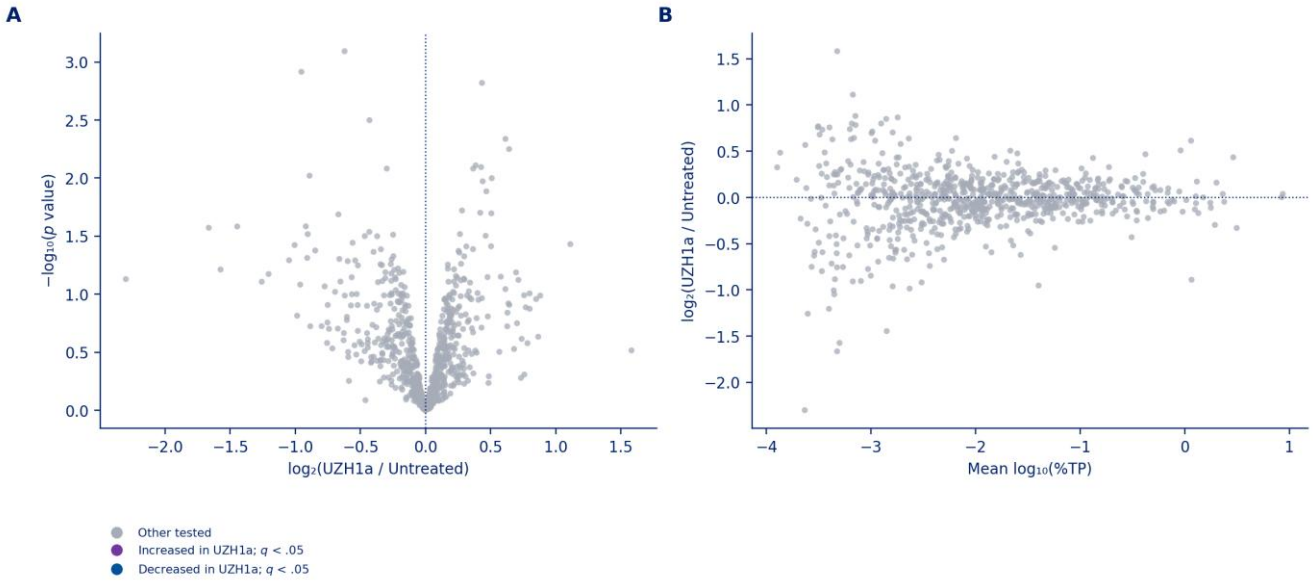


Figure 18. Differential analyses of filtered GO RNA-binding proteins between UZH1a and Untreated. 0 of 782 tested proteins met $q < .05$. **(A)** Volcano plot showing $-\log_{10}$-transformed *p* values before FDR correction as a function of $\log_2$(UZH1a/Untreated). Point colors indicate differential abundance after Benjamini–Hochberg correction ($q < .05$) in both panels. **(B)** MA plot showing $\log_2$(UZH1a/Untreated) as a function of mean $\log_{10}$(%TP) across all samples.

Of the 782 proteins tested, 0 (0.0%) differed significantly in abundance, including 0 with increased and 0 with decreased abundance in UZH1a relative to Untreated.

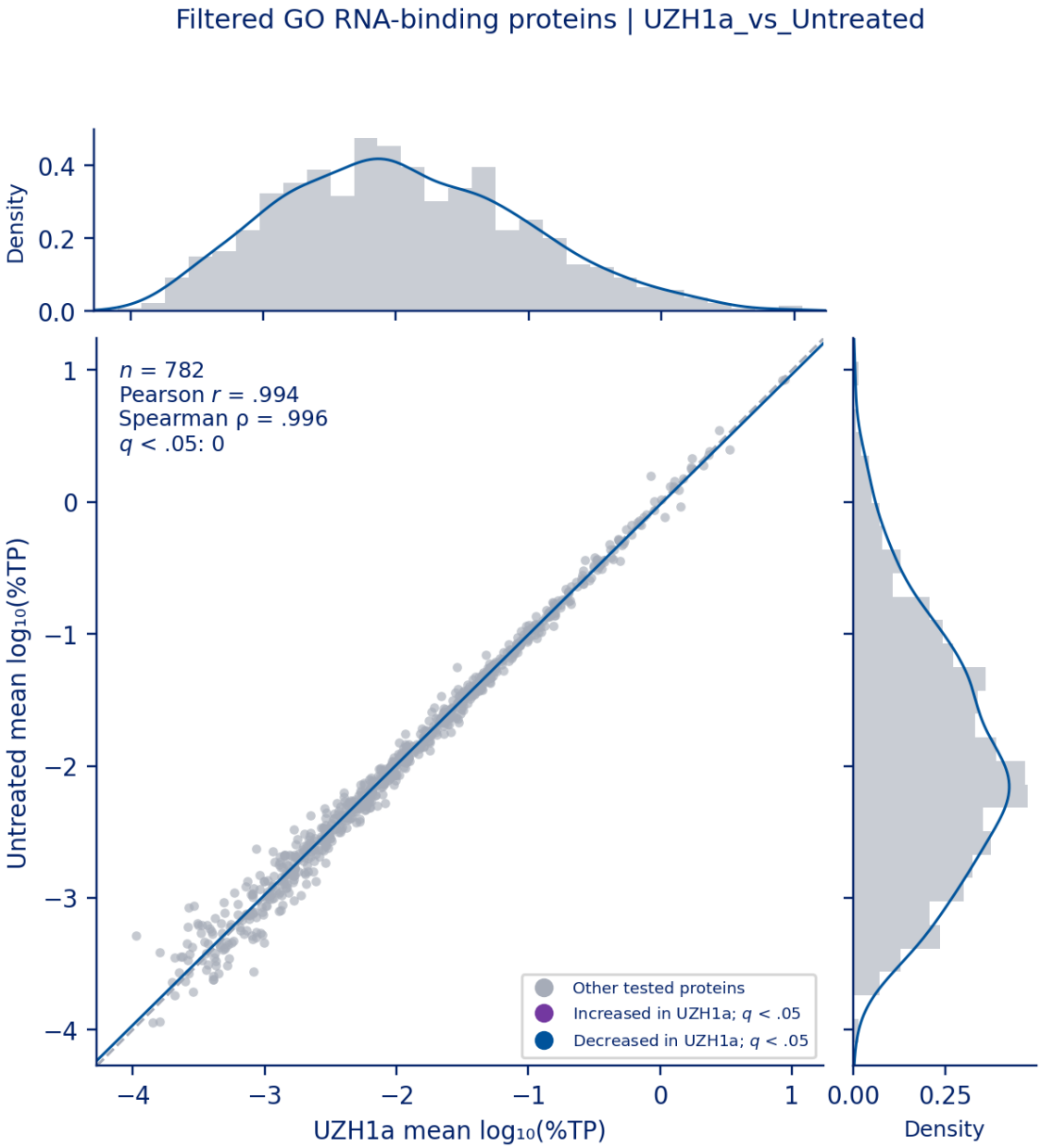


Figure 19. Comparison of observed protein abundances between UZH1a and Untreated. Scatterplot comparing group means of $\log_{10}$(%TP) for filtered GO RNA-binding proteins. Each point represents a protein tested for differential abundance. Corresponding histograms and probability density curves show the distributions for the horizontal-axis group (top) and vertical-axis group (right). Purple and blue identify proteins with significantly increased and decreased abundance, respectively, in UZH1a relative to Untreated after Benjamini–Hochberg correction ($q < .05$). Other tested proteins are shown in gray. The dashed line indicates equal abundance, and the solid blue line shows the linear regression fit.

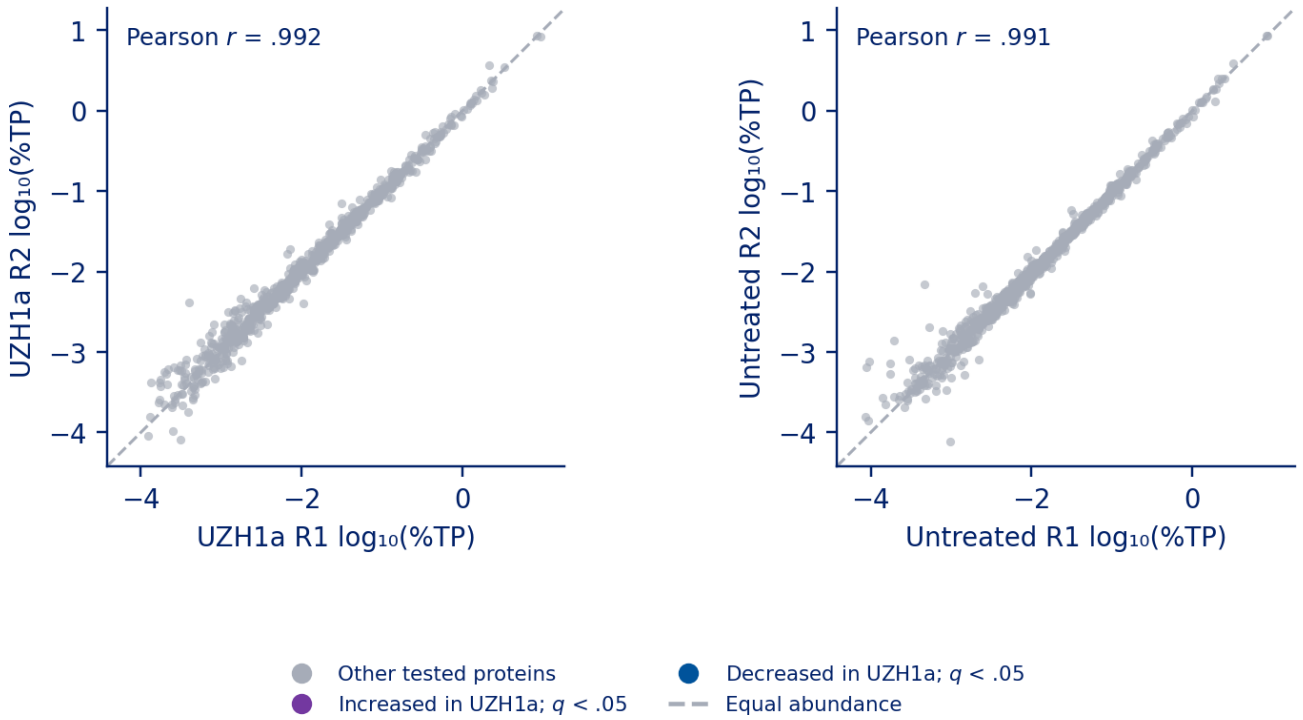


Figure 20. Within-group comparisons of biological replicates for UZH1a and Untreated. Each point represents a protein tested in the filtered GO RNA-binding proteins panel; axes show $\log_{10}$(%TP) in the analyzed RNP fractions for individual replicates. Pearson *r* summarizes all plotted proteins. The dashed line indicates equal abundance. Purple and blue identify proteins with significantly increased and decreased abundance, respectively, in UZH1a relative to Untreated (BH-adjusted $q < .05$). Other tested proteins are gray. The colors refer to the between-group comparison, not a within-group test.

9. Functional Annotations

Functional categories were curated in-house using UniProtKB Gene Ontology annotations and keywords. Proteins could be assigned to more than one category. The classification approach is described in Methods_and_Data_Analysis.docx; category assignments and supporting database annotations are provided in the 06_Functional_Annotations folders.

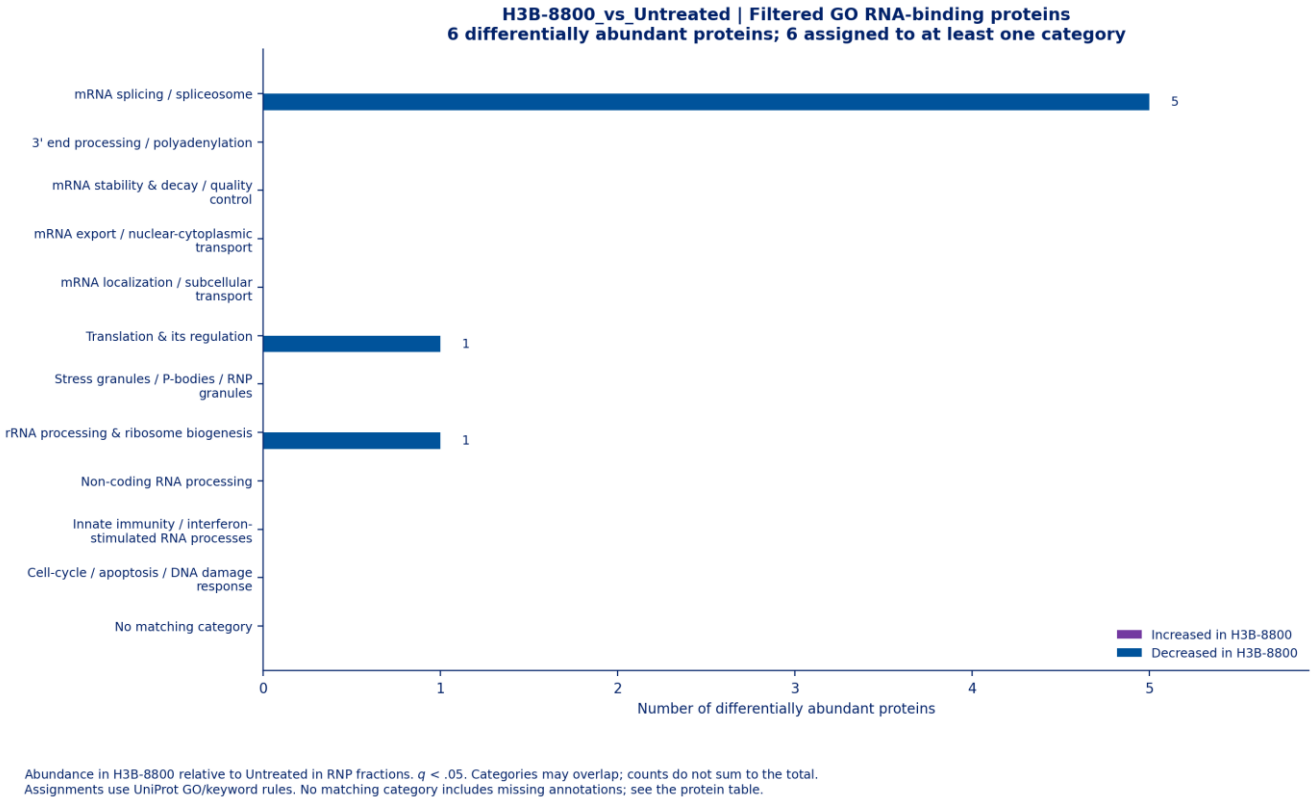


Figure 21. Annotated functions of differentially abundant proteins. Bar chart showing the numbers of differentially abundant filtered GO RNA-binding proteins assigned automatically to categories defined in-house using UniProtKB Gene Ontology annotations and keywords. Purple and blue bars indicate proteins with increased and decreased abundance in H3B-8800 relative to Untreated, respectively ($q < .05$). Categories overlap, and individual proteins may contribute to multiple categories. Proteins that did not match the predefined categories are shown under “No matching category.” Counts are descriptive and do not represent functional-enrichment tests.

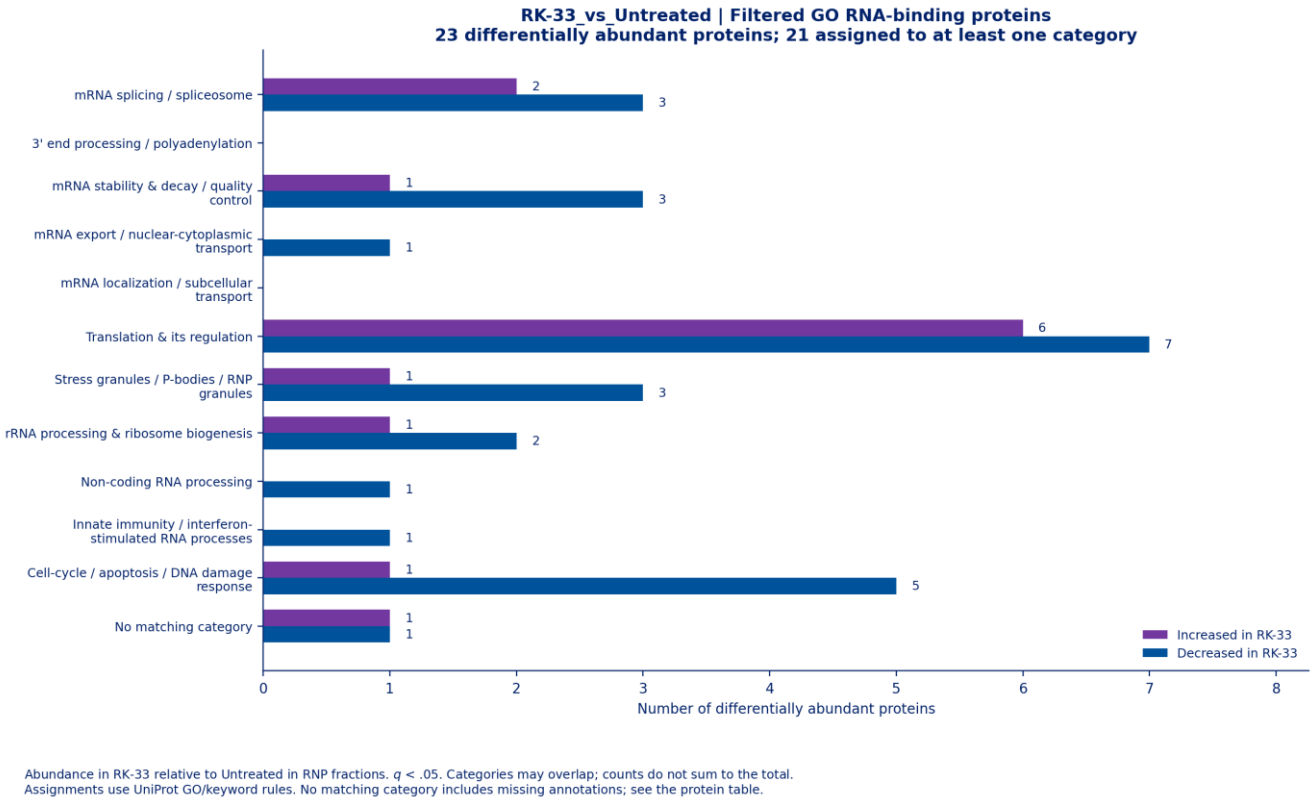


Figure 22. Annotated functions of differentially abundant proteins. Bar chart showing the numbers of differentially abundant filtered GO RNA-binding proteins assigned automatically to categories defined in-house using UniProtKB Gene Ontology annotations and keywords. Purple and blue bars indicate proteins with increased and decreased abundance in RK-33 relative to Untreated, respectively ($q < .05$). Categories overlap, and individual proteins may contribute to multiple categories. Proteins that did not match the predefined categories are shown under “No matching category.” Counts are descriptive and do not represent functional-enrichment tests.

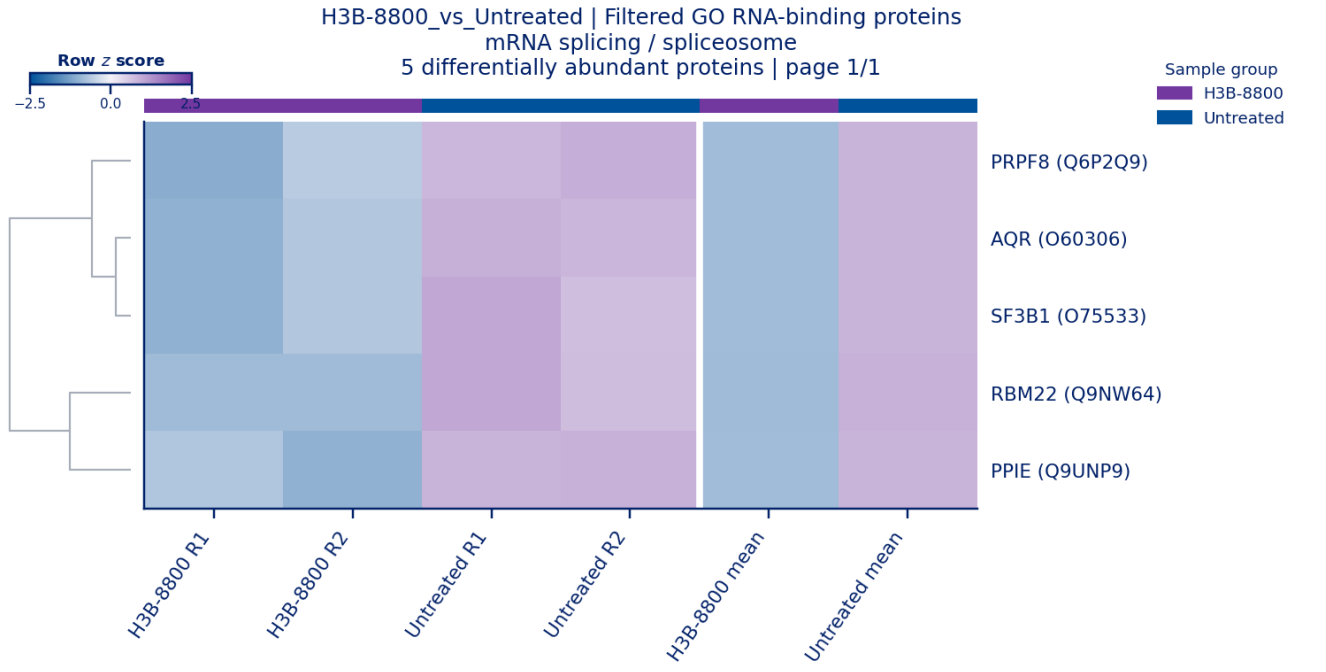


Figure 23. Protein abundance patterns within the mRNA splicing / spliceosome category. Heatmap showing $\log_2$(%TP) values in the analyzed RNP fractions, standardized within each protein across biological replicates (row *z* scores). Category membership was assigned automatically using in-house classification rules applied to positive UniProtKB Gene Ontology annotations and keywords relating to RNA splicing, the spliceosome, or U1, U2, U4, U5, or U6 snRNPs. Purple and blue indicate abundances above and below the mean for each protein, respectively; the color scale is limited to ±2.5. Rows were clustered using average linkage and correlation distance across replicate samples. The dendrogram branches show the hierarchical clustering of proteins by their abundance patterns; the merge positions reflect average correlation distances, not evidence of direct interactions. Sample columns retain their experimental order. The final columns show the group means of the row *z* scores and were excluded from clustering. Proteins may appear in more than one category.

Protein functions and features (Figure 23)

PRPF8 (Q6P2Q9). Plays a role in pre-mRNA splicing as core component of precatalytic, catalytic and postcatalytic spliceosomal complexes, both of the predominant U2-type spliceosome and the minor U12-type spliceosome. Annotated features: JAB1/Mov34/MPN/PAD-1 ubiquitin protease; PRO8NT (NUC069), PrP8 N-terminal domain.

AQR (O60306). Involved in pre-mRNA splicing as component of the spliceosome; GO annotations include 3'-5' RNA helicase activity; mRNA splicing, via spliceosome. Annotated features: AAA domain; Intron-binding protein aquarius insert domain.

SF3B1 (O75533). Component of the 17S U2 SnRNP complex of the spliceosome, a large ribonucleoprotein complex that removes introns from transcribed pre-mRNAs. Annotated features: Splicing factor 3B subunit 1; PPP2R1A-like HEAT repeat (repeat).

RBM22 (Q9NW64). Required for pre-mRNA splicing as component of the activated spliceosome; GO annotations include U6 snRNA binding; positive regulation of protein import into nucleus. Annotated features: RBM22 CCCH zinc finger domain; RNA recognition motif.

PPIE (Q9UNP9). Involved in pre-mRNA splicing as component of the spliceosome; GO annotations include poly(A) binding; mRNA splicing, via spliceosome. Annotated features: Cyclophilin type peptidyl-prolyl cis-trans isomerase/CLD; RNA recognition motif.

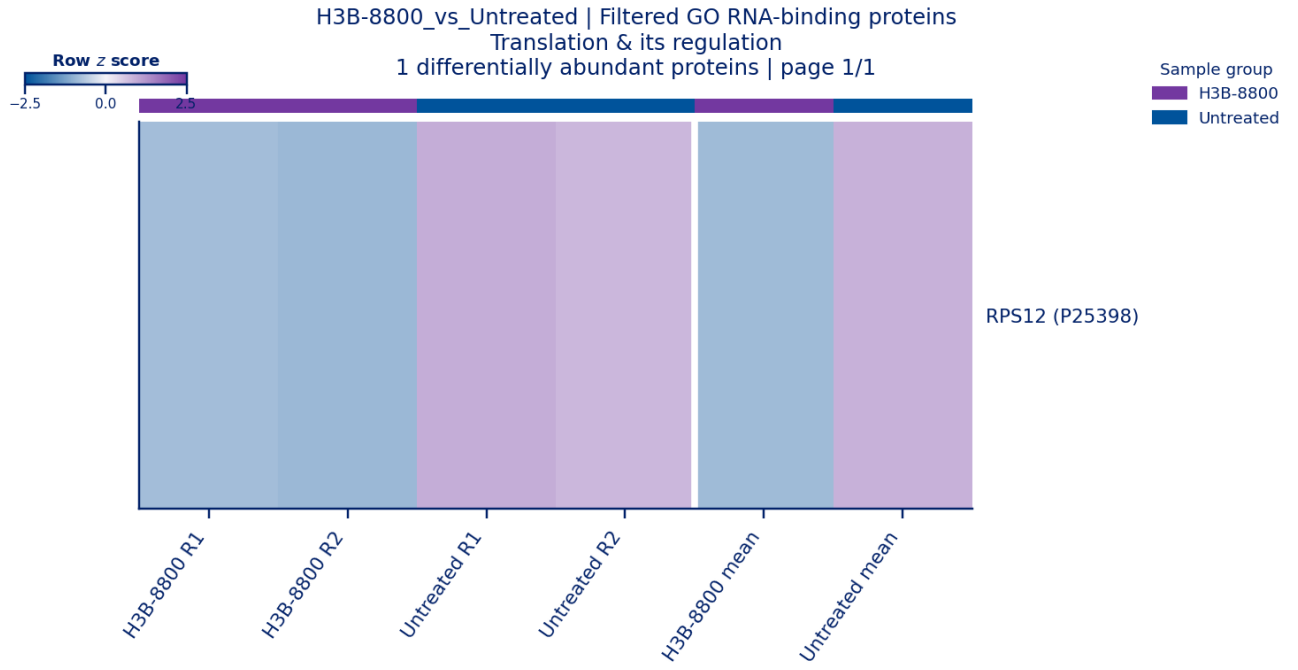


Figure 24. Protein abundance patterns within the Translation & its regulation category. Heatmap showing $\log_2$(%TP) values in the analyzed RNP fractions, standardized within each protein across biological replicates (row *z* scores). Category membership was assigned automatically using in-house classification rules applied to positive UniProtKB Gene Ontology annotations and keywords relating to translation or its regulation, ribosomal proteins, or structural constituents of the ribosome. Purple and blue indicate abundances above and below the mean for each protein, respectively; the color scale is limited to ±2.5. Rows were clustered using average linkage and correlation distance across replicate samples. The dendrogram branches show the hierarchical clustering of proteins by their abundance patterns; the merge positions reflect average correlation distances, not evidence of direct interactions. Sample columns retain their experimental order. The final columns show the group means of the row *z* scores and were excluded from clustering. Proteins may appear in more than one category.

Protein functions and features (Figure 24)

RPS12 (P25398). Part of the small subunit (SSU) processome, first precursor of the small eukaryotic ribosomal subunit. Annotated features: Ribosomal protein L7Ae/L30e/S12e/Gadd45 family.

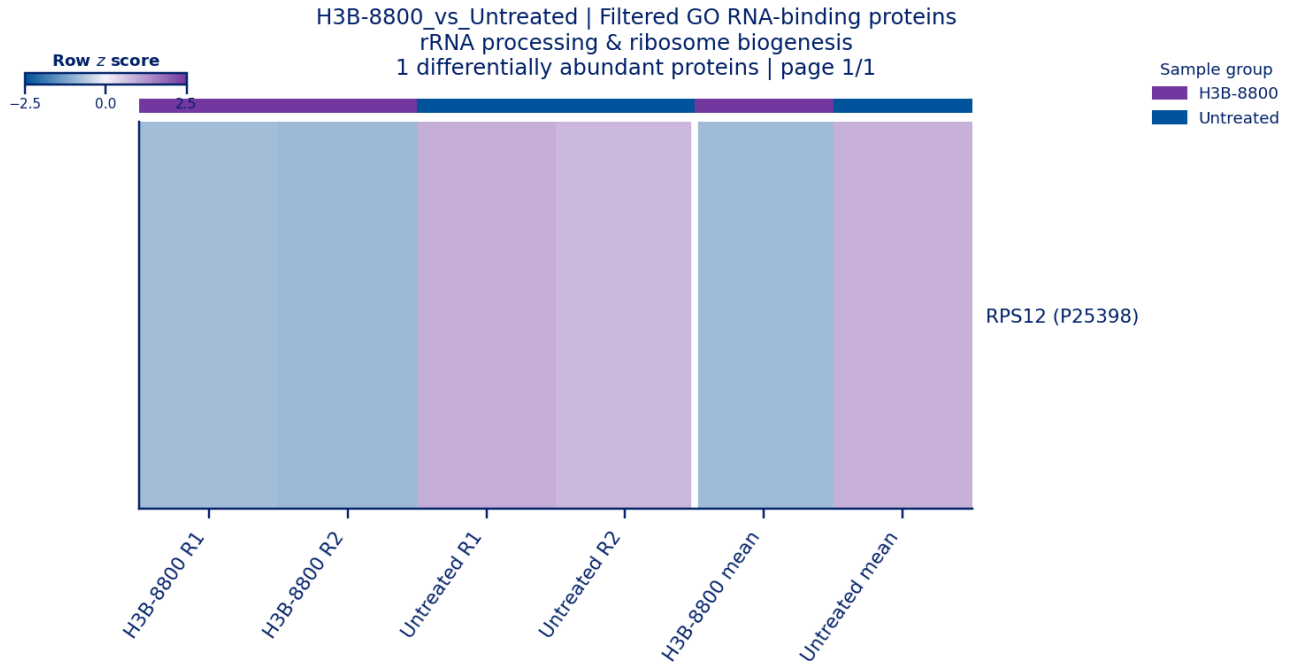


Figure 25. Protein abundance patterns within the rRNA processing & ribosome biogenesis category. Heatmap showing $\log_2$(%TP) values in the analyzed RNP fractions, standardized within each protein across biological replicates (row *z* scores). Category membership was assigned automatically using in-house classification rules applied to positive UniProtKB Gene Ontology annotations and keywords relating to rRNA processing, maturation, or modification, ribosome or ribosomal-subunit biogenesis or assembly, or the small-subunit processome. Purple and blue indicate abundances above and below the mean for each protein, respectively; the color scale is limited to ±2.5. Rows were clustered using average linkage and correlation distance across replicate samples. The dendrogram branches show the hierarchical clustering of proteins by their abundance patterns; the merge positions reflect average correlation distances, not evidence of direct interactions. Sample columns retain their experimental order. The final columns show the group means of the row *z* scores and were excluded from clustering. Proteins may appear in more than one category.

Protein functions and features (Figure 25)

RPS12 (P25398). Part of the small subunit (SSU) processome, first precursor of the small eukaryotic ribosomal subunit. Annotated features: Ribosomal protein L7Ae/L30e/S12e/Gadd45 family.

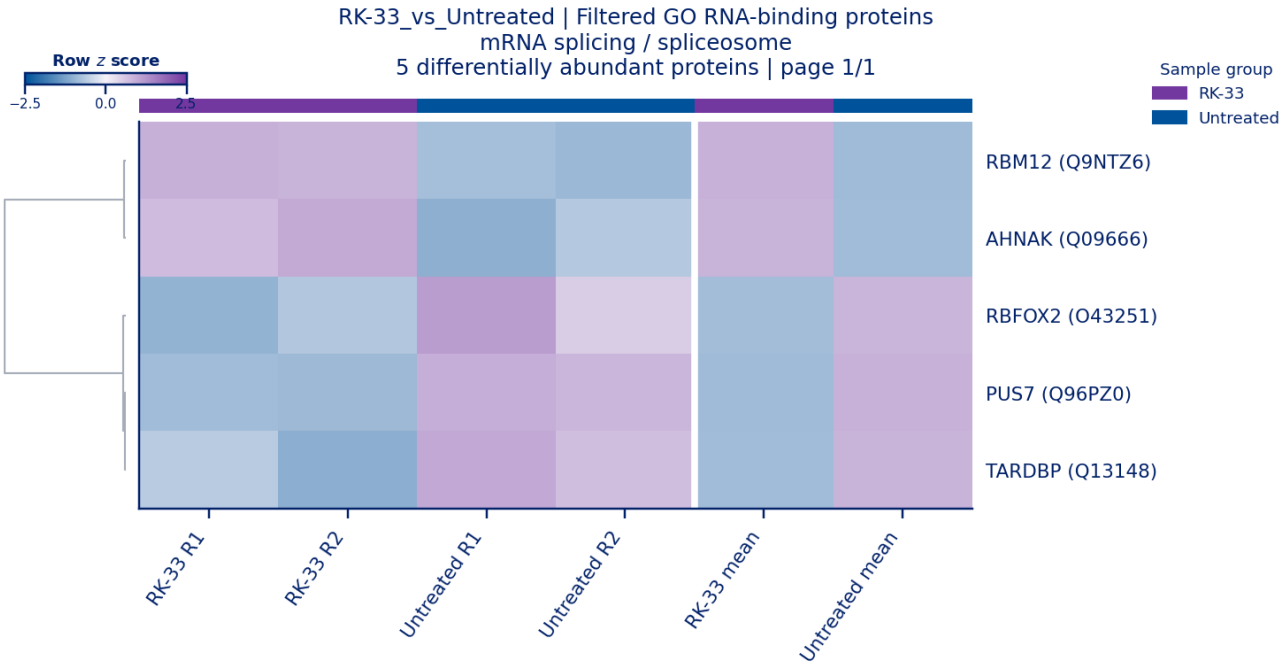


Figure 26. Protein abundance patterns within the mRNA splicing / spliceosome category. Heatmap showing $\log_2$(%TP) values in the analyzed RNP fractions, standardized within each protein across biological replicates (row *z* scores). Category membership was assigned automatically using in-house classification rules applied to positive UniProtKB Gene Ontology annotations and keywords relating to RNA splicing, the spliceosome, or U1, U2, U4, U5, or U6 snRNPs. Purple and blue indicate abundances above and below the mean for each protein, respectively; the color scale is limited to ±2.5. Rows were clustered using average linkage and correlation distance across replicate samples. The dendrogram branches show the hierarchical clustering of proteins by their abundance patterns; the merge positions reflect average correlation distances, not evidence of direct interactions. Sample columns retain their experimental order. The final columns show the group means of the row *z* scores and were excluded from clustering. Proteins may appear in more than one category.

Protein functions and features (Figure 26)

RBM12 (Q9NTZ6). RNA binding protein; GO annotations include nucleic acid binding; negative regulation of cAMP/PKA signal transduction. Annotated features: RNA recognition motif; RRM domain.

AHNAK (Q09666). May be required for neuronal cell differentiation; GO annotations include cadherin binding; positive regulation of plasma membrane repair. Annotated features: PDZ domain.

RBFOX2 (O43251). RNA-binding protein that regulates alternative splicing events by binding to 5'-UGCAUGU-3' elements. Annotated features: RNA recognition motif.

PUS7 (Q96PZ0). Pseudouridylate synthase that catalyzes pseudouridylation of RNAs; GO annotations include tRNA pseudouridine(13) synthase activity; negative regulation of translation. Annotated features: Pseudouridine synthase, TruD, insertion domain.

TARDBP (Q13148). RNA-binding protein that is involved in various steps of RNA biogenesis and processing. Annotated features: RNA recognition motif; TAR DNA-binding protein 43, N-terminal domain.

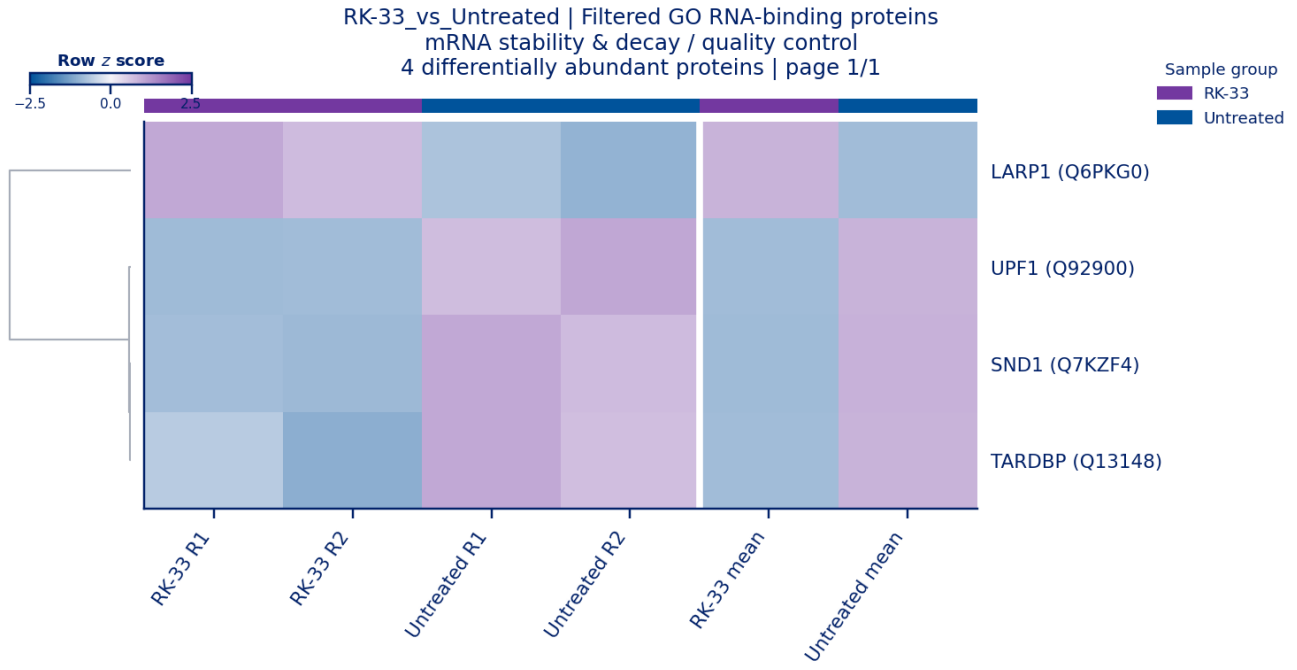


Figure 27. Protein abundance patterns within the mRNA stability & decay / quality control category. Heatmap showing $\log_2$(%TP) values in the analyzed RNP fractions, standardized within each protein across biological replicates (row *z* scores). Category membership was assigned automatically using in-house classification rules applied to positive UniProtKB Gene Ontology annotations and keywords relating to RNA stability, turnover, decay, degradation, or surveillance, including deadenylation, decapping, and translation-associated RNA decay. Purple and blue indicate abundances above and below the mean for each protein, respectively; the color scale is limited to ±2.5. Rows were clustered using average linkage and correlation distance across replicate samples. The dendrogram branches show the hierarchical clustering of proteins by their abundance patterns; the merge positions reflect average correlation distances, not evidence of direct interactions. Sample columns retain their experimental order. The final columns show the group means of the row *z* scores and were excluded from clustering. Proteins may appear in more than one category.

Protein functions and features (Figure 27)

LARP1 (Q6PKG0). RNA-binding protein that regulates the translation of specific target mRNA species downstream of the mTORC1 complex, in function of growth signals and nutrient availability. Annotated features: La domain; LARP1 HEAT repeat region (repeat).

UPF1 (Q92900). RNA-dependent helicase required for nonsense-mediated decay (NMD) of aberrant mRNAs containing premature stop codons and which modulates the expression level of normal mRNAs. Annotated features: AAA domain; RNA helicase (UPF2 interacting domain).

SND1 (Q7KZF4). Endonuclease that mediates miRNA decay of both protein-free and AGO2-loaded miRNAs; GO annotations include 3' overhang single-stranded DNA endonuclease activity; mRNA catabolic process. Annotated features: Staphylococcal nuclease homologue; Tudor domain.

TARDBP (Q13148). RNA-binding protein that is involved in various steps of RNA biogenesis and processing. Annotated features: RNA recognition motif; TAR DNA-binding protein 43, N-terminal domain.

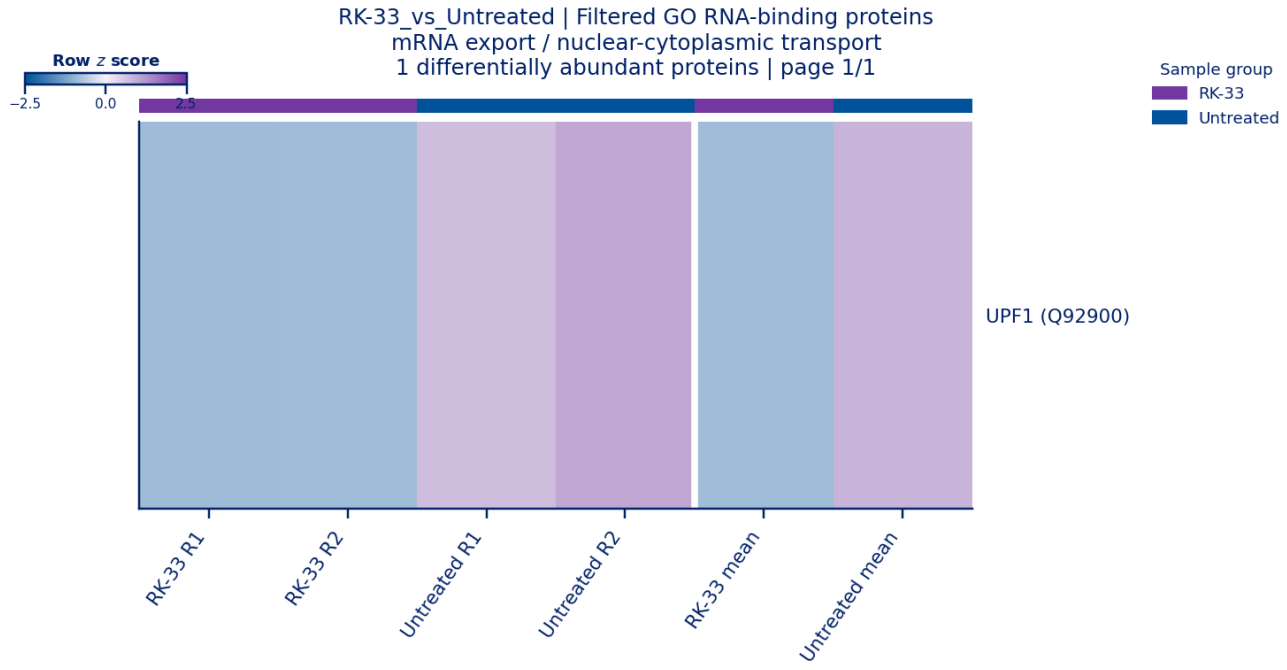


Figure 28. Protein abundance patterns within the mRNA export / nuclear-cytoplasmic transport category. Heatmap showing $\log_2$(%TP) values in the analyzed RNP fractions, standardized within each protein across biological replicates (row *z* scores). Category membership was assigned automatically using in-house classification rules applied to positive UniProtKB Gene Ontology annotations and keywords relating to RNA or ribonucleoprotein-complex export or nucleocytoplasmic transport; supporting annotations may describe a transport complex. Purple and blue indicate abundances above and below the mean for each protein, respectively; the color scale is limited to ±2.5. Rows were clustered using average linkage and correlation distance across replicate samples. The dendrogram branches show the hierarchical clustering of proteins by their abundance patterns; the merge positions reflect average correlation distances, not evidence of direct interactions. Sample columns retain their experimental order. The final columns show the group means of the row *z* scores and were excluded from clustering. Proteins may appear in more than one category.

Protein functions and features (Figure 28)

UPF1 (Q92900). RNA-dependent helicase required for nonsense-mediated decay (NMD) of aberrant mRNAs containing premature stop codons and which modulates the expression level of normal mRNAs. Annotated features: AAA domain; RNA helicase (UPF2 interacting domain).

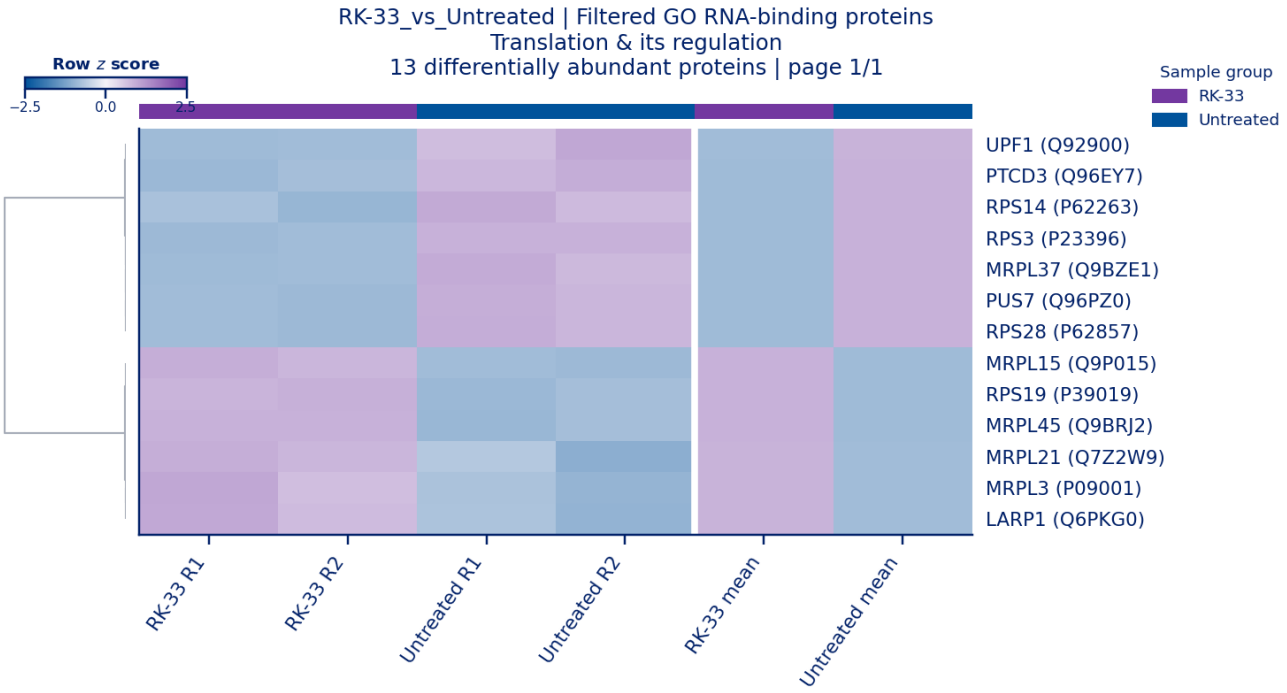


Figure 29. Protein abundance patterns within the Translation & its regulation category. Heatmap showing $\log_2$(%TP) values in the analyzed RNP fractions, standardized within each protein across biological replicates (row *z* scores). Category membership was assigned automatically using in-house classification rules applied to positive UniProtKB Gene Ontology annotations and keywords relating to translation or its regulation, ribosomal proteins, or structural constituents of the ribosome. Purple and blue indicate abundances above and below the mean for each protein, respectively; the color scale is limited to ±2.5. Rows were clustered using average linkage and correlation distance across replicate samples. The dendrogram branches show the hierarchical clustering of proteins by their abundance patterns; the merge positions reflect average correlation distances, not evidence of direct interactions. Sample columns retain their experimental order. The final columns show the group means of the row *z* scores and were excluded from clustering. Proteins may appear in more than one category.

Protein functions and features (Figure 29)

UPF1 (Q92900). RNA-dependent helicase required for nonsense-mediated decay (NMD) of aberrant mRNAs containing premature stop codons and which modulates the expression level of normal mRNAs. Annotated features: AAA domain; RNA helicase (UPF2 interacting domain).

PTCD3 (Q96EY7). Mitochondrial RNA-binding protein that has a role in mitochondrial translation. ; GO annotations include ribosomal small subunit binding; mitochondrial translation. Annotated features: Pentatricopeptide repeat domain (repeat); Small ribosomal subunit protein mS39, PPR (repeat).

RPS14 (P62263). Component of the small ribosomal subunit; GO annotations include mRNA 5'-UTR binding; negative regulation of transcription by RNA polymerase II. Annotated features: Ribosomal protein S11 (family).

RPS3 (P23396). Component of the small ribosomal subunit; GO annotations include class I DNA-(apurinic or apyrimidinic site) endonuclease activity; positive regulation of intrinsic apoptotic signaling pathway in response to DNA damage. Annotated features: KH domain; Ribosomal protein S3, C-terminal domain.

MRPL37 (Q9BZE1). GO annotations include structural constituent of ribosome; mitochondrial translation. Annotated features: Mitochondrial 28S ribosomal protein S30 (PDCD9) (family).

PUS7 (Q96PZ0). Pseudouridylate synthase that catalyzes pseudouridylation of RNAs; GO annotations include tRNA pseudouridine(13) synthase activity; negative regulation of translation. Annotated features: Pseudouridine synthase, TruD, insertion domain.

RPS28 (P62857). Component of the small ribosomal subunit; GO annotations include structural constituent of ribosome; cytoplasmic translation. Annotated features: Ribosomal protein S28e.

MRPL15 (Q9P015). GO annotations include structural constituent of ribosome; mitochondrial translation. Annotated features: Ribosomal proteins 50S-L15, 50S-L18e, 60S-L27A.

RPS19 (P39019). Component of the small ribosomal subunit; GO annotations include fibroblast growth factor binding; antimicrobial humoral immune response mediated by antimicrobial peptide. Annotated features: Ribosomal protein S19e (family).

MRPL45 (Q9BRJ2). Component of the mitochondrial large ribosomal subunit (mt-LSU); GO annotations include mitochondrial translation. Annotated features: Tim44-like domain.

MRPL21 (Q7Z2W9). GO annotations include structural constituent of ribosome; mitochondrial translation. Annotated features: Ribosomal prokaryotic L21 protein (family).

MRPL3 (P09001). GO annotations include structural constituent of ribosome; mitochondrial translation. Annotated features: Ribosomal protein L3 (family).

LARP1 (Q6PKG0). RNA-binding protein that regulates the translation of specific target mRNA species downstream of the mTORC1 complex, in function of growth signals and nutrient availability. Annotated features: La domain; LARP1 HEAT repeat region (repeat).

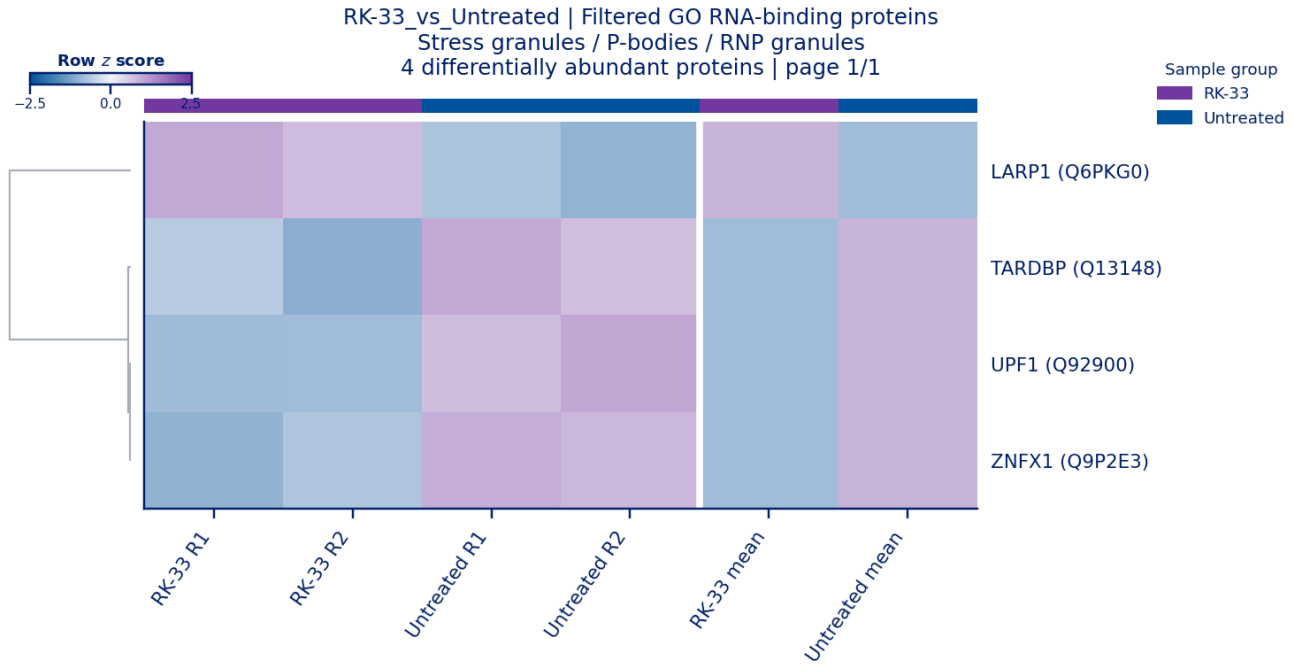


Figure 30. Protein abundance patterns within the Stress granules / P-bodies / RNP granules category. Heatmap showing $\log_2$(%TP) values in the analyzed RNP fractions, standardized within each protein across biological replicates (row *z* scores). Category membership was assigned automatically using in-house classification rules applied to positive UniProtKB Gene Ontology annotations and keywords describing stress granules, P-bodies, processing bodies, or ribonucleoprotein granules; membership can reflect cellular association rather than a demonstrated role in granule formation. Purple and blue indicate abundances above and below the mean for each protein, respectively; the color scale is limited to ±2.5. Rows were clustered using average linkage and correlation distance across replicate samples. The dendrogram branches show the hierarchical clustering of proteins by their abundance patterns; the merge positions reflect average correlation distances, not evidence of direct interactions. Sample columns retain their experimental order. The final columns show the group means of the row *z* scores and were excluded from clustering. Proteins may appear in more than one category.

Protein functions and features (Figure 30)

LARP1 (Q6PKG0). RNA-binding protein that regulates the translation of specific target mRNA species downstream of the mTORC1 complex, in function of growth signals and nutrient availability. Annotated features: La domain; LARP1 HEAT repeat region (repeat).

TARDBP (Q13148). RNA-binding protein that is involved in various steps of RNA biogenesis and processing. Annotated features: RNA recognition motif; TAR DNA-binding protein 43, N-terminal domain.

UPF1 (Q92900). RNA-dependent helicase required for nonsense-mediated decay (NMD) of aberrant mRNAs containing premature stop codons and which modulates the expression level of normal mRNAs. Annotated features: AAA domain; RNA helicase (UPF2 interacting domain).

ZNFX1 (Q9P2E3). RNA-activated non-canonical E3 ubiquitin ligase required for cell survival during interferon (IFN) responses. Annotated features: AAA domain; RZ type zinc finger domain.

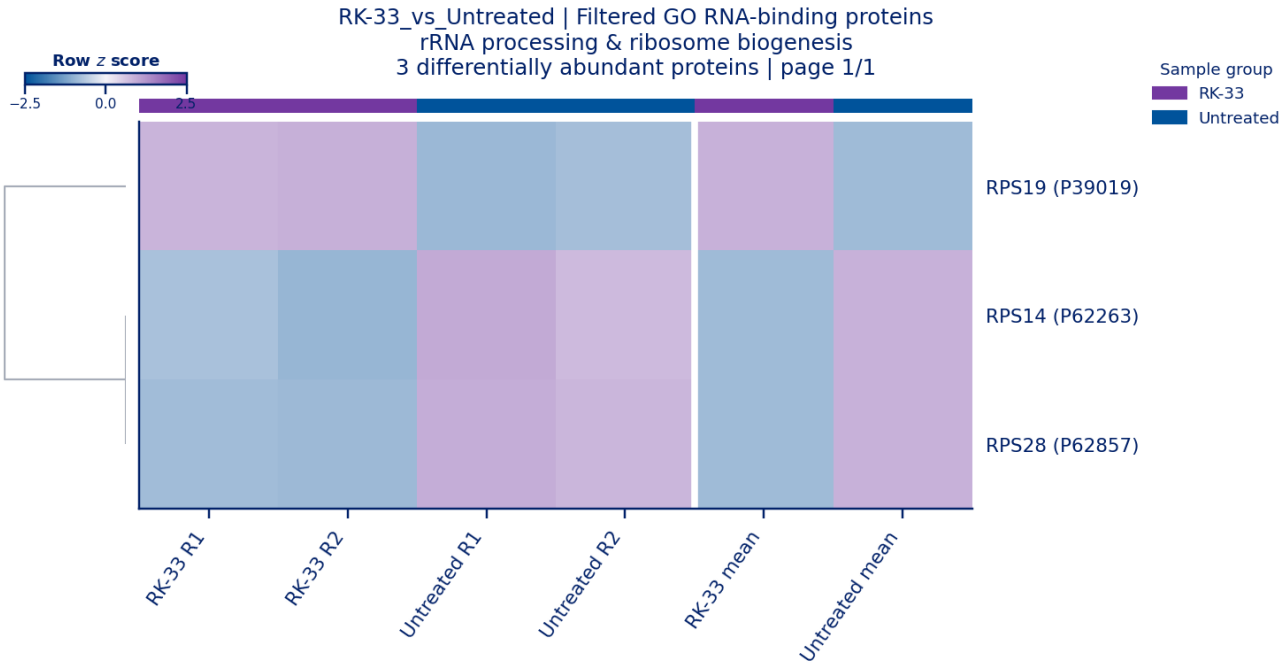


Figure 31. Protein abundance patterns within the rRNA processing & ribosome biogenesis category. Heatmap showing $\log_2$(%TP) values in the analyzed RNP fractions, standardized within each protein across biological replicates (row *z* scores). Category membership was assigned automatically using in-house classification rules applied to positive UniProtKB Gene Ontology annotations and keywords relating to rRNA processing, maturation, or modification, ribosome or ribosomal-subunit biogenesis or assembly, or the small-subunit processome. Purple and blue indicate abundances above and below the mean for each protein, respectively; the color scale is limited to ±2.5. Rows were clustered using average linkage and correlation distance across replicate samples. The dendrogram branches show the hierarchical clustering of proteins by their abundance patterns; the merge positions reflect average correlation distances, not evidence of direct interactions. Sample columns retain their experimental order. The final columns show the group means of the row *z* scores and were excluded from clustering. Proteins may appear in more than one category.

Protein functions and features (Figure 31)

RPS19 (P39019). Component of the small ribosomal subunit; GO annotations include fibroblast growth factor binding; antimicrobial humoral immune response mediated by antimicrobial peptide. Annotated features: Ribosomal protein S19e (family).

RPS14 (P62263). Component of the small ribosomal subunit; GO annotations include mRNA 5'-UTR binding; negative regulation of transcription by RNA polymerase II. Annotated features: Ribosomal protein S11 (family).

RPS28 (P62857). Component of the small ribosomal subunit; GO annotations include structural constituent of ribosome; cytoplasmic translation. Annotated features: Ribosomal protein S28e.

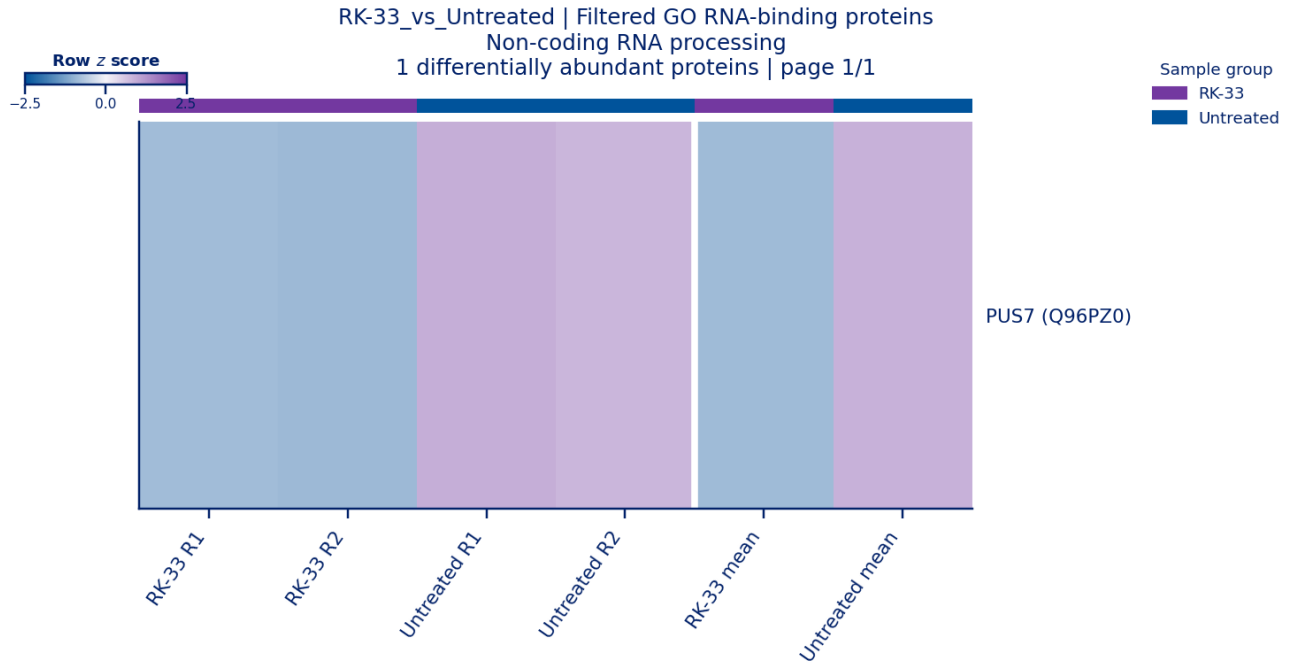


Figure 32. Protein abundance patterns within the Non-coding RNA processing category. Heatmap showing $\log_2$(%TP) values in the analyzed RNP fractions, standardized within each protein across biological replicates (row *z* scores). Category membership was assigned automatically using in-house classification rules applied to positive UniProtKB Gene Ontology annotations and keywords relating to processing, maturation, modification, aminoacylation, or splicing of tRNA, miRNA, snRNA, snoRNA, lncRNA, or other noncoding RNA. Purple and blue indicate abundances above and below the mean for each protein, respectively; the color scale is limited to ±2.5. Rows were clustered using average linkage and correlation distance across replicate samples. The dendrogram branches show the hierarchical clustering of proteins by their abundance patterns; the merge positions reflect average correlation distances, not evidence of direct interactions. Sample columns retain their experimental order. The final columns show the group means of the row *z* scores and were excluded from clustering. Proteins may appear in more than one category.

Protein functions and features (Figure 32)

PUS7 (Q96PZ0). Pseudouridylate synthase that catalyzes pseudouridylation of RNAs; GO annotations include tRNA pseudouridine(13) synthase activity; negative regulation of translation. Annotated features: Pseudouridine synthase, TruD, insertion domain.

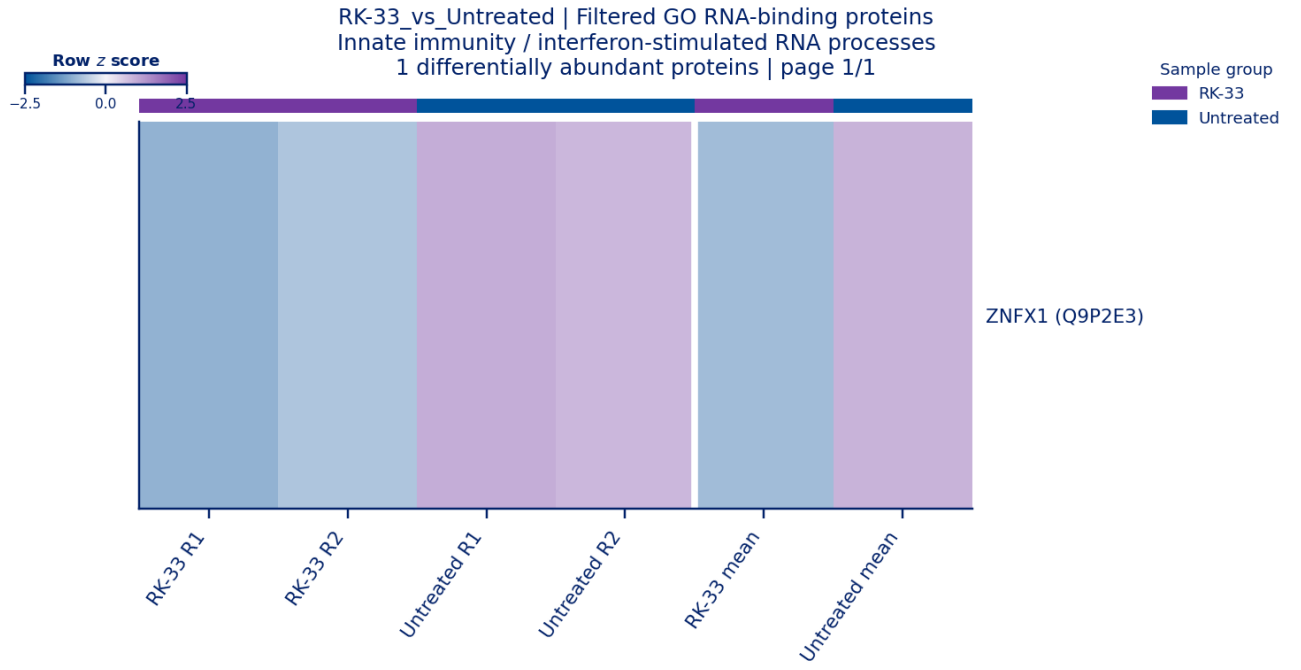


Figure 33. Protein abundance patterns within the Innate immunity / interferon-stimulated RNA processes category. Heatmap showing $\log_2$(%TP) values in the analyzed RNP fractions, standardized within each protein across biological replicates (row *z* scores). Category membership was assigned automatically using in-house classification rules applied to positive UniProtKB Gene Ontology annotations and keywords relating to interferon, innate immune responses, antiviral functions, viral RNA sensing, or RNA-mediated immunity. Purple and blue indicate abundances above and below the mean for each protein, respectively; the color scale is limited to ±2.5. Rows were clustered using average linkage and correlation distance across replicate samples. The dendrogram branches show the hierarchical clustering of proteins by their abundance patterns; the merge positions reflect average correlation distances, not evidence of direct interactions. Sample columns retain their experimental order. The final columns show the group means of the row *z* scores and were excluded from clustering. Proteins may appear in more than one category.

Protein functions and features (Figure 33)

ZNFX1 (Q9P2E3). RNA-activated non-canonical E3 ubiquitin ligase required for cell survival during interferon (IFN) responses. Annotated features: AAA domain; RZ type zinc finger domain.

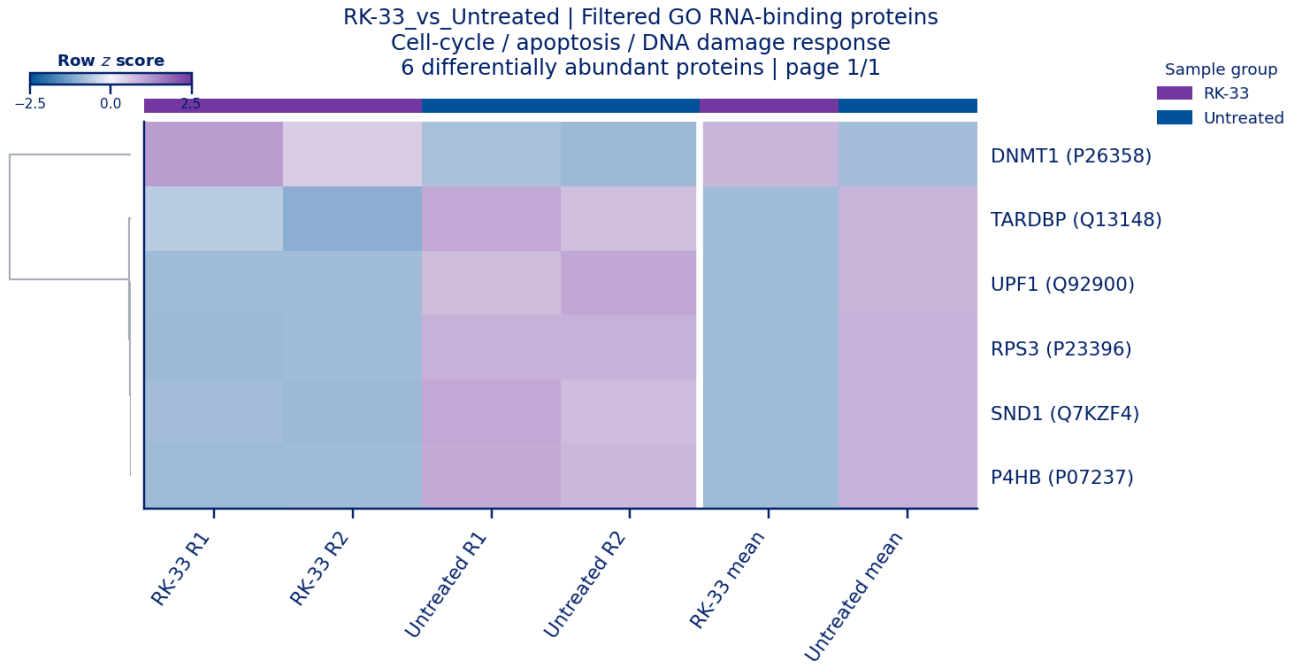


Figure 34. Protein abundance patterns within the Cell-cycle / apoptosis / DNA damage response category. Heatmap showing $\log_2$(%TP) values in the analyzed RNP fractions, standardized within each protein across biological replicates (row *z* scores). Category membership was assigned automatically using in-house classification rules applied to positive UniProtKB Gene Ontology annotations and keywords relating to the cell cycle, mitosis, apoptosis, programmed cell death, DNA-damage responses or checkpoints, or DNA repair. Purple and blue indicate abundances above and below the mean for each protein, respectively; the color scale is limited to ±2.5. Rows were clustered using average linkage and correlation distance across replicate samples. The dendrogram branches show the hierarchical clustering of proteins by their abundance patterns; the merge positions reflect average correlation distances, not evidence of direct interactions. Sample columns retain their experimental order. The final columns show the group means of the row *z* scores and were excluded from clustering. Proteins may appear in more than one category.

Protein functions and features (Figure 34)

DNMT1 (P26358). DNA methyltransferase that methylates CpG residues; GO annotations include DNA (cytosine-5-)-methyltransferase activity; negative regulation of gene expression via chromosomal CpG island methylation. Annotated features: BAH domain; C-5 cytosine-specific DNA methylase.

TARDBP (Q13148). RNA-binding protein that is involved in various steps of RNA biogenesis and processing. Annotated features: RNA recognition motif; TAR DNA-binding protein 43, N-terminal domain.

UPF1 (Q92900). RNA-dependent helicase required for nonsense-mediated decay (NMD) of aberrant mRNAs containing premature stop codons and which modulates the expression level of normal mRNAs. Annotated features: AAA domain; RNA helicase (UPF2 interacting domain).

RPS3 (P23396). Component of the small ribosomal subunit; GO annotations include class I DNA-(apurinic or apyrimidinic site) endonuclease activity; positive regulation of intrinsic apoptotic signaling pathway in response to DNA damage. Annotated features: KH domain; Ribosomal protein S3, C-terminal domain.

SND1 (Q7KZF4). Endonuclease that mediates miRNA decay of both protein-free and AGO2-loaded miRNAs; GO annotations include 3' overhang single-stranded DNA endonuclease activity; mRNA catabolic process. Annotated features: Staphylococcal nuclease homologue; Tudor domain.

P4HB (P07237). This multifunctional protein catalyzes the formation, breakage and rearrangement of disulfide bonds. Annotated features: Thioredoxin; Thioredoxin-like domain.

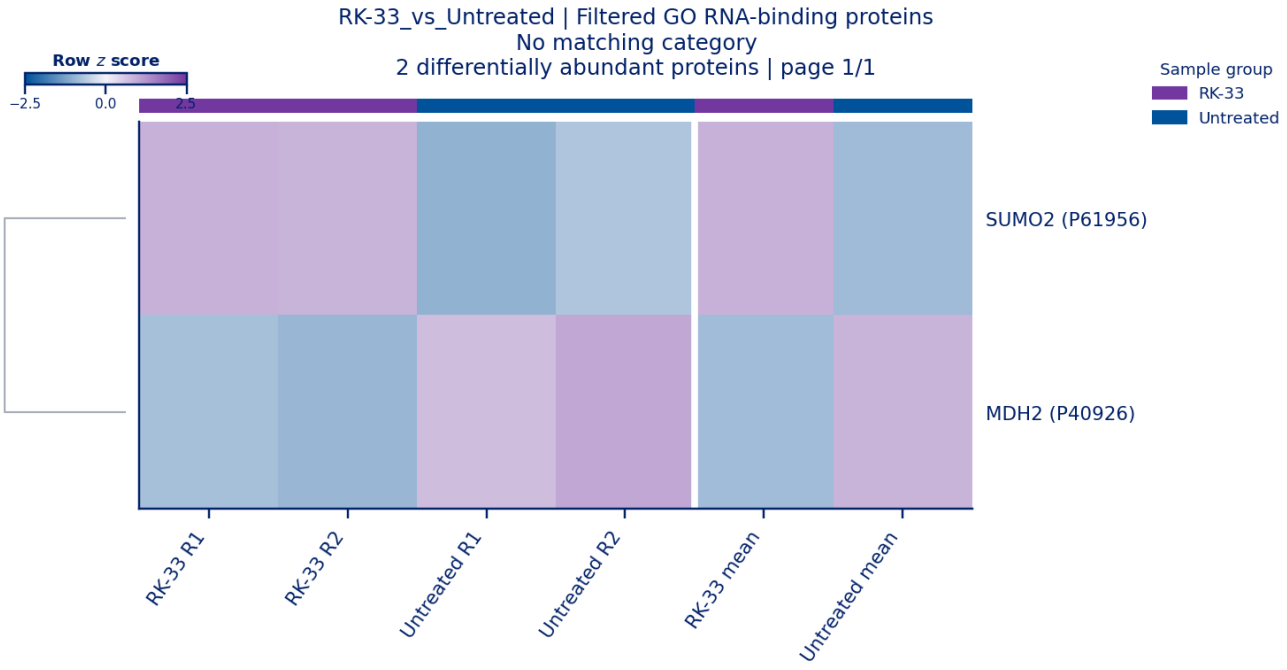


Figure 35. Protein abundance patterns of proteins without a matching functional category. Heatmap showing $\log_2$(%TP) values in the analyzed RNP fractions, standardized within each protein across biological replicates (row *z* scores). These proteins did not match the predefined annotation categories; this does not indicate an absence of known functions. Purple and blue indicate abundances above and below the mean for each protein, respectively; the color scale is limited to ±2.5. Rows were clustered using average linkage and correlation distance across replicate samples. The dendrogram branches show the hierarchical clustering of proteins by their abundance patterns; the merge positions reflect average correlation distances, not evidence of direct interactions. Sample columns retain their experimental order. The final columns show the group means of the row *z* scores and were excluded from clustering. Proteins may appear in more than one category.

Protein functions and features (Figure 35)

SUMO2 (P61956). Ubiquitin-like protein that can be covalently attached to proteins as a monomer or as a lysine-linked polymer. Annotated features: Rad60/SUMO-like domain; Ubiquitin-like domain.

MDH2 (P40926). Mitochondrial malate dehydrogenase that catalyzes the reversible conversion of malate to oxaloacetate using NAD(+) as a cofactor. Annotated features: lactate/malate dehydrogenase, NAD binding domain; lactate/malate dehydrogenase, alpha/beta C-terminal domain.

10. Over-representation and Gene Set Enrichment Analyses

H3B-8800 versus Untreated

Functional enrichment was evaluated using genes corresponding to tested proteins. The comparison included 797 unique, unambiguously mapped genes, of which 6 corresponded to differentially abundant proteins (0 with increased and 6 with decreased %TP in H3B-8800 relative to Untreated). Missing or ambiguous gene symbols were excluded without alias substitution. Multiple protein entries mapping to the same gene were counted once; their signed *t* statistics were averaged for ranked enrichment.

Gene sets were obtained from GOA/QuickGO, Enrichr, Reactome, and InterPro/UniProtKB as listed below (retrieved 2026-11-14). Enrichr library years identify provider exports; the upstream release is not necessarily specified. Direct Reactome and InterPro library labels identify recorded source releases; InterPro domain assignments use reviewed human UniProtKB cross-references. GO gene sets use positive human GOA protein annotations, all evidence codes, and is_a and part_of propagation within each GO aspect using the recorded QuickGO ontology release. These gene sets were analyzed separately from the descriptive categories in Section 9.

RK-33 versus Untreated

Functional enrichment was evaluated using genes corresponding to tested proteins. The comparison included 797 unique, unambiguously mapped genes, of which 23 corresponded to differentially abundant proteins (10 with increased and 13 with decreased %TP in RK-33 relative to Untreated). Missing or ambiguous gene symbols were excluded without alias substitution. Multiple protein entries mapping to the same gene were counted once; their signed *t* statistics were averaged for ranked enrichment.

Gene sets were obtained from GOA/QuickGO, Enrichr, Reactome, and InterPro/UniProtKB as listed below (retrieved 2026-11-14). Enrichr library years identify provider exports; the upstream release is not necessarily specified. Direct Reactome and InterPro library labels identify recorded source releases; InterPro domain assignments use reviewed human UniProtKB cross-references. GO gene sets use positive human GOA protein annotations, all evidence codes, and is_a and part_of propagation within each GO aspect using the recorded QuickGO ontology release. These gene sets were analyzed separately from the descriptive categories in Section 9.

MS-444 versus Untreated

Functional enrichment was evaluated using genes corresponding to tested proteins. The comparison included 804 unique, unambiguously mapped genes. Missing or ambiguous gene symbols were excluded without alias substitution. Multiple protein entries mapping to the same gene were counted once; their signed *t* statistics were averaged for ranked enrichment.

Gene sets were obtained from GOA/QuickGO, Enrichr, Reactome, and InterPro/UniProtKB as listed below (retrieved 2026-11-14). Enrichr library years identify provider exports; the upstream release is not necessarily specified. Direct Reactome and InterPro library labels identify recorded source releases; InterPro domain assignments use reviewed human UniProtKB cross-references. GO gene sets use positive human GOA protein annotations, all evidence codes, and is_a and part_of propagation within each GO aspect using the recorded QuickGO ontology release. These gene sets were analyzed separately from the descriptive categories in Section 9.

UZH1a versus Untreated

Functional enrichment was evaluated using genes corresponding to tested proteins. The comparison included 782 unique, unambiguously mapped genes. Missing or ambiguous gene symbols were excluded without alias substitution. Multiple protein entries mapping to the same gene were counted once; their signed *t* statistics were averaged for ranked enrichment.

Gene sets were obtained from GOA/QuickGO, Enrichr, Reactome, and InterPro/UniProtKB as listed below (retrieved 2026-11-14). Enrichr library years identify provider exports; the upstream release is not necessarily specified. Direct Reactome and InterPro library labels identify recorded source releases; InterPro domain assignments use reviewed human UniProtKB cross-references. GO gene sets use positive human GOA protein annotations, all evidence codes, and is_a and part_of propagation within each GO aspect using the recorded QuickGO ontology release. These gene sets were analyzed separately from the descriptive categories in Section 9.

Over-representation analysis

Over-representation analysis was performed separately for all differentially abundant proteins and for each abundance direction, using all 797 tested genes as the background. Gene sets containing 3–500 background genes were tested using a one-sided hypergeometric test. The Benjamini–Hochberg procedure was applied across all eligible terms, including terms with no overlap, separately for each library and selected list. The adjusted *p* values are reported as *q* values ($q < .05$). Fold enrichment is the observed overlap divided by its expectation under random selection from the tested background.

H3B-8800 versus Untreated

Gene-set library	Terms tested	Significant terms: all proteins	Significant terms: increased in H3B-8800	Significant terms: decreased in H3B-8800
GO biological process (2026-11-13)	1492	0	0	0
GO molecular function (2026-11-13)	367	0	0	0
GO cellular component (2026-11-13)	340	10	0	10
Reactome pathways (98)	463	12	0	12
KEGG 2026	71	1	0	1
InterPro domains (111.0)	108	0	0	0

The final three columns give the numbers of terms meeting $q < .05$ in each selected list. Increased and decreased refer to H3B-8800 relative to Untreated. Terms overlap, and counts are not numbers of independent biological processes. All libraries and selected lists are included, including those with no significant terms.

Over-representation analysis was performed separately for all differentially abundant proteins and for each abundance direction, using all 797 tested genes as the background. Gene sets containing 3–500 background genes were tested using a one-sided hypergeometric test. The Benjamini–Hochberg procedure was applied across all eligible terms, including terms with no overlap, separately for each library and selected list. The adjusted *p* values are reported as *q* values ($q < .05$). Fold enrichment is the observed overlap divided by its expectation under random selection from the tested background.

RK-33 versus Untreated

Gene-set library	Terms tested	Significant terms: all proteins	Significant terms: increased in RK-33	Significant terms: decreased in RK-33
GO biological process (2026-11-13)	1459	0	0	0
GO molecular function (2026-11-13)	362	0	0	0
GO cellular component (2026-11-13)	332	16	9	0
Reactome pathways (98)	451	6	5	0
KEGG 2026	67	1	0	0
InterPro domains (111.0)	109	0	0	0

The final three columns give the numbers of terms meeting $q < .05$ in each selected list. Increased and decreased refer to RK-33 relative to Untreated. Terms overlap, and counts are not numbers of independent biological processes. All libraries and selected lists are included, including those with no significant terms.

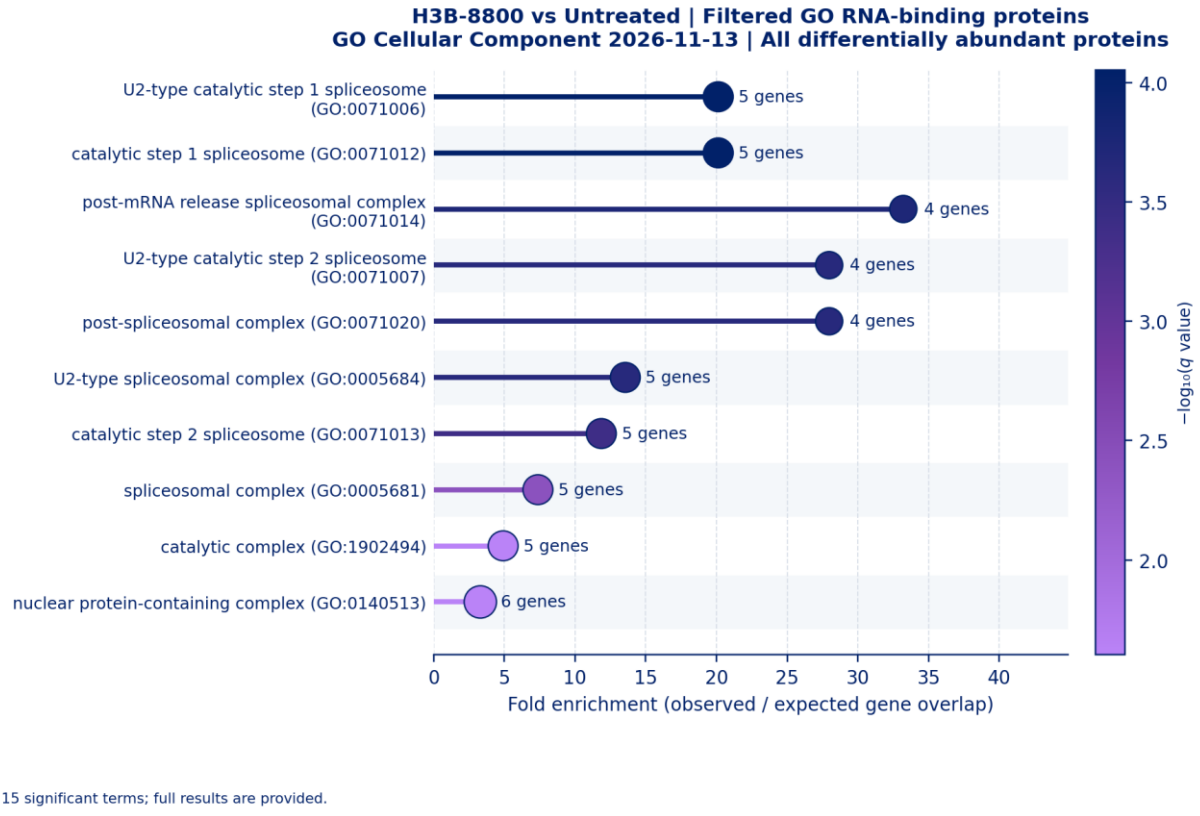


Figure 36. Over-representation of GO cellular component (2026-11-13) terms among all differentially abundant proteins. Shown are all 10 significant terms, ordered by *q* value, then *p* value and term name. Horizontal positions indicate fold enrichment (observed divided by expected gene overlap); dot size indicates the number of overlapping genes, and color indicates $-\log_{10}(q)$. Terms meet $q < .05$ after correction across 340 eligible terms in this library and selected list. Complete results and supporting genes are provided in the corresponding over-representation tables.

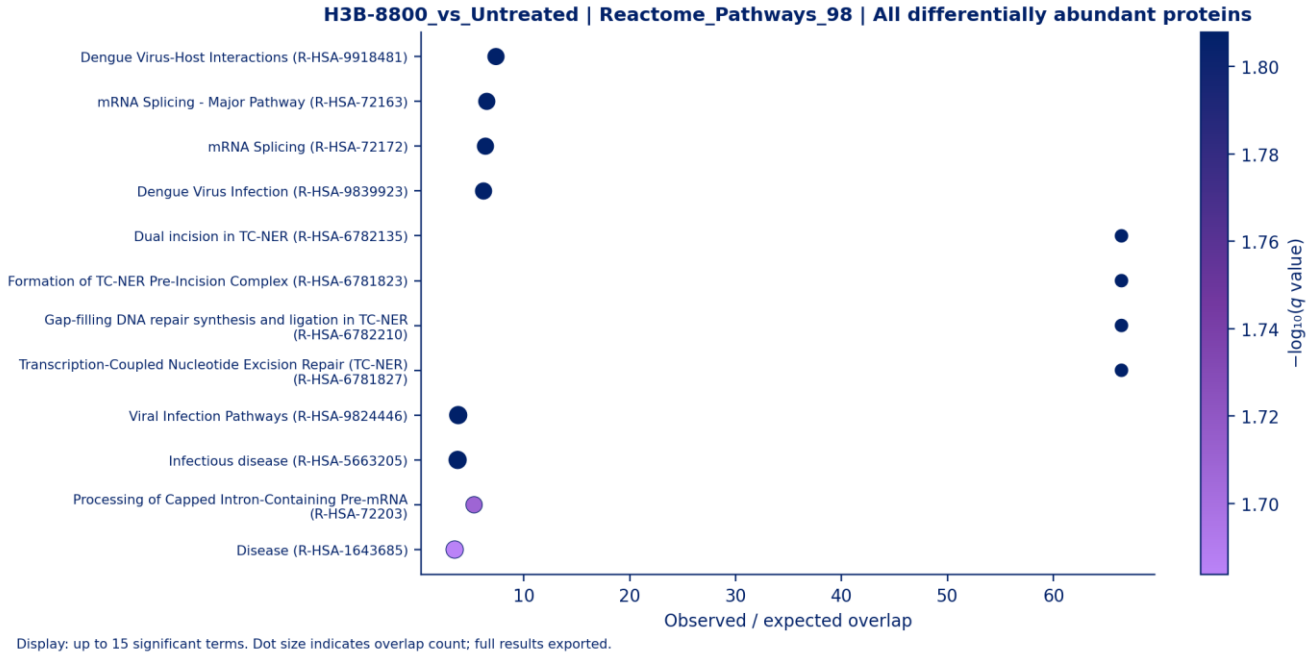


Figure 37. Over-representation of Reactome pathways (98) terms among all differentially abundant proteins. Shown are all 12 significant terms, ordered by *q* value, then *p* value and term name. Horizontal positions indicate fold enrichment (observed divided by expected gene overlap); dot size indicates the number of overlapping genes, and color indicates $-\log_{10}(q)$. Terms meet $q < .05$ after correction across 463 eligible terms in this library and selected list. Complete results and supporting genes are provided in the corresponding over-representation tables.

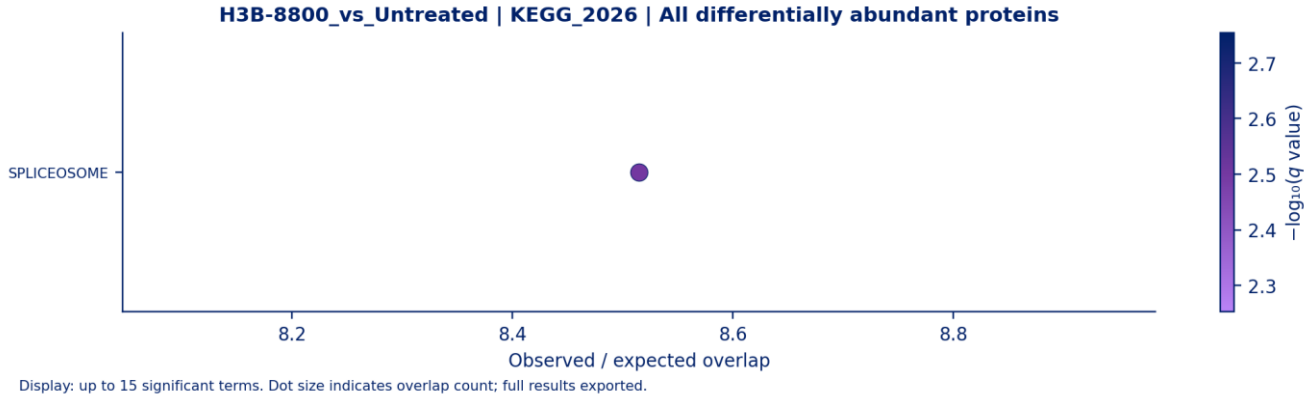
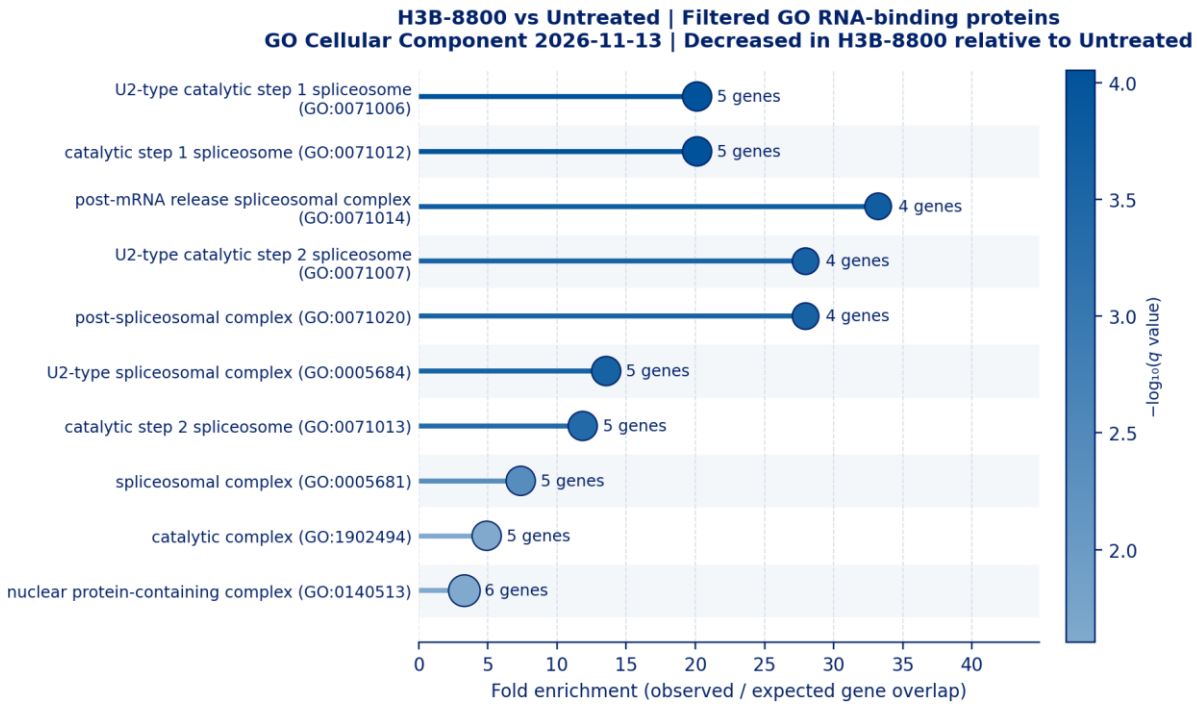


Figure 38. Over-representation of KEGG 2026 terms among all differentially abundant proteins. Shown is the significant term, ordered by *q* value, then *p* value and term name. Horizontal positions indicate fold enrichment (observed divided by expected gene overlap); dot size indicates the number of overlapping genes, and color indicates $-\log_{10}(q)$. Terms meet $q < .05$ after correction across 71 eligible terms in this library and selected list. Complete results and supporting genes are provided in the corresponding over-representation tables.



Display: up to 15 significant terms; full results are provided.

Figure 39. Over-representation of GO cellular component (2026-11-13) terms among proteins with decreased %TP in H3B-8800 relative to Untreated. Shown are all 10 significant terms, ordered by *q* value, then *p* value and term name. Horizontal positions indicate fold enrichment (observed divided by expected gene overlap); dot size indicates the number of overlapping genes, and color indicates $-\log_{10}(q)$. Terms meet $q < .05$ after correction across 340 eligible terms in this library and selected list. Complete results and supporting genes are provided in the corresponding over-representation tables.

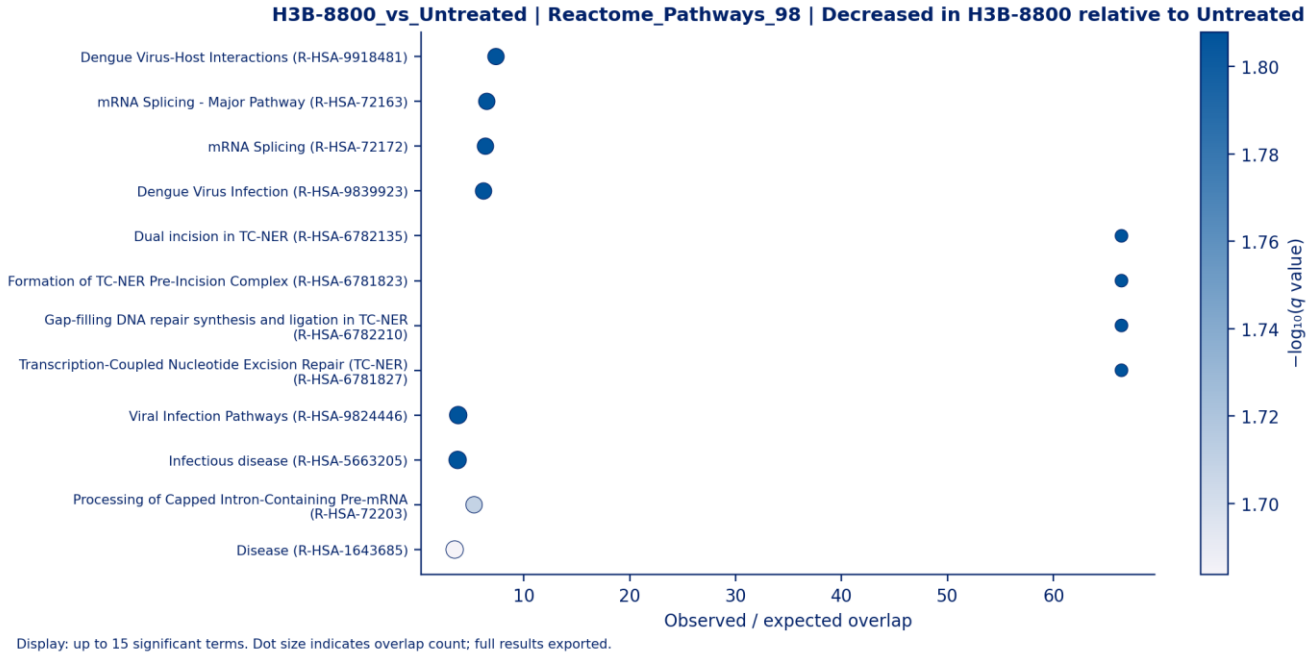


Figure 40. Over-representation of Reactome pathways (98) terms among proteins with decreased %TP in H3B-8800 relative to Untreated. Shown are all 12 significant terms, ordered by *q* value, then *p* value and term name. Horizontal positions indicate fold enrichment (observed divided by expected gene overlap); dot size indicates the number of overlapping genes, and color indicates $-\log_{10}(q)$. Terms meet $q < .05$ after correction across 463 eligible terms in this library and selected list. Complete results and supporting genes are provided in the corresponding over-representation tables.

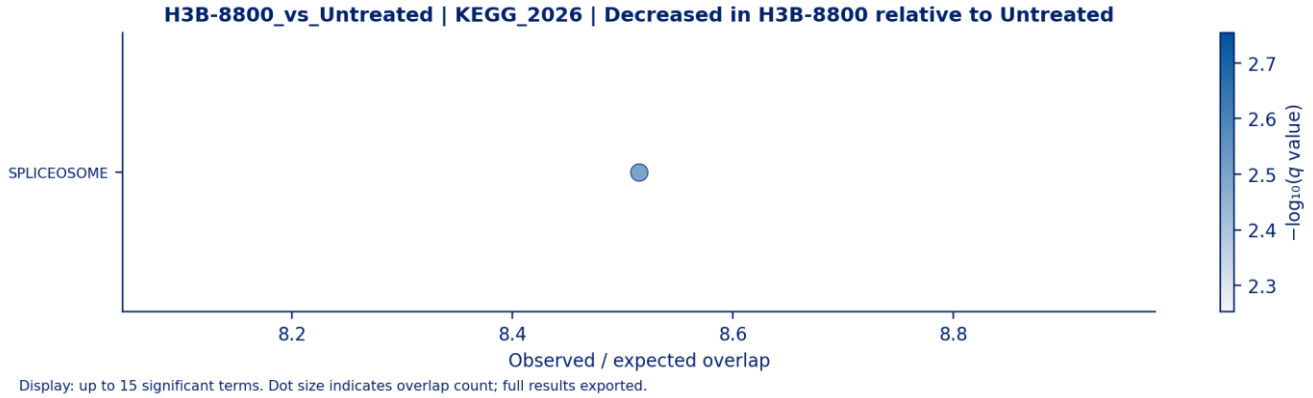
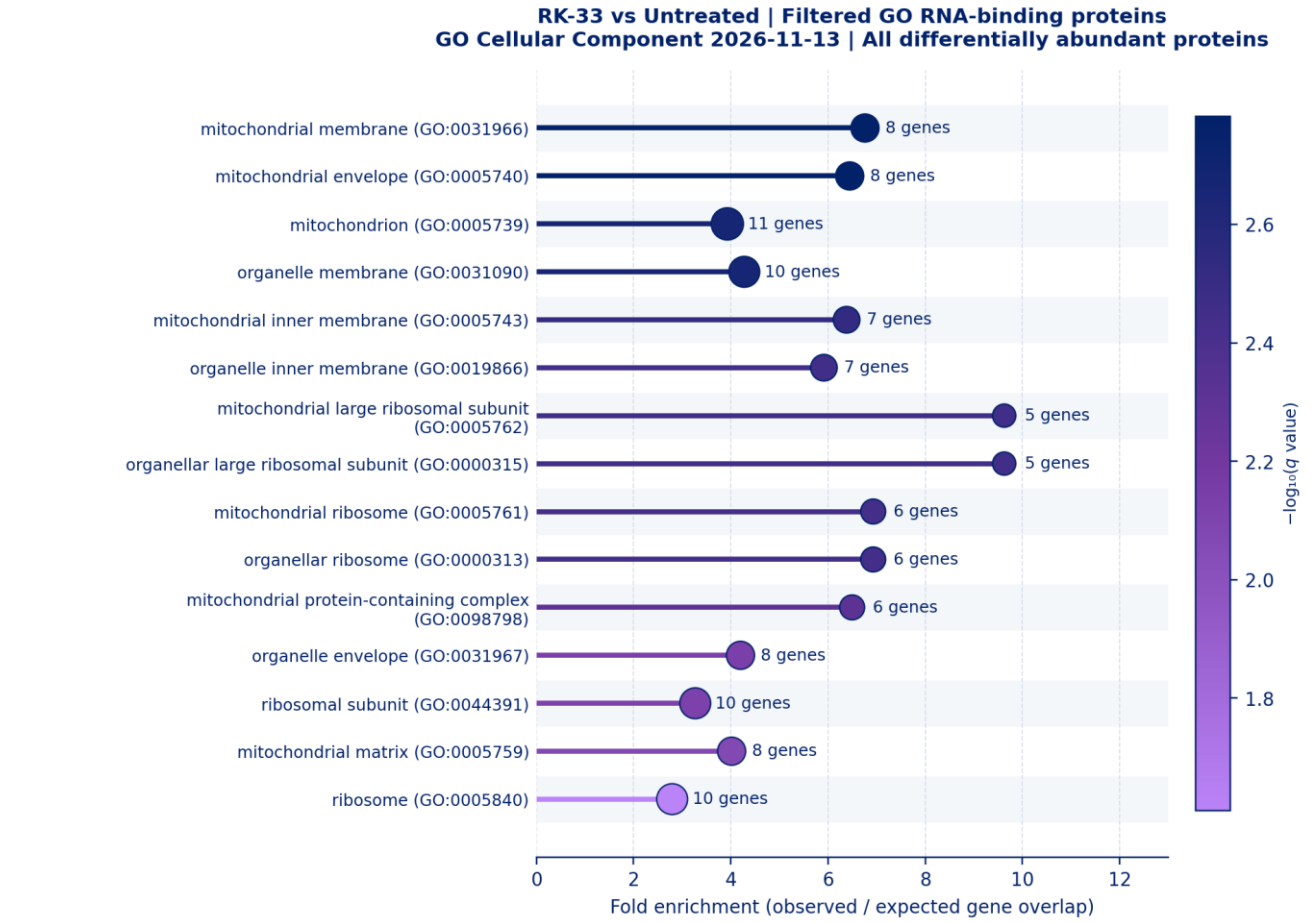


Figure 41. Over-representation of KEGG 2026 terms among proteins with decreased %TP in H3B-8800 relative to Untreated. Shown is the significant term, ordered by *q* value, then *p* value and term name. Horizontal positions indicate fold enrichment (observed divided by expected gene overlap); dot size indicates the number of overlapping genes, and color indicates $-\log_{10}(q)$. Terms meet $q < .05$ after correction across 71 eligible terms in this library and selected list. Complete results and supporting genes are provided in the corresponding over-representation tables.



Display: up to 15 significant terms; full results are provided.

Figure 42. Over-representation of GO cellular component (2026-11-13) terms among all differentially abundant proteins. Shown are 15 of 16 significant terms, ordered by *q* value, then *p* value and term name. Horizontal positions indicate fold enrichment (observed divided by expected gene overlap); dot size indicates the number of overlapping genes, and color indicates $-\log_{10}(q)$. Terms meet $q < .05$ after correction across 332 eligible terms in this library and selected list. Complete results and supporting genes are provided in the corresponding over-representation tables.

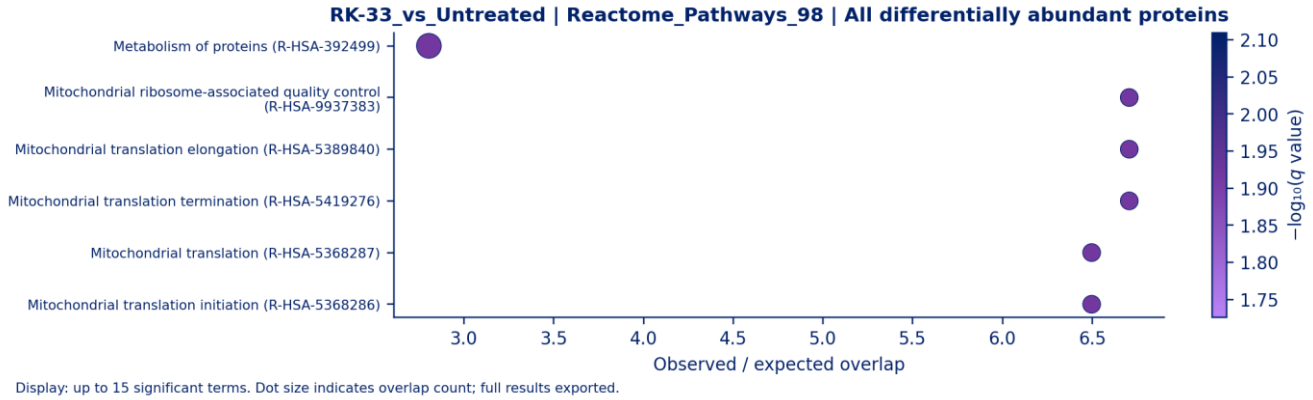


Figure 43. Over-representation of Reactome pathways (98) terms among all differentially abundant proteins. Shown are all 6 significant terms, ordered by *q* value, then *p* value and term name. Horizontal positions indicate fold enrichment (observed divided by expected gene overlap); dot size indicates the number of overlapping genes, and color indicates $-\log_{10}(q)$. Terms meet $q < .05$ after correction across 451 eligible terms in this library and selected list. Complete results and supporting genes are provided in the corresponding over-representation tables.

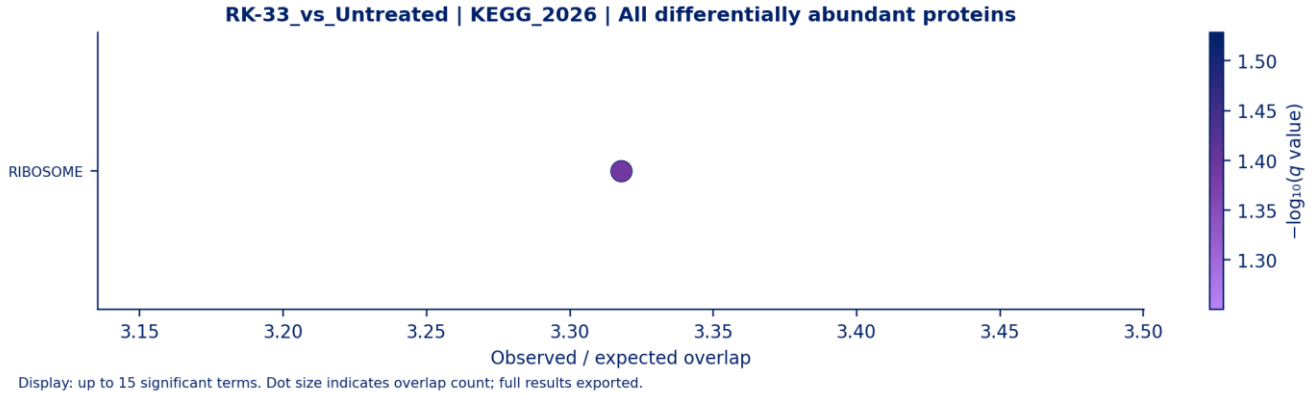


Figure 44. Over-representation of KEGG 2026 terms among all differentially abundant proteins. Shown is the significant term, ordered by *q* value, then *p* value and term name. Horizontal positions indicate fold enrichment (observed divided by expected gene overlap); dot size indicates the number of overlapping genes, and color indicates $-\log_{10}(q)$. Terms meet $q < .05$ after correction across 67 eligible terms in this library and selected list. Complete results and supporting genes are provided in the corresponding over-representation tables.

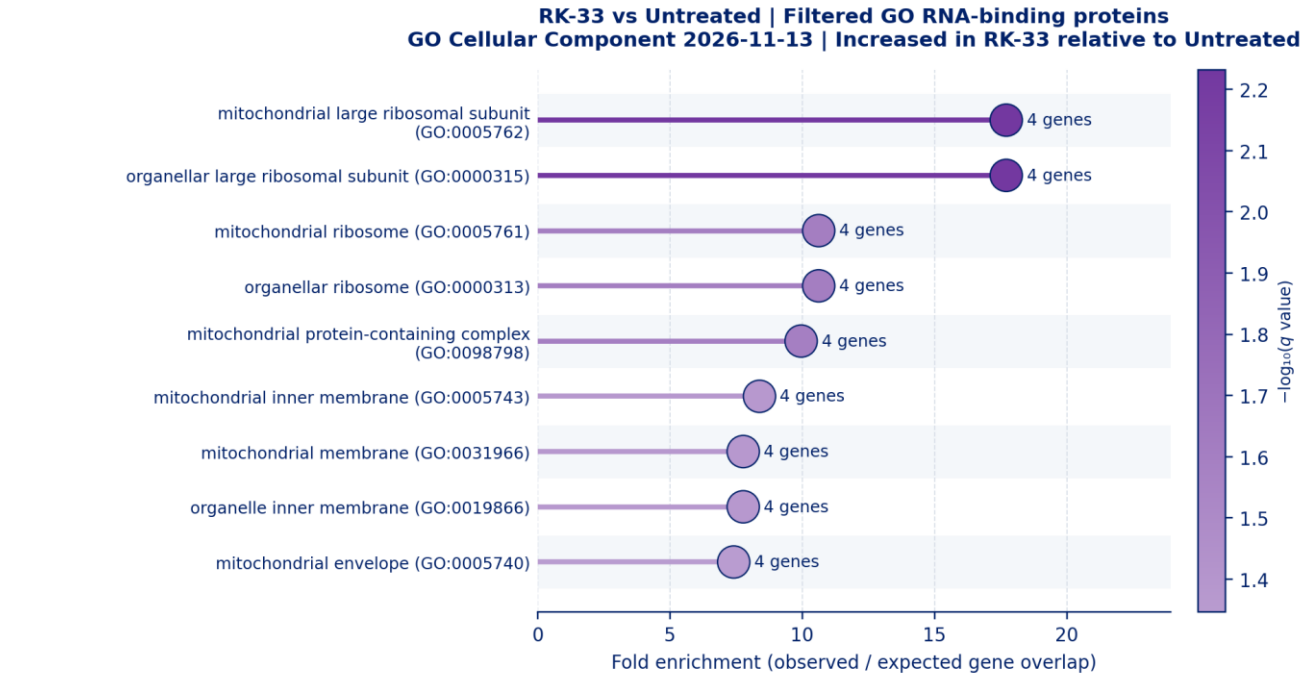


Figure 45. Over-representation of GO cellular component (2026-11-13) terms among proteins with increased %TP in RK-33 relative to Untreated. Shown are all 9 significant terms, ordered by *q* value, then *p* value and term name. Horizontal positions indicate fold enrichment (observed divided by expected gene overlap); dot size indicates the number of overlapping genes, and color indicates $-\log_{10}(q)$. Terms meet $q < .05$ after correction across 332 eligible terms in this library and selected list. Complete results and supporting genes are provided in the corresponding over-representation tables.

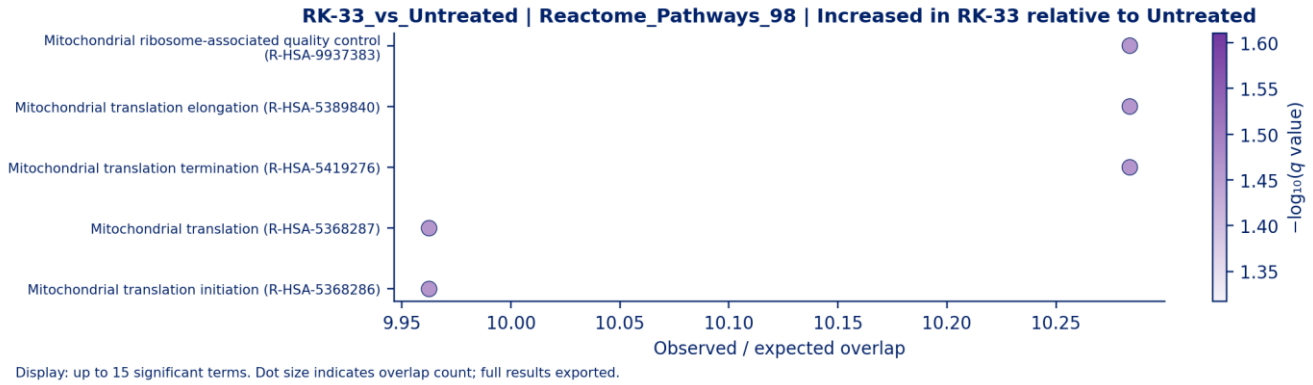


Figure 46. Over-representation of Reactome pathways (98) terms among proteins with increased %TP in RK-33 relative to Untreated. Shown are all 5 significant terms, ordered by *q* value, then *p* value and term name. Horizontal positions indicate fold enrichment (observed divided by expected gene overlap); dot size indicates the number of overlapping genes, and color indicates $-\log_{10}(q)$. Terms meet $q < .05$ after correction across 451 eligible terms in this library and selected list. Complete results and supporting genes are provided in the corresponding over-representation tables.

Ranked gene set enrichment analysis

Preranked gene set enrichment analysis (GSEA) used the full gene list ordered by decreasing signed *t* statistic. Positive and negative scores indicate increased and decreased relative protein abundance in H3B-8800 relative to Untreated, respectively. Gene sets containing 15–500 ranked genes were eligible. Weighted enrichment scores (weight = 1) were evaluated using 1,000 gene-set permutations (seed = 1729); sample-group labels were not permuted. GSEA's permutation-based adjusted *p* values are reported as *q* values and were estimated separately within each library ($q < .05$). Leading-edge genes are the subset contributing to a gene set's enrichment score; they need not be individually differentially abundant. Enrichment FDR is distinct from the protein-level Benjamini–Hochberg correction and is not pooled across libraries.

H3B-8800 versus Untreated

Gene-set library	Sets tested	Significant sets: NES > 0	Significant sets: NES < 0
GO biological process (2026-11-13)	396	0	0
GO molecular function (2026-11-13)	124	0	0
GO cellular component (2026-11-13)	125	0	16
Reactome pathways (98)	105	0	11
KEGG 2026	8	0	1
InterPro domains (111.0)	10	1	0

The final two columns give the numbers of gene sets with $q < .05$, separated by enrichment direction. All libraries are included. Summary figures show up to 15 significant sets per library; complete results and supporting genes are retained in the data package.

Preranked gene set enrichment analysis (GSEA) used the full gene list ordered by decreasing signed *t* statistic. Positive and negative scores indicate increased and decreased relative protein abundance in RK-33 relative to Untreated, respectively. Gene sets containing 15–500 ranked genes were eligible. Weighted enrichment scores (weight = 1) were evaluated using 1,000 gene-set permutations (seed = 1729); sample-group labels were not permuted. GSEA's permutation-based adjusted *p* values are reported as *q* values and were estimated separately within each library ($q < .05$). Leading-edge genes are the subset contributing to a gene set's enrichment score; they need not be individually differentially abundant. Enrichment FDR is distinct from the protein-level Benjamini–Hochberg correction and is not pooled across libraries.

RK-33 versus Untreated

Gene-set library	Sets tested	Significant sets: NES > 0	Significant sets: NES < 0
GO biological process (2026-11-13)	388	0	0
GO molecular function (2026-11-13)	128	0	0
GO cellular component (2026-11-13)	125	2	0
Reactome pathways (98)	106	5	0
KEGG 2026	8	0	0
InterPro domains (111.0)	10	0	0

The final two columns give the numbers of gene sets with $q < .05$, separated by enrichment direction. All libraries are included. Summary figures show up to 15 significant sets per library; complete results and supporting genes are retained in the data package.

Preranked gene set enrichment analysis (GSEA) used the full gene list ordered by decreasing signed *t* statistic. Positive and negative scores indicate increased and decreased relative protein abundance in MS-444 relative to Untreated, respectively. Gene sets containing 15–500 ranked genes were eligible. Weighted enrichment scores (weight = 1) were evaluated using 1,000 gene-set permutations (seed = 1729); sample-group labels were not permuted. GSEA's permutation-based adjusted *p* values are reported as *q* values and were estimated separately within each library ($q < .05$). Leading-edge genes are the subset contributing to a gene set's enrichment score; they need not be individually differentially abundant. Enrichment FDR is distinct from the protein-level Benjamini–Hochberg correction and is not pooled across libraries.

MS-444 versus Untreated

Gene-set library	Sets tested	Significant sets: NES > 0	Significant sets: NES < 0
GO biological process (2026-11-13)	402	1	11
GO molecular function (2026-11-13)	129	0	0
GO cellular component (2026-11-13)	127	2	10
Reactome pathways (98)	108	0	11
KEGG 2026	8	1	2
InterPro domains (111.0)	10	0	1

The final two columns give the numbers of gene sets with $q < .05$, separated by enrichment direction. All libraries are included. Summary figures show up to 15 significant sets per library; complete results and supporting genes are retained in the data package.

Preranked gene set enrichment analysis (GSEA) used the full gene list ordered by decreasing signed *t* statistic. Positive and negative scores indicate increased and decreased relative protein abundance in UZH1a relative to Untreated, respectively. Gene sets containing 15–500 ranked genes were eligible. Weighted enrichment scores (weight = 1) were evaluated using 1,000 gene-set permutations (seed = 1729); sample-group labels were not permuted. GSEA's permutation-based adjusted *p* values are reported as *q* values and were estimated separately within each library ($q < .05$). Leading-edge genes are the subset contributing to a gene set's enrichment score; they need not be individually differentially abundant. Enrichment FDR is distinct from the protein-level Benjamini–Hochberg correction and is not pooled across libraries.

UZH1a versus Untreated

Gene-set library	Sets tested	Significant sets: NES > 0	Significant sets: NES < 0
GO biological process (2026-11-13)	396	1	0
GO molecular function (2026-11-13)	121	0	0
GO cellular component (2026-11-13)	123	0	0
Reactome pathways (98)	101	0	0
KEGG 2026	8	0	0

Gene-set library	Sets tested	Significant sets: NES > 0	Significant sets: NES < 0
InterPro domains (111.0)	10	0	0

The final two columns give the numbers of gene sets with $q < .05$, separated by enrichment direction. All libraries are included. Summary figures show up to 15 significant sets per library; complete results and supporting genes are retained in the data package.

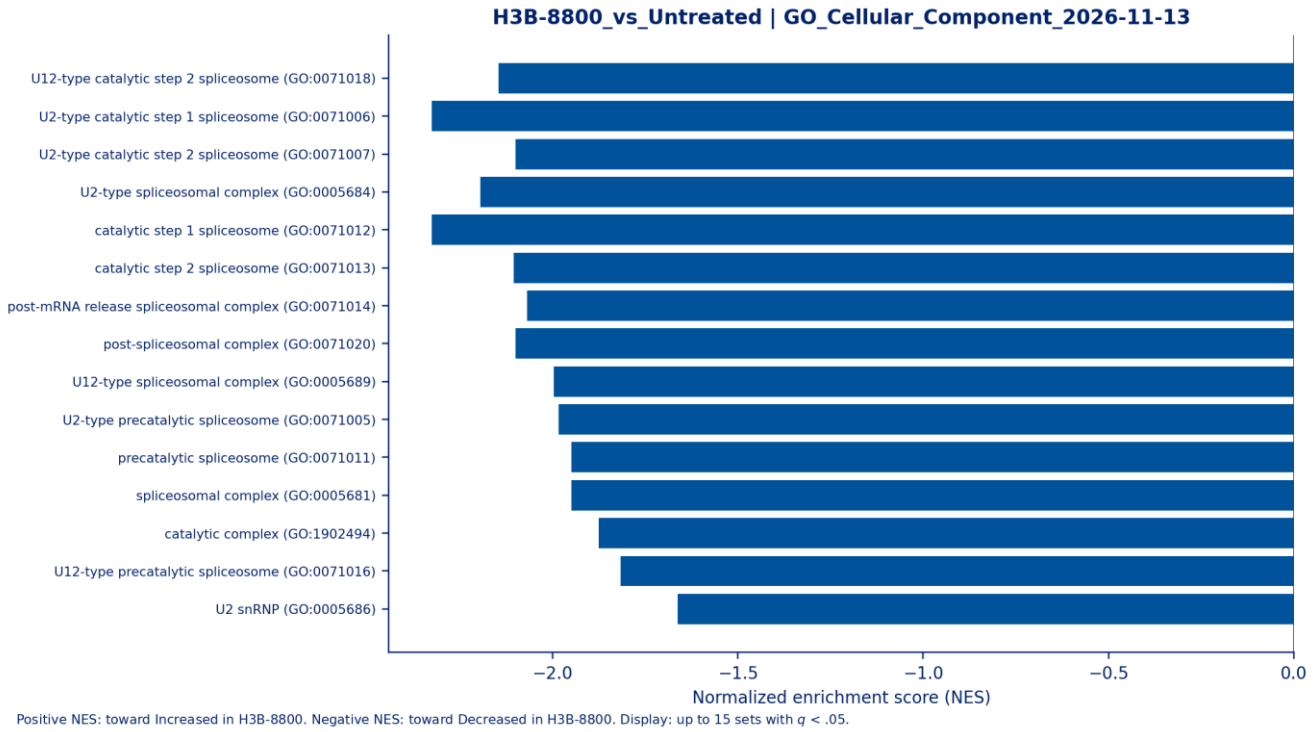


Figure 47. Ranked enrichment of GO cellular component (2026-11-13) gene sets. Shown are 15 of 16 significant gene sets, ordered by *q* value, then nominal *p* value and term name. Bars show normalized enrichment scores (NES). Positive and negative NES indicate enrichment toward the H3B-8800 and Untreated ends of the signed *t*-statistic ranking, respectively. Gene sets meet $q < .05$ within this library (125 sets tested). Complete results, ranked genes, leading-edge genes, and running enrichment curves are provided in the corresponding ranked-enrichment folder.

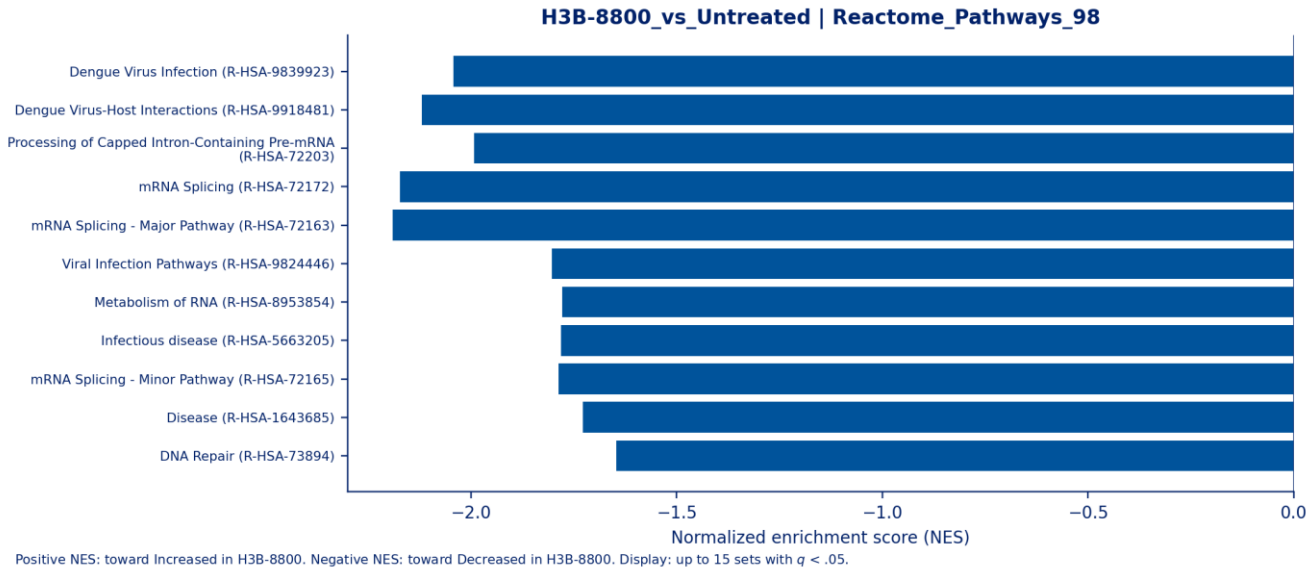


Figure 48. Ranked enrichment of Reactome pathways (98) gene sets. Shown are all 11 significant gene sets, ordered by *q* value, then nominal *p* value and term name. Bars show normalized enrichment scores (NES). Positive and negative NES indicate enrichment toward the H3B-8800 and Untreated ends of the signed *t*-statistic ranking, respectively. Gene sets meet $q < .05$ within this library (105 sets tested). Complete results, ranked genes, leading-edge genes, and running enrichment curves are provided in the corresponding ranked-enrichment folder.

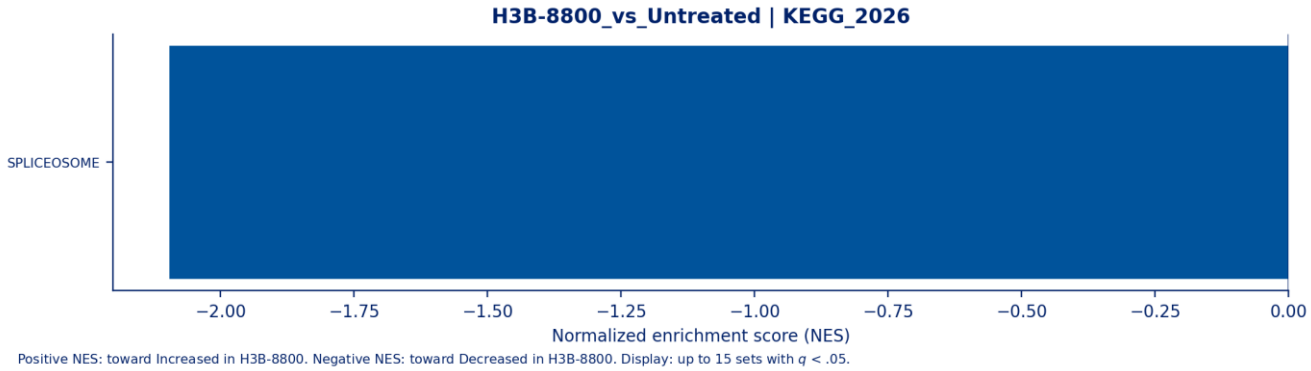


Figure 49. Ranked enrichment of KEGG 2026 gene sets. Shown is the significant gene set, ordered by *q* value, then nominal *p* value and term name. Bars show normalized enrichment scores (NES). Positive and negative NES indicate enrichment toward the H3B-8800 and Untreated ends of the signed *t*-statistic ranking, respectively. Gene sets meet $q < .05$ within this library (8 sets tested). Complete results, ranked genes, leading-edge genes, and running enrichment curves are provided in the corresponding ranked-enrichment folder.

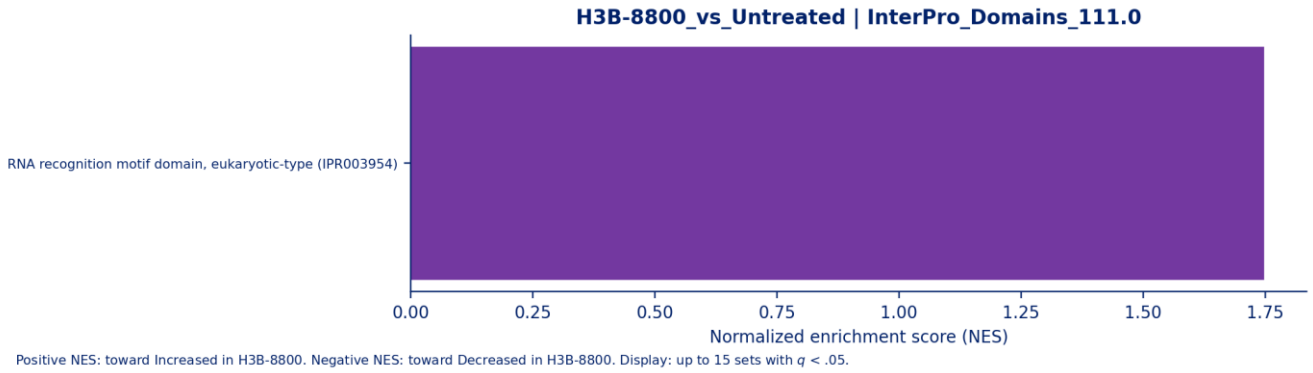


Figure 50. Ranked enrichment of InterPro domains (111.0) gene sets. Shown is the significant gene set, ordered by *q* value, then nominal *p* value and term name. Bars show normalized enrichment scores (NES). Positive and negative NES indicate enrichment toward the H3B-8800 and Untreated ends of the signed *t*-statistic ranking, respectively. Gene sets meet $q < .05$ within this library (10 sets tested). Complete results, ranked genes, leading-edge genes, and running enrichment curves are provided in the corresponding ranked-enrichment folder.

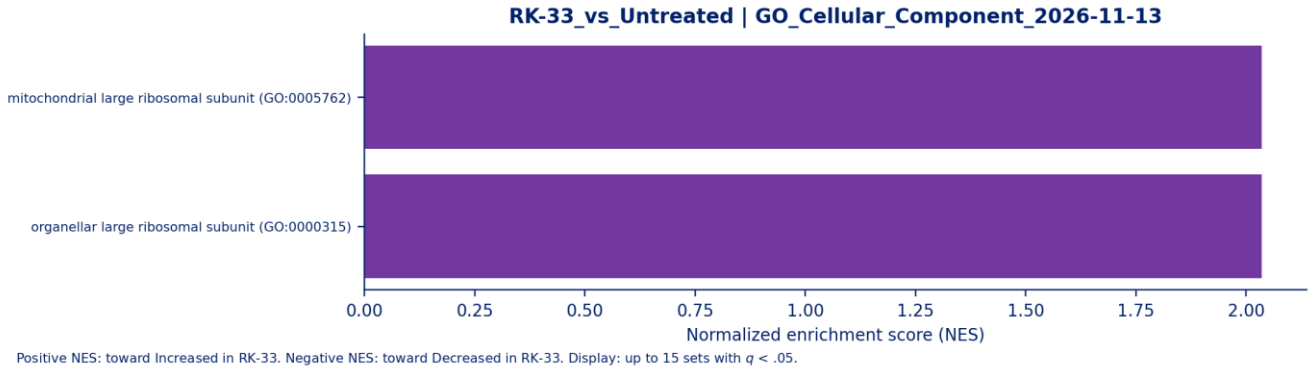


Figure 51. Ranked enrichment of GO cellular component (2026-11-13) gene sets. Shown are all 2 significant gene sets, ordered by *q* value, then nominal *p* value and term name. Bars show normalized enrichment scores (NES). Positive and negative NES indicate enrichment toward the RK-33 and Untreated ends of the signed *t*-statistic ranking, respectively. Gene sets meet $q < .05$ within this library (125 sets tested). Complete results, ranked genes, leading-edge genes, and running enrichment curves are provided in the corresponding ranked-enrichment folder.

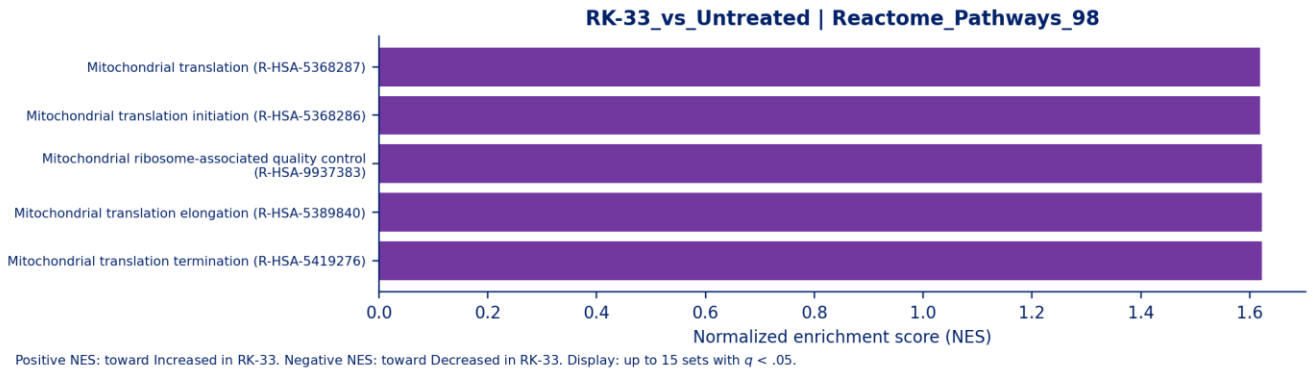


Figure 52. Ranked enrichment of Reactome pathways (98) gene sets. Shown are all 5 significant gene sets, ordered by *q* value, then nominal *p* value and term name. Bars show normalized enrichment scores (NES). Positive and negative NES indicate enrichment toward the RK-33 and Untreated ends of the signed *t*-statistic ranking, respectively. Gene sets meet $q < .05$ within this library (106 sets tested). Complete results, ranked genes, leading-edge genes, and running enrichment curves are provided in the corresponding ranked-enrichment folder.

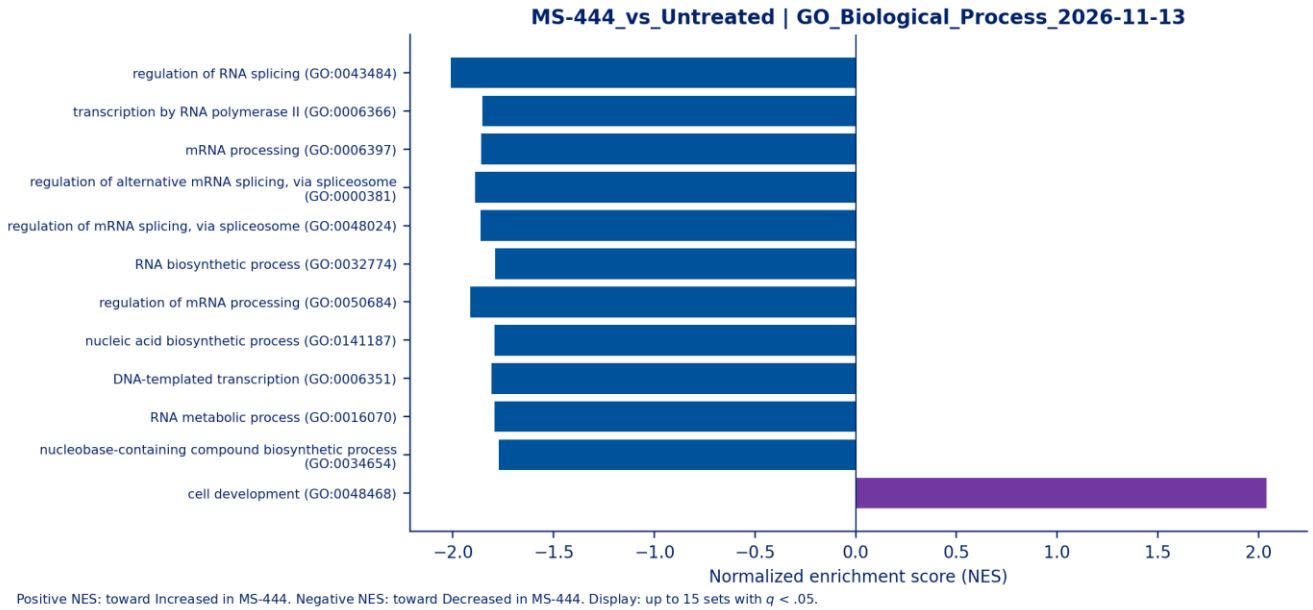


Figure 53. Ranked enrichment of GO biological process (2026-11-13) gene sets. Shown are all 12 significant gene sets, ordered by *q* value, then nominal *p* value and term name. Bars show normalized enrichment scores (NES). Positive and negative NES indicate enrichment toward the MS-444 and Untreated ends of the signed *t*-statistic ranking, respectively. Gene sets meet $q < .05$ within this library (402 sets tested). Complete results, ranked genes, leading-edge genes, and running enrichment curves are provided in the corresponding ranked-enrichment folder.

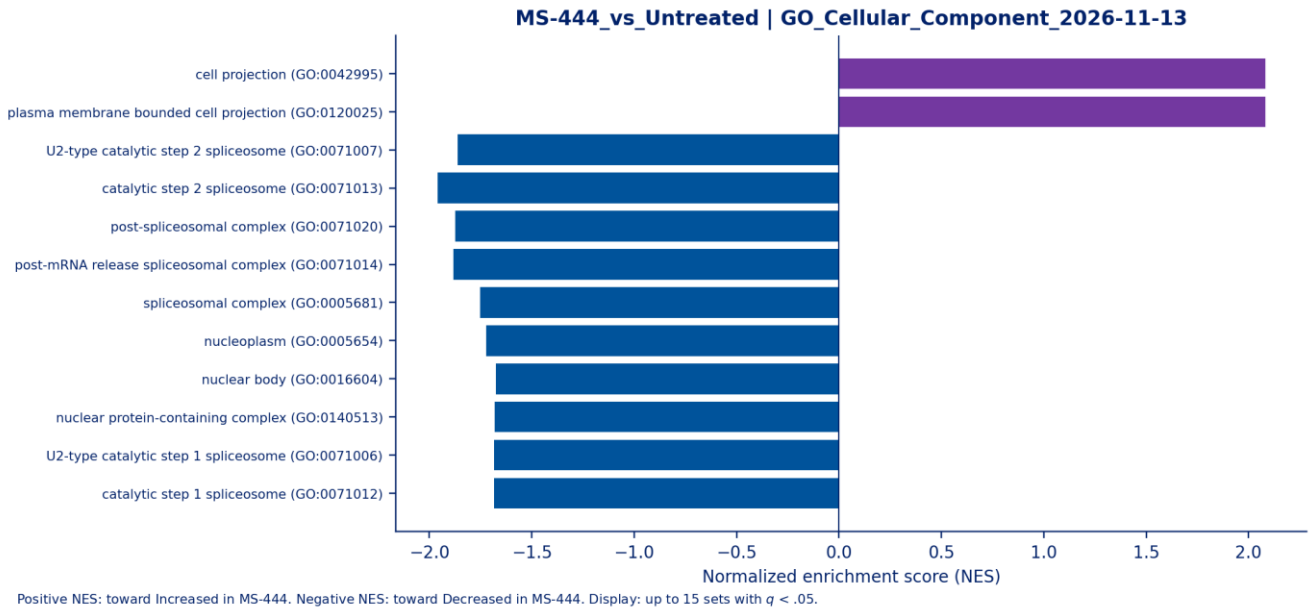


Figure 54. Ranked enrichment of GO cellular component (2026-11-13) gene sets. Shown are all 12 significant gene sets, ordered by *q* value, then nominal *p* value and term name. Bars show normalized enrichment scores (NES). Positive and negative NES indicate enrichment toward the MS-444 and Untreated ends of the signed *t*-statistic ranking, respectively. Gene sets meet $q < .05$ within this library (127 sets tested). Complete results, ranked genes, leading-edge genes, and running enrichment curves are provided in the corresponding ranked-enrichment folder.

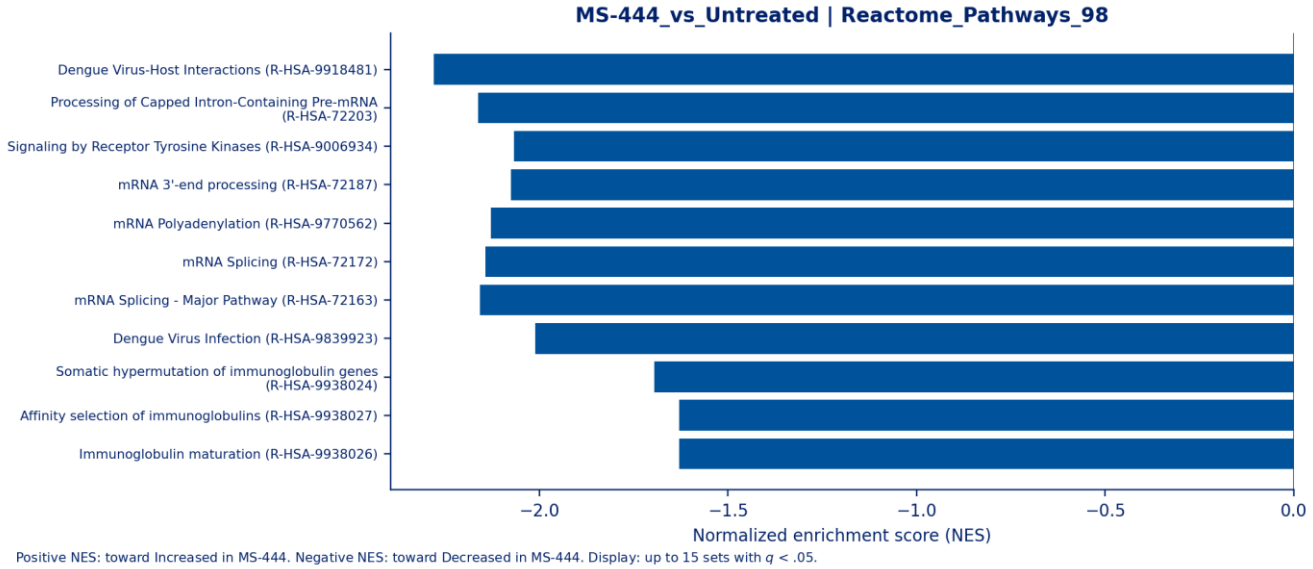


Figure 55. Ranked enrichment of Reactome pathways (98) gene sets. Shown are all 11 significant gene sets, ordered by *q* value, then nominal *p* value and term name. Bars show normalized enrichment scores (NES). Positive and negative NES indicate enrichment toward the MS-444 and Untreated ends of the signed *t*-statistic ranking, respectively. Gene sets meet $q < .05$ within this library (108 sets tested). Complete results, ranked genes, leading-edge genes, and running enrichment curves are provided in the corresponding ranked-enrichment folder.

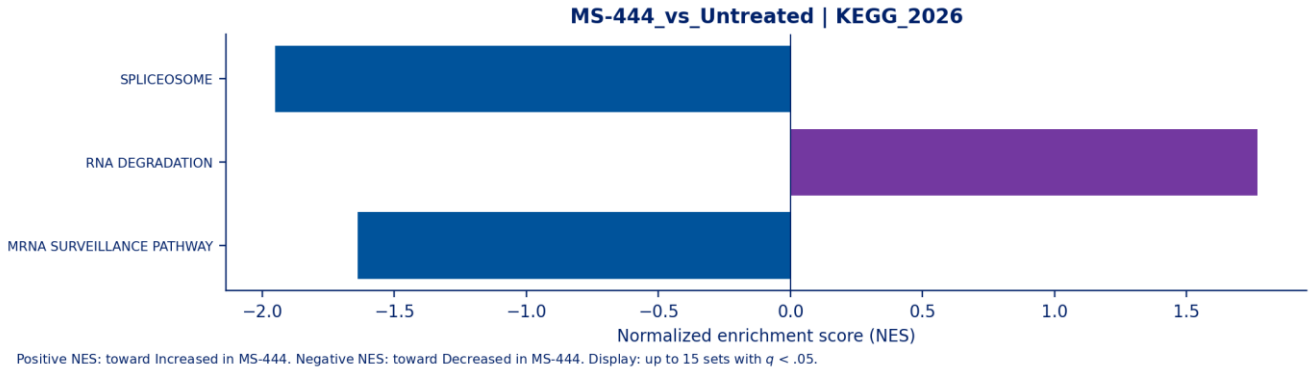


Figure 56. Ranked enrichment of KEGG 2026 gene sets. Shown are all 3 significant gene sets, ordered by *q* value, then nominal *p* value and term name. Bars show normalized enrichment scores (NES). Positive and negative NES indicate enrichment toward the MS-444 and Untreated ends of the signed *t*-statistic ranking, respectively. Gene sets meet $q < .05$ within this library (8 sets tested). Complete results, ranked genes, leading-edge genes, and running enrichment curves are provided in the corresponding ranked-enrichment folder.

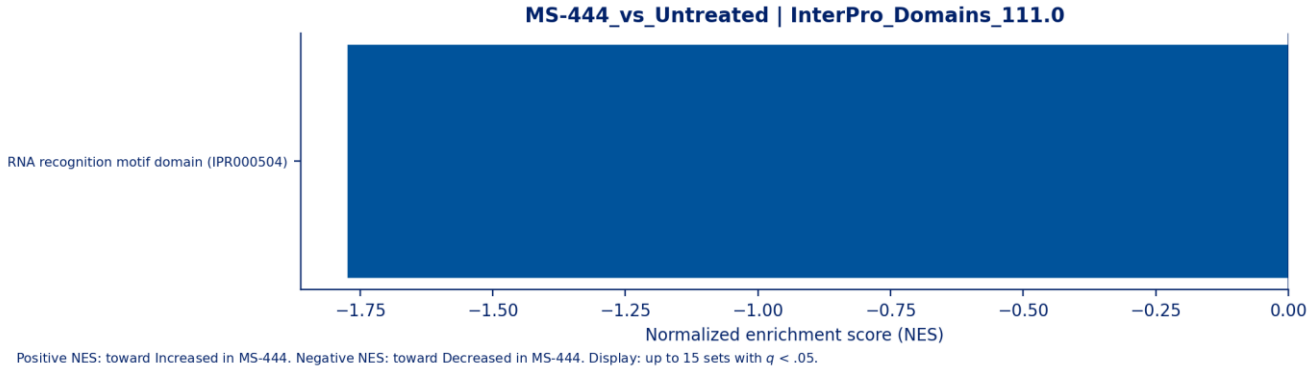


Figure 57. Ranked enrichment of InterPro domains (111.0) gene sets. Shown is the significant gene set, ordered by *q* value, then nominal *p* value and term name. Bars show normalized enrichment scores (NES). Positive and negative NES indicate enrichment toward the MS-444 and Untreated ends of the signed *t*-statistic ranking, respectively. Gene sets meet $q < .05$ within this library (10 sets tested). Complete results, ranked genes, leading-edge genes, and running enrichment curves are provided in the corresponding ranked-enrichment folder.

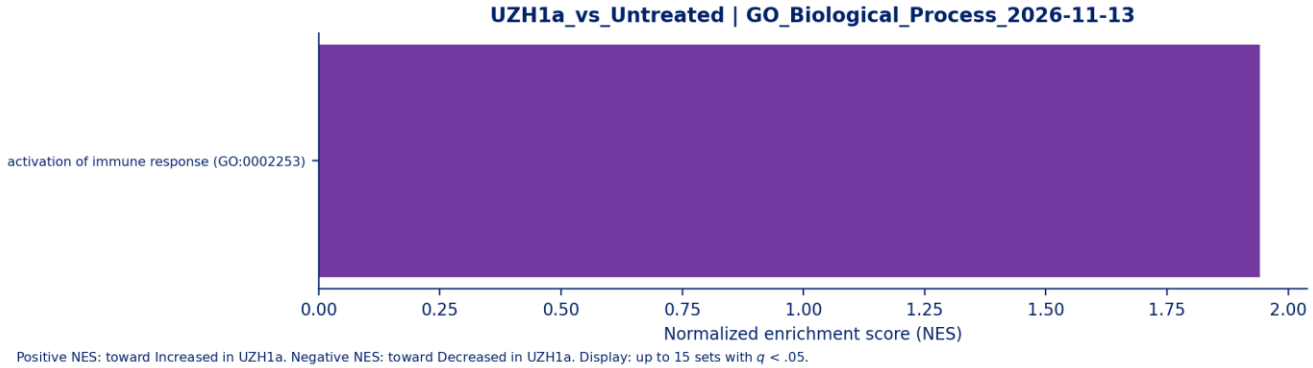


Figure 58. Ranked enrichment of GO biological process (2026-11-13) gene sets. Shown is the significant gene set, ordered by *q* value, then nominal *p* value and term name. Bars show normalized enrichment scores (NES). Positive and negative NES indicate enrichment toward the UZH1a and Untreated ends of the signed *t*-statistic ranking, respectively. Gene sets meet $q < .05$ within this library (396 sets tested). Complete results, ranked genes, leading-edge genes, and running enrichment curves are provided in the corresponding ranked-enrichment folder.

Functional enrichment describes the distribution of annotations among selected or ranked proteins in the analyzed fractions. Overlapping terms may reflect the same proteins. These results do not establish changes in total cellular protein abundance, RNA-binding occupancy, or pathway activity.

11. Protein Networks

STRING functional-association networks show proteins with BH-adjusted $q < .05$ in each selected comparison and protein panel. Colored lines show the sources of evidence for reference associations; node and line colors do not show the direction of the measured change. The mapping and association tables accompany the figures. No additional proteins were added.

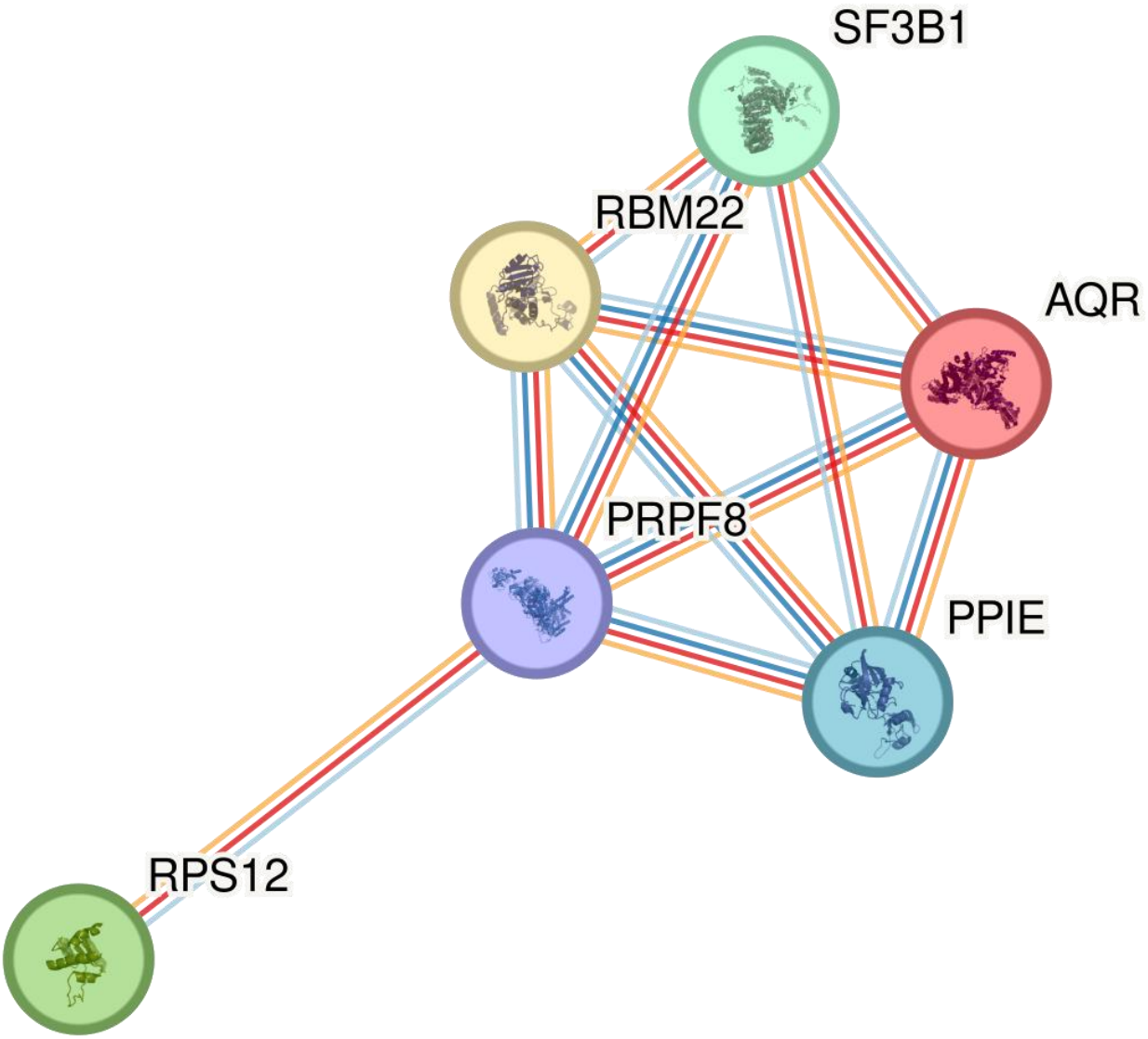


Figure 59. STRING functional-association network for H3B-8800 versus Untreated. The input comprises 6 proteins with protein-level BH-adjusted $q < .05$; 6 mapped uniquely to STRING. Colored lines identify evidence sources; nodes and line colors do not encode fold-change direction. STRING v12.5; combined confidence ≥ 0.40; no additional proteins were added. Protein mappings and association scores are provided in the source tables. The report image is cropped to remove transparent margins. STRING network image and data: https://string-db.org, CC BY 4.0.

STRING line colors: ● light blue: curated databases; ● purple: experiments; ● yellow: text mining; ● black: co-expression; ● green: gene neighborhood; ● red: gene fusion; ● blue: gene co-occurrence. Multiple colors can support the same association. Node colors distinguish proteins and do not indicate the direction of change.

Source data: protein nodes; connections; selection

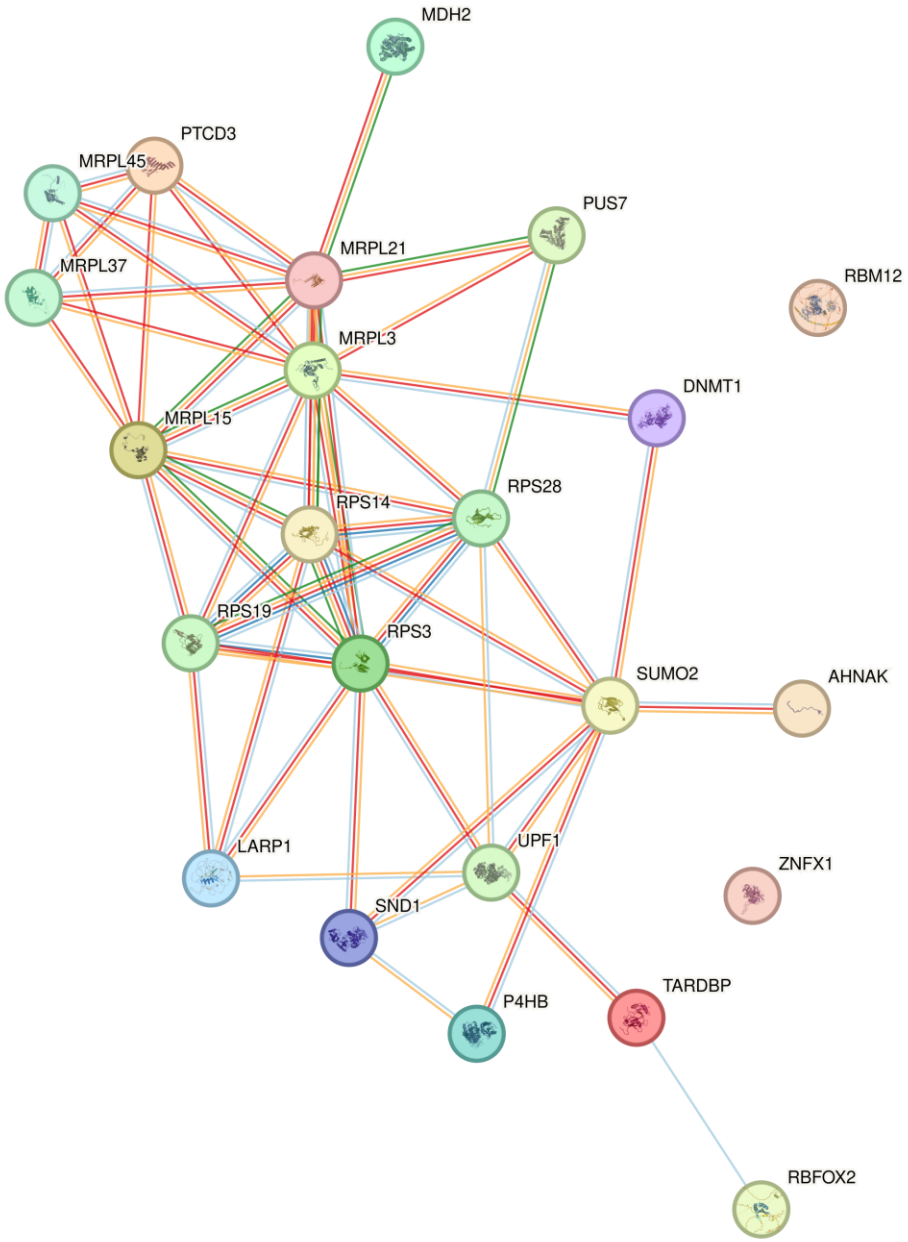


Figure 60. STRING functional-association network for RK-33 versus Untreated. The input comprises 23 proteins with protein-level BH-adjusted $q < .05$; 23 mapped uniquely to STRING. Colored lines identify evidence sources; nodes and line colors do not encode fold-change direction. STRING v12.5; combined confidence ≥ 0.40; no additional proteins were added. Protein mappings and association scores are provided in the source tables. The report image is cropped to remove transparent margins. STRING network image and data: https://string-db.org, CC BY 4.0.

STRING line colors: ● light blue: curated databases; ● purple: experiments; ● yellow: text mining; ● black: co-expression; ● green: gene neighborhood; ● red: gene fusion; ● blue: gene co-occurrence. Multiple colors can support the same association. Node colors distinguish proteins and do not indicate the direction of change.

Source data: protein nodes; connections; selection

12. Treatment Selectivity

Selectivity scores summarize the fraction of evaluated proteins whose abundance in the analyzed RNP fractions changes by at least the stated fold threshold relative to the explicitly nominated control. Increases and reciprocal decreases are counted without a *p*-value or *q*-value filter. These counts are separate from the differential-abundance calls in Section 8.

The following summary uses the common eligible protein set across nominated comparisons sharing the same control and protein panel. Lower scores describe a response concentrated among fewer evaluated proteins at that threshold. Comparison-specific scores, complete protein values and response memberships are provided in the data package. Scores describe the recorded treatment conditions.

Treatment	Control	*N*	S(1.25-fold)	S(1.5-fold)	S(2-fold)
H3B-8800	Untreated	762	0.1312	0.0591	0.0223
RK-33	Untreated	762	0.2192	0.0945	0.0341
MS-444	Untreated	762	0.1535	0.0420	0.0118
UZH1a	Untreated	762	0.1864	0.0735	0.0105

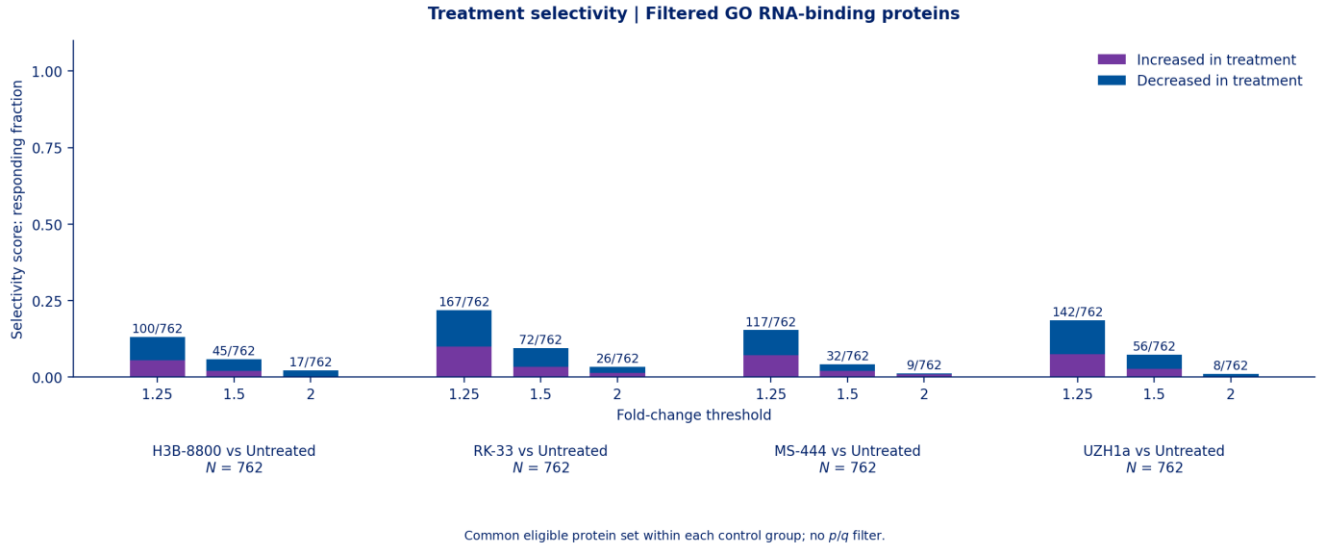


Figure 61. Treatment selectivity across fold-change thresholds. Stacked bars show the fraction of evaluated proteins with an increase (purple) or decrease (blue) of at least 1.25, 1.5, 2-fold relative to the nominated control. The total bar height is S(f-fold); no *p*-value or *q*-value filter is applied. The denominator is the common eligible protein set across nominated comparisons sharing a control and protein panel, with its size shown as *N*. Reciprocal decreases are counted: for example, a twofold decrease corresponds to a treatment/control ratio of 0.5. Fold changes retain the original %TP normalization. The source tables contain counts, scores, complete evaluated protein values, and threshold memberships; comparison-specific scores are also provided.

13. Additional Detection Evidence

Comparison	Panel	Criterion met in	Additional proteins
H3B-8800_vs_Untreated	Filtered GO RNA-binding proteins	H3B-8800	23
H3B-8800_vs_Untreated	Filtered GO RNA-binding proteins	Untreated	22
RK-33_vs_Untreated	Filtered GO RNA-binding proteins	RK-33	24
RK-33_vs_Untreated	Filtered GO RNA-binding proteins	Untreated	22
MS-444_vs_Untreated	Filtered GO RNA-binding proteins	MS-444	24
MS-444_vs_Untreated	Filtered GO RNA-binding proteins	Untreated	15
UZH1a_vs_Untreated	Filtered GO RNA-binding proteins	UZH1a	12
UZH1a_vs_Untreated	Filtered GO RNA-binding proteins	Untreated	37

These proteins meet the peptide criterion in every replicate of one group and fail it in at least one replicate of the other. They are listed separately from differential-abundance results. Missing detection does not demonstrate biological absence; no imputed fold changes or significance values are assigned.

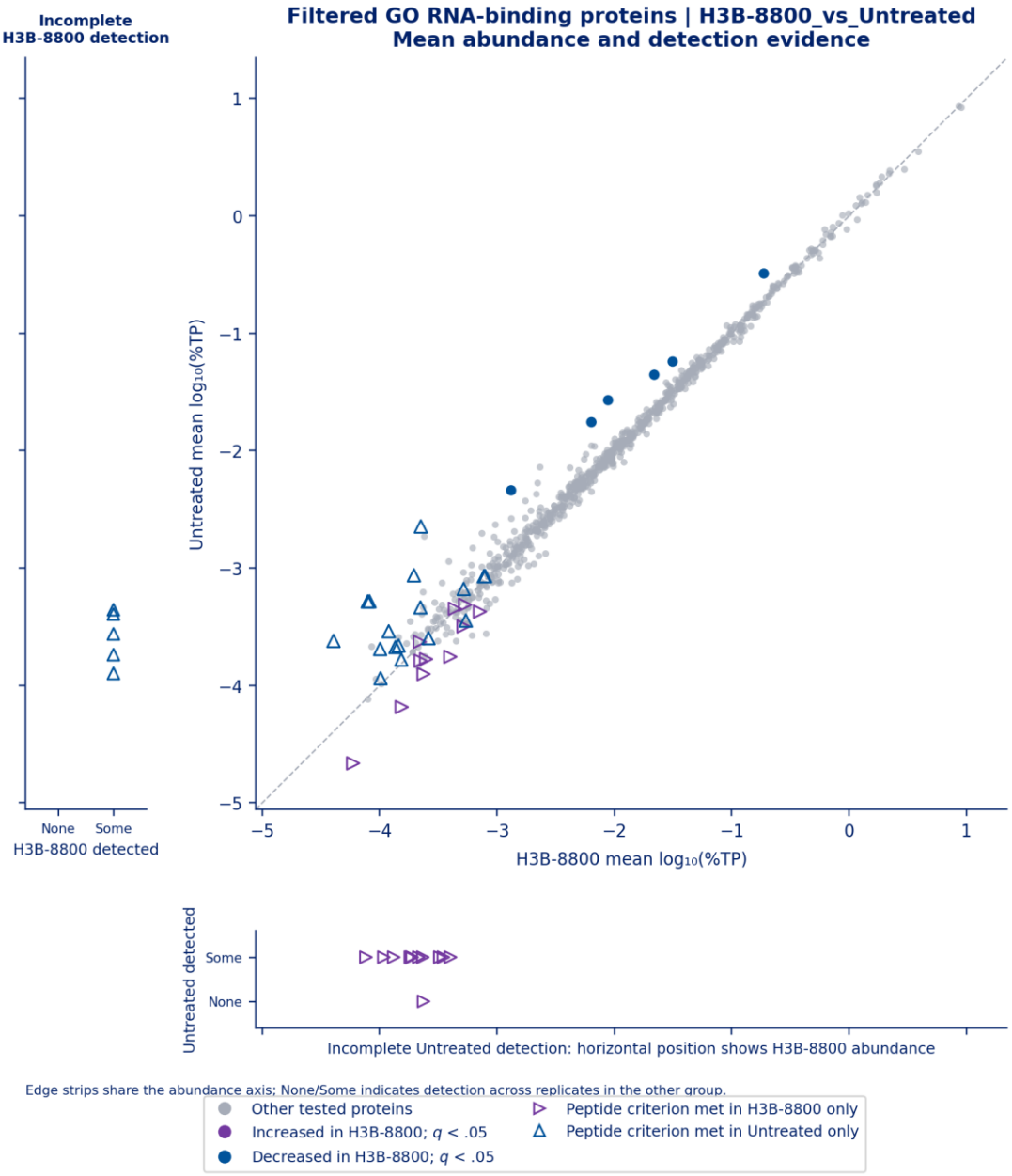


Figure 62. H3B-8800_vs_Untreated: measured abundance and incomplete detection evidence. Proteins meeting the peptide criterion in only one group are descriptive observations and have no assigned differential-abundance *p* values or fold changes.

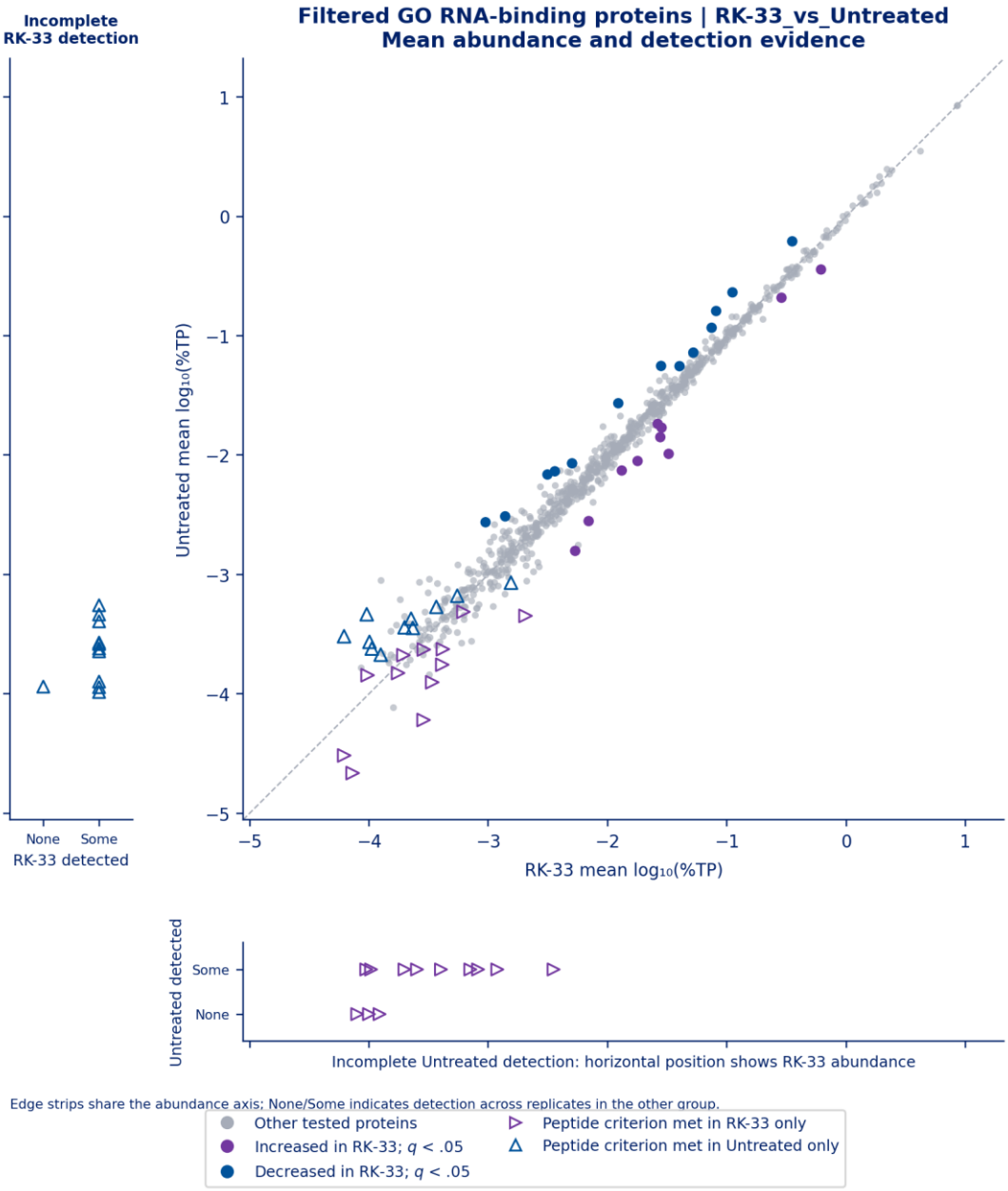


Figure 63. RK-33_vs_Untreated: measured abundance and incomplete detection evidence. Proteins meeting the peptide criterion in only one group are descriptive observations and have no assigned differential-abundance *p* values or fold changes.

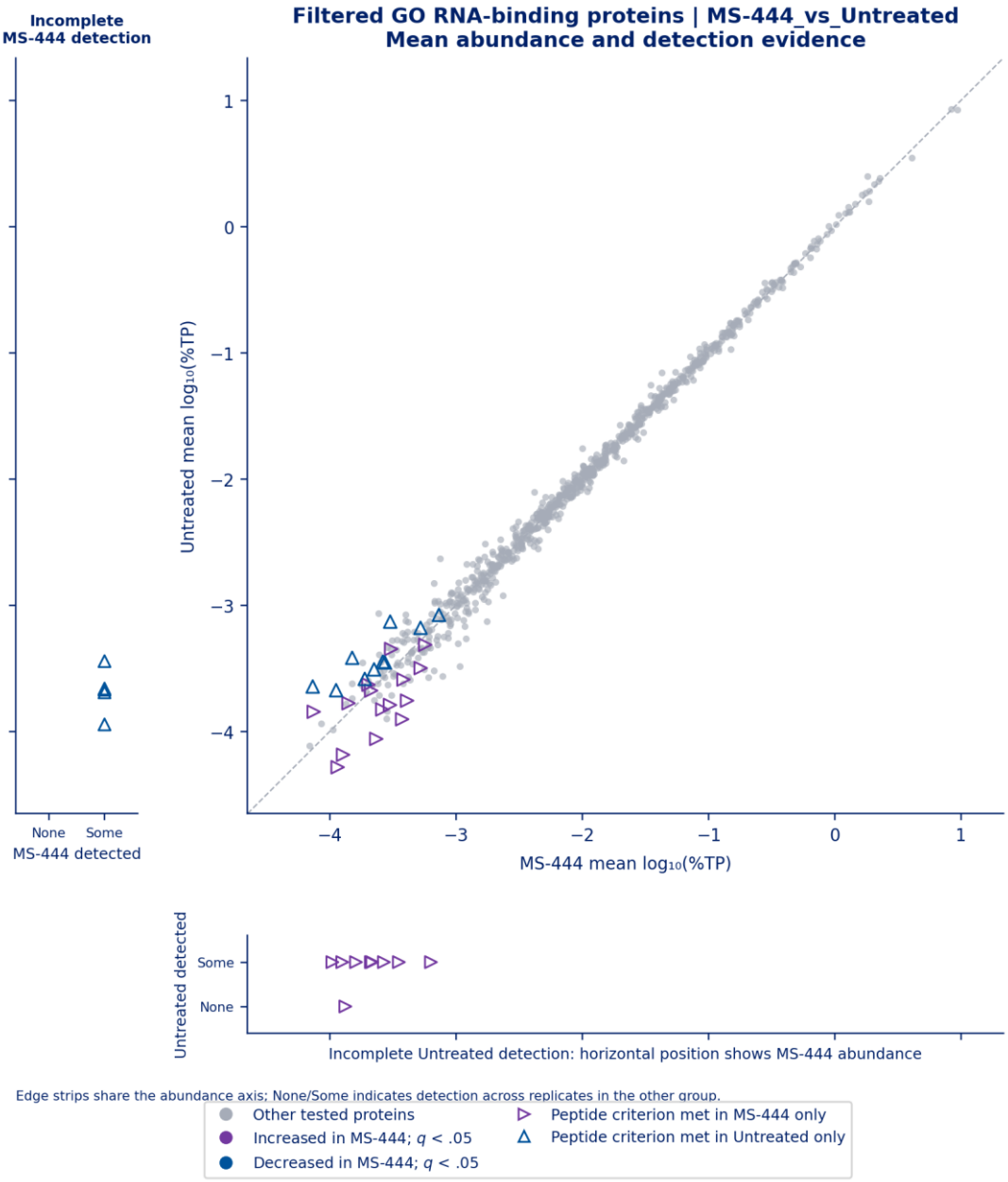


Figure 64. MS-444_vs_Untreated: measured abundance and incomplete detection evidence. Proteins meeting the peptide criterion in only one group are descriptive observations and have no assigned differential-abundance *p* values or fold changes.

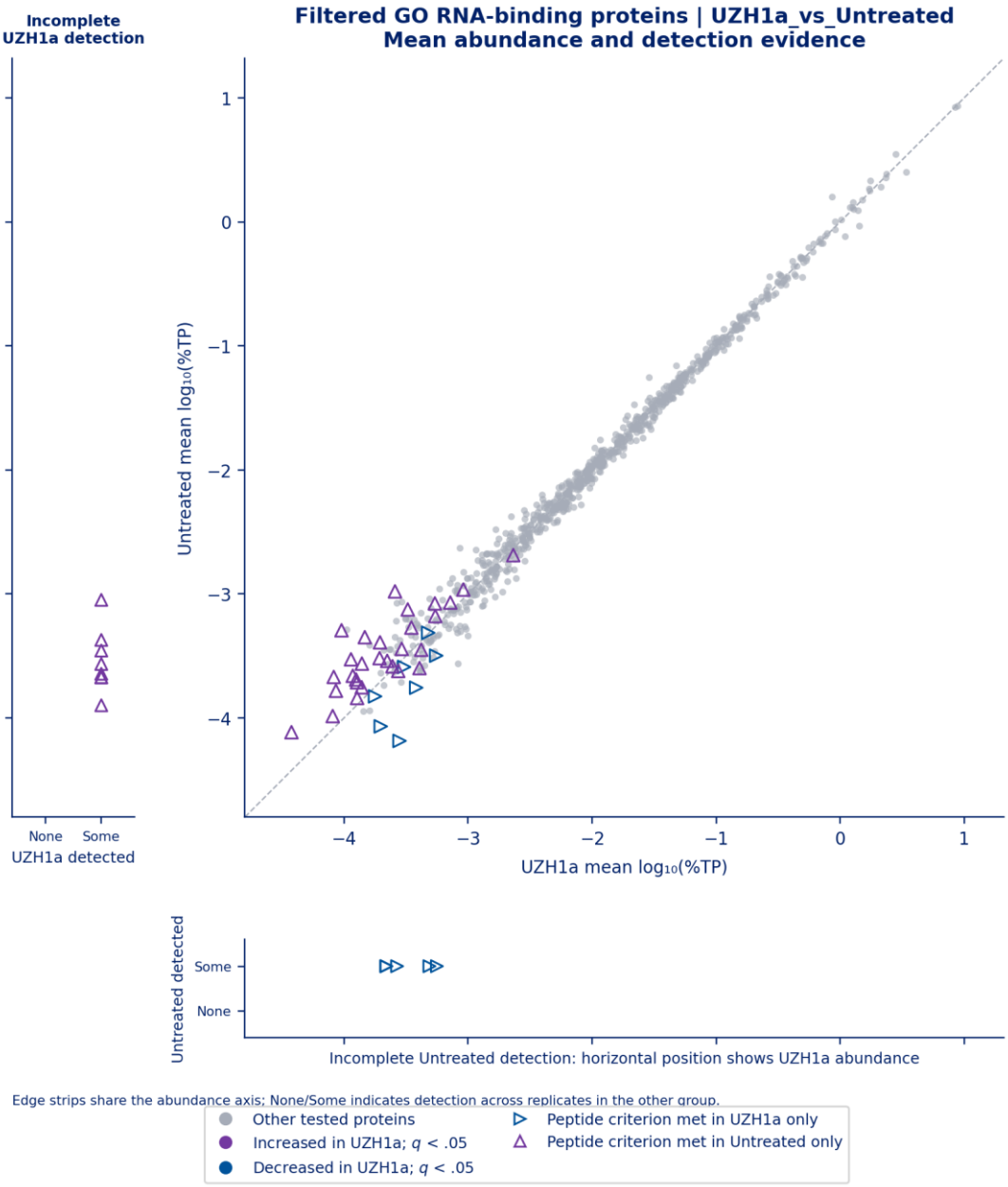


Figure 65. UZH1a_vs_Untreated: measured abundance and incomplete detection evidence. Proteins meeting the peptide criterion in only one group are descriptive observations and have no assigned differential-abundance *p* values or fold changes.

14. Interpretation

This study profiles the cellular responses of HCT116 cells to four RBP-targeting compounds. H3B-8800 produced a focused response involving SF3B1 and other spliceosome proteins, consistent with its reported mechanism. RK-33 produced a broader response that included mitochondrial and cytoplasmic ribosomal proteins. Ranked enrichment also identified coordinated protein patterns following MS-444 and UZH1a treatment. The responding proteins and functional themes provide candidate markers of compound activity under the tested conditions.

H3B-8800 (10 µM) was associated with decreased relative abundance in the RNP fractions for six of 797 tested proteins ($q < .05$). These included SF3B1 (0.55-fold), AQR (0.33-fold), RBM22 (0.49-fold), PRPF8 (0.58-fold), and PPIE (0.29-fold). H3B-8800 targets the SF3b complex and inhibits U2 snRNP assembly in biochemical studies; it also modulates splicing in cellular models (Seiler et al., 2018). The coordinated response of SF3B1 and additional spliceosome proteins is consistent with activity involving the reported target complex and identifies a potential protein signature of compound activity. Negative ranked enrichment of spliceosome-related gene sets extends this pattern across the tested proteins. Conversely, PABPC1, PABPC4, TIA1, and TIAL1 contributed to a positively enriched RNA-recognition-motif set, indicating that the ranked response included proteins shifted in the opposite direction.

RK-33 (10 µM) was associated with differential abundance of 23 of 797 tested proteins ($q < .05$). MRPL15 (3.17-fold), MRPL21 (3.40-fold), MRPL3 (1.77-fold), and MRPL45 (1.44-fold) were increased, whereas MRPL37 (0.72-fold), PTCD3 (0.72-fold), RPS3 (0.48-fold), RPS14 (0.45-fold), and RPS28 (0.35-fold) were decreased. Positive ranked enrichment of mitochondrial large-ribosomal-subunit and mitochondrial-translation sets highlighted overlapping groups of mitochondrial ribosomal proteins. These proteins identify a mitochondrial translation-related response alongside changes in cytoplasmic ribosomal proteins.

RK-33 was developed as a DDX3 inhibitor (Bol et al., 2015). In breast cancer models, Heerma van Voss et al. (2018) reported that RK-33 treatment or DDX3 depletion affected mitochondrial translation and reduced mitochondrial translation-related proteins. The present HCT116 data likewise highlight mitochondrial ribosomal proteins, but the RNP-fraction measurements, treatment duration, and directions of individual protein changes differ from those prior experiments. DDX3X did not meet the protein-level significance threshold in this comparison. In another model, Hecht and Parker (2026) reported RK-33-associated cellular effects that persisted after DDX3 depletion. Together, these findings frame the mitochondrial protein response as a candidate signature of RK-33 activity while leaving its target dependence to be established.

MS-444 (100 µM) produced negative ranked enrichment of proteins annotated to regulation of RNA splicing and the U2-type catalytic step 2 spliceosome. RBFOX2, PTBP1, PRPF8, and RBM22 contributed to the leading edge of these related sets, providing a coordinated spliceosome-related pattern for the compound profile. MS-444 was reported to interfere with HuR RNA binding and dimerization in biochemical and cell-based experiments (Meisner et al., 2007). ELAVL1 (HuR) and the other 803 tested proteins did not meet the protein-level significance threshold in this comparison; the gene-set result provides complementary evidence of the ranked protein response.

UZH1a (100 µM) produced positive ranked enrichment of the activation-of-immune-response gene set (NES = 1.94, $q = .044$), with NONO, PSPC1, TRIM25, SFPQ, and DDX3X among its leading-edge proteins. UZH1a was characterized as a cell-permeable METTL3 inhibitor, with reduced mRNA m^6A levels reported in cellular studies using longer exposures (Moroz-Omori et al., 2021). No individual protein met the protein-level significance

threshold among the 782 tested here. The ranked set identifies a coordinated group of proteins for the 90-minute compound response; its annotation describes their reported functions rather than a direct measurement of immune activation.

The selectivity scores summarize response breadth across the 762 proteins eligible in all four comparisons without applying a protein-level significance filter. At the twofold threshold, 17 proteins responded to H3B-8800, 26 to RK-33, 9 to MS-444, and 8 to UZH1a. The scores describe the breadth of relative abundance changes at the tested concentrations and time point, rather than direct compound binding or target specificity.

Under the signal-to-noise (*S*/*N*) analytical framework underlying the analyses in this report, differential abundance can serve as a proxy for altered relative RNA-interaction levels (Kristofich & Nicchitta, 2023, Supplementary Notes 4f and 6b–c). The filtered panel excludes proteins with historical *S*/*N* < 3 and retains proteins without historical measurements. Current-study protein-specific *S*/*N* was not measured; cellular protein abundance and the shared %TP denominator can also influence these relative measurements.

References

Bol, G. M., Vesuna, F., Xie, M., Zeng, J., Aziz, K., Gandhi, N., Levine, A., Irving, A., Korz, D., Tantravedi, S., Heerma van Voss, M. R., Gabrielson, K., Bordt, E. A., Polster, B. M., Cope, L., van der Groep, P., Kondaskar, A., Rudek, M. A., Hosmane, R. S., … Raman, V. (2015). Targeting DDX3 with a small molecule inhibitor for lung cancer therapy. *EMBO Molecular Medicine*, *7*(5), 648–669. https://doi.org/10.15252/emmm.201404368

Heerma van Voss, M. R., Vesuna, F., Bol, G. M., Afzal, J., Tantravedi, S., Bergman, Y., Kammers, K., Lehar, M., Malek, R., Ballew, M., ter Hoeve, N., Abou, D., Thorek, D., Berlinicke, C., Yazdankhah, M., Sinha, D., Le, A., Abrahams, R., Tran, P. T., … Raman, V. (2018). Targeting mitochondrial translation by inhibiting DDX3: a novel radiosensitization strategy for cancer treatment. *Oncogene*, *37*(1), 63–74. https://doi.org/10.1038/onc.2017.308

Hecht, C. J. S., & Parker, R. R. (2026). RK-33 inhibits the OC43 coronavirus and induces stress granules via DDX3X-independent mechanisms. *RNA*, *32*(5), 724–735. https://doi.org/10.1261/rna.080931.125

Kristofich, J., & Nicchitta, C. V. (2023). Signal-noise metrics for RNA binding protein identification reveal broad spectrum protein-RNA interaction frequencies and dynamics. *Nature Communications*, *14*(1), 5868. https://doi.org/10.1038/s41467-023-41284-9

Meisner, N.-C., Hintersteiner, M., Mueller, K., Bauer, R., Seifert, J.-M., Naegeli, H.-U., Ottl, J., Oberer, L., Guenat, C., Moss, S., Harrer, N., Woisetschlaeger, M., Buehler, C., Uhl, V., & Auer, M. (2007). Identification and mechanistic characterization of low-molecular-weight inhibitors for HuR. *Nature Chemical Biology*, *3*(8), 508–515. https://doi.org/10.1038/nchembio.2007.14

Moroz-Omori, E. V., Huang, D., Kumar Bedi, R., Cheriyamkunnel, S. J., Bochenkova, E., Dolbois, A., Rzeczkowski, M. D., Li, Y., Wiedmer, L., & Caflisch, A. (2021). METTL3 inhibitors for epitranscriptomic modulation of cellular processes. *ChemMedChem*, *16*(19), 3035–3043. https://doi.org/10.1002/cmdc.202100291

Seiler, M., Yoshimi, A., Darman, R., Chan, B., Keaney, G., Thomas, M., Agrawal, A. A., Caleb, B., Csibi, A., Sean, E., Fekkes, P., Karr, C., Klimek, V., Lai, G., Lee, L., Kumar, P., Lee, S. C.-W., Liu, X., Mackenzie, C., … Buonamici, S. (2018). H3B-8800, an orally available small-molecule splicing modulator, induces lethality in spliceosome-mutant cancers. *Nature Medicine*, *24*(4), 497–504. https://doi.org/10.1038/nm.4493

Supporting Data and Methods

README.md describes the package contents. Methods_and_Data_Analysis.docx contains the separate methods. The numbered panel folders contain complete result tables and available figures, including figures not selected for this report. SHA256SUMS.txt records package file checksums.